А.М. Никишин
Соляная тектоника

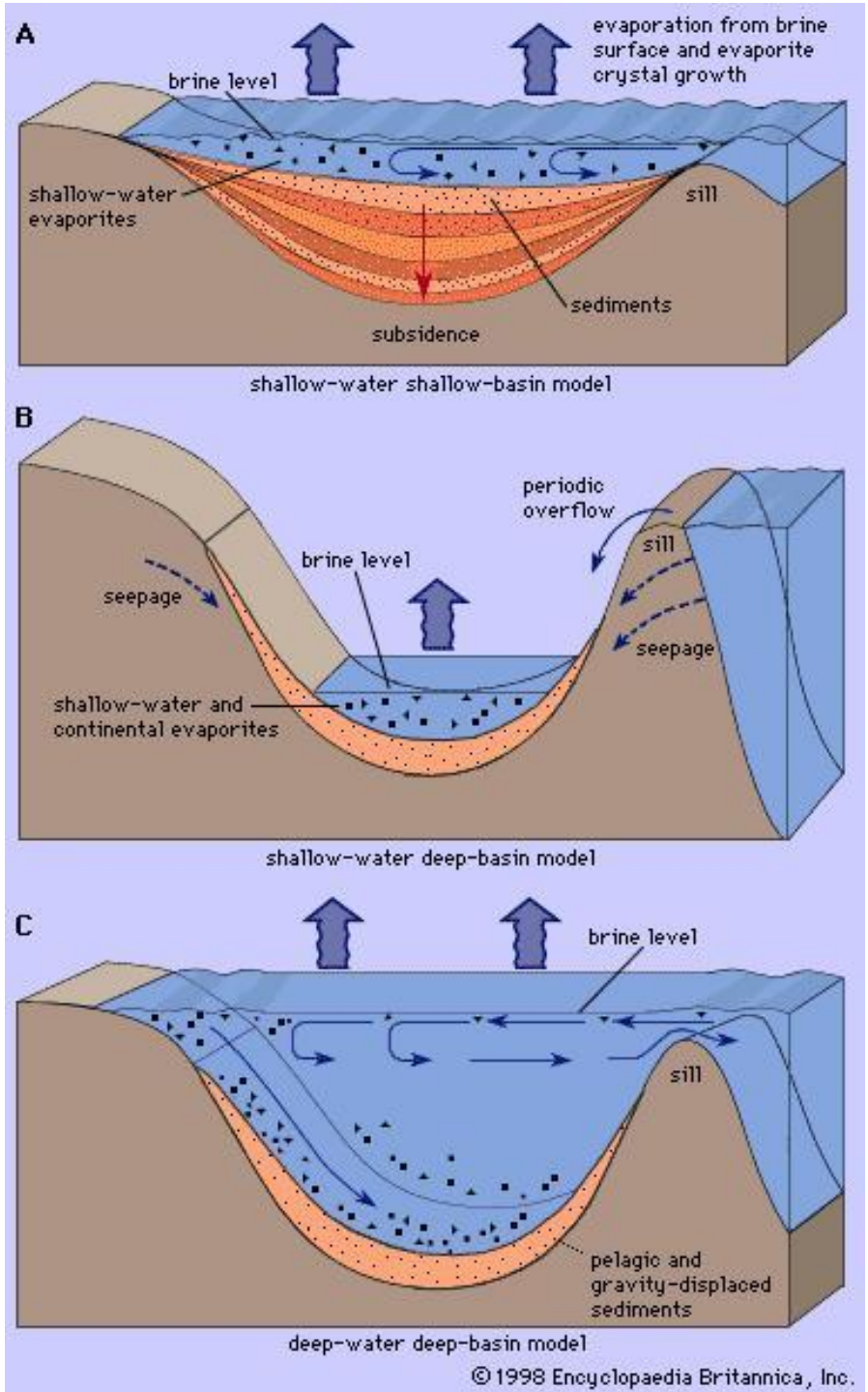

Три разных концепции формирования эвапоритов

Evaporites precipitation order of seawater

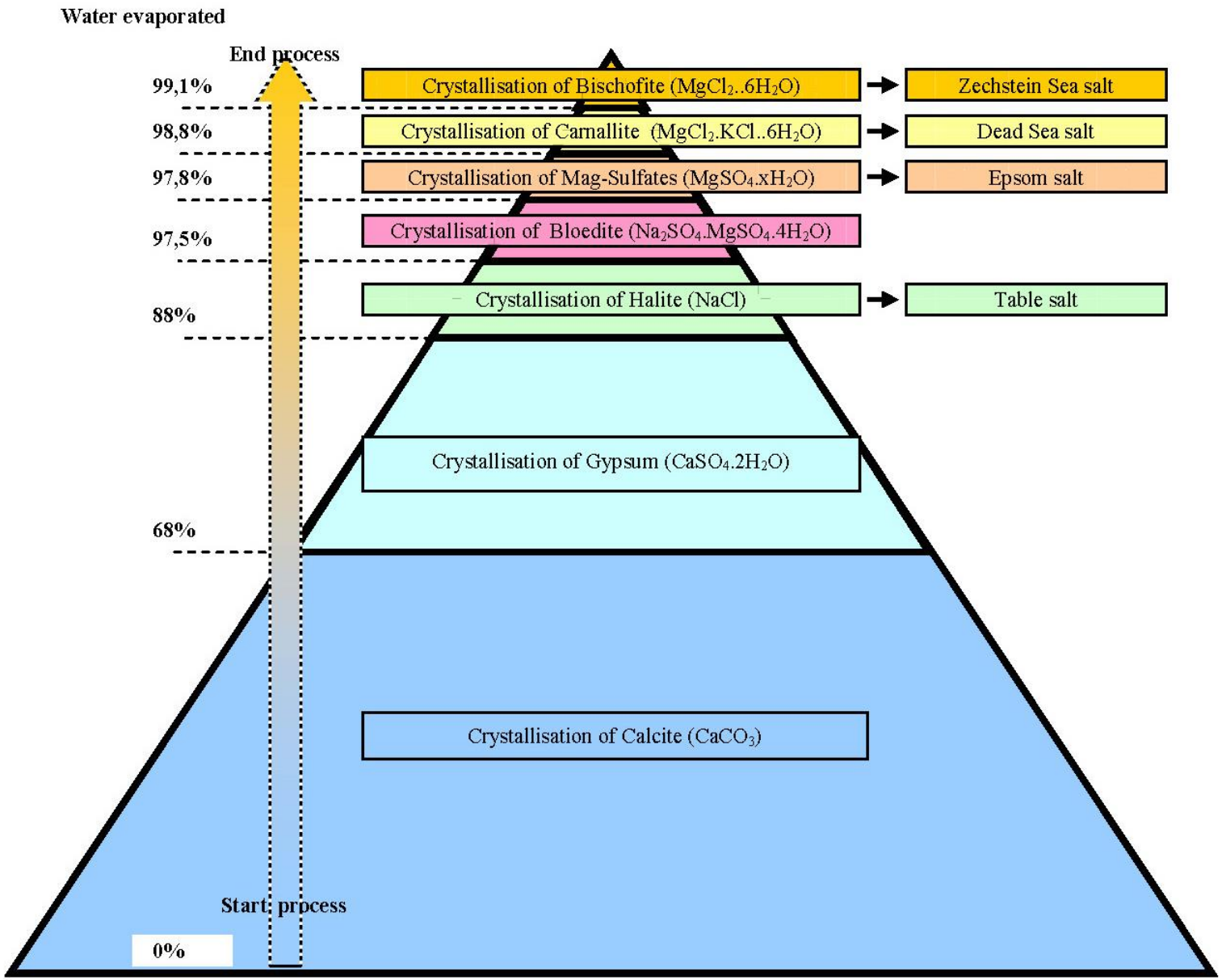

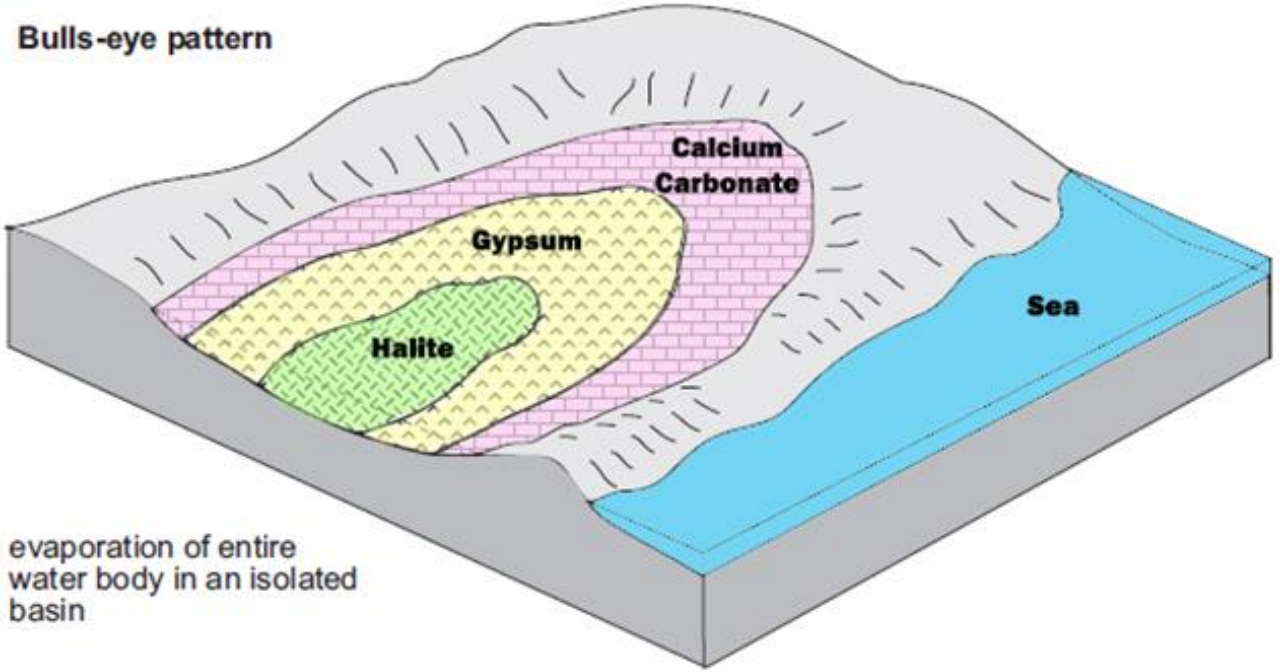
Bulls-eye pattern
Calcium
Carbonate
Gypsum
Halite
Sea
evaporation of entire
water body in an isolated
basin

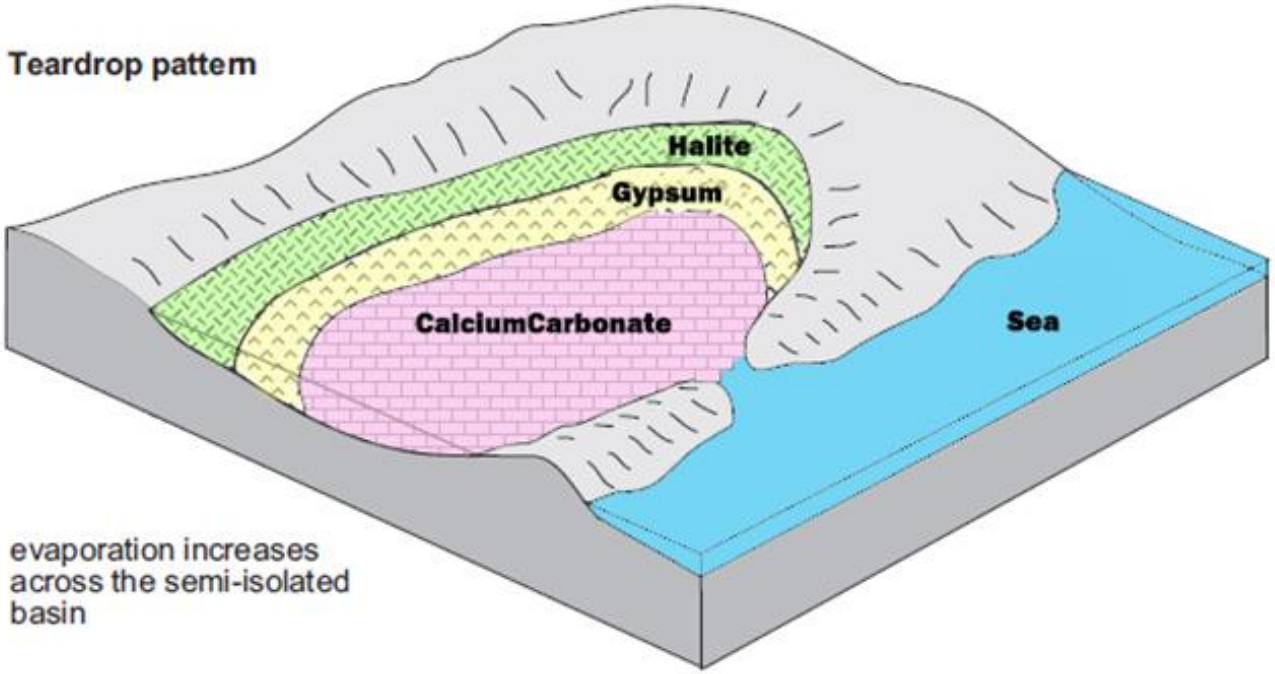
Teardrop pattern
Halite
Gypsum
CalciumCarbonate
Sea
evaporation increases
across the semi-isolated
basin

Marine Geology 395 (2018) 48–64

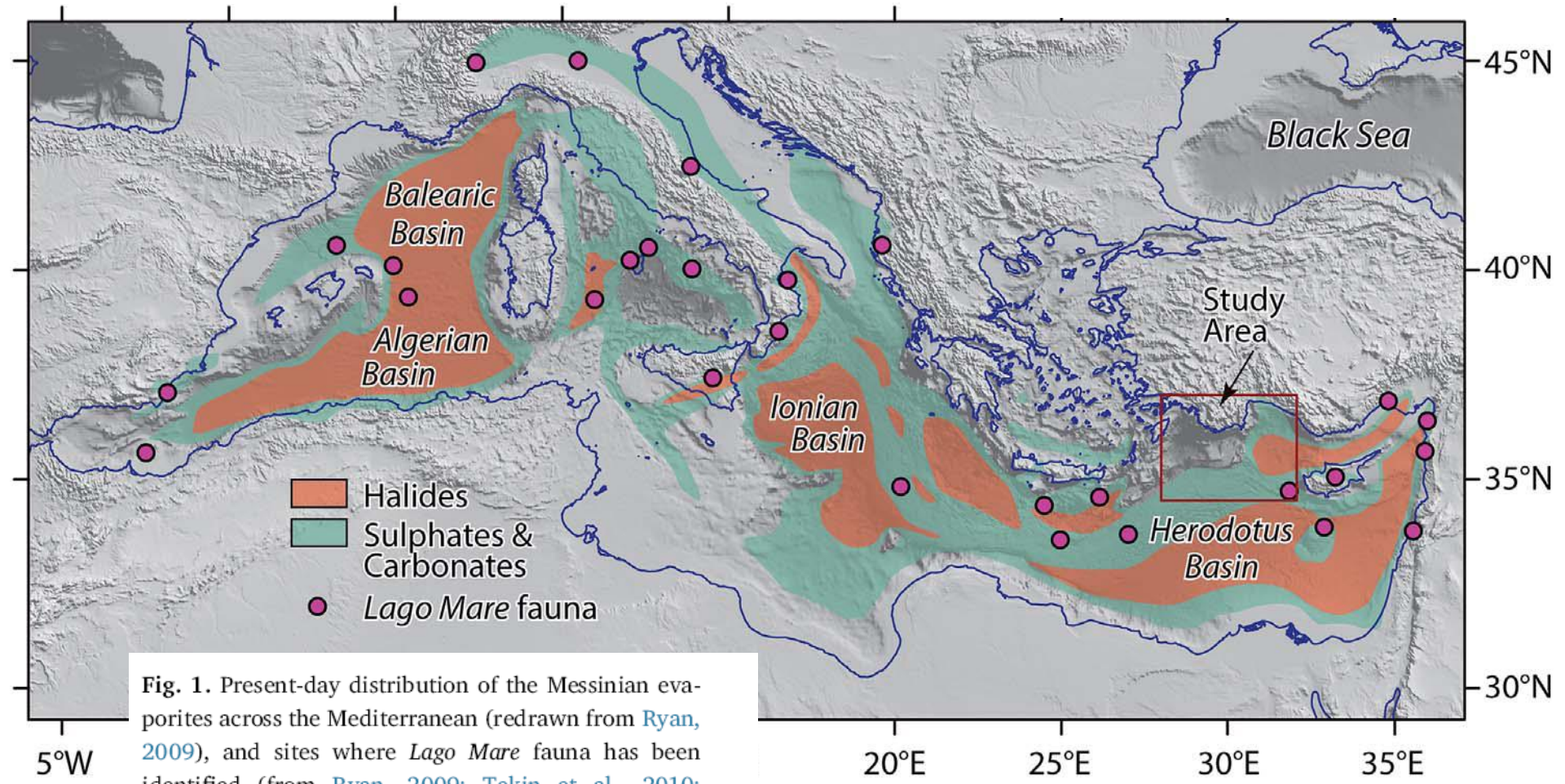

Fig. 1. Present-day distribution of the Messinian evaporites across the Mediterranean (redrawn from Ryan, 2009), and sites where *Lago Mare* fauna has been identified (from Ryan, 2009; Tekin et al., 2010; Bowman, 2011; Cipollari et al., 2013a, 2013b; Manzi et al., 2014). The morphological basemap of the Mediterranean region is compiled using GeoMapApp (Ryan et al., 2009), and shaded using Caris Base Editor (4.1). Coastline is from the International Bathymetric Charts of the Mediterranean (IOC, 1981). (For interpretation of the references to color in this figure legend, the reader is referred to the web version of this article.)

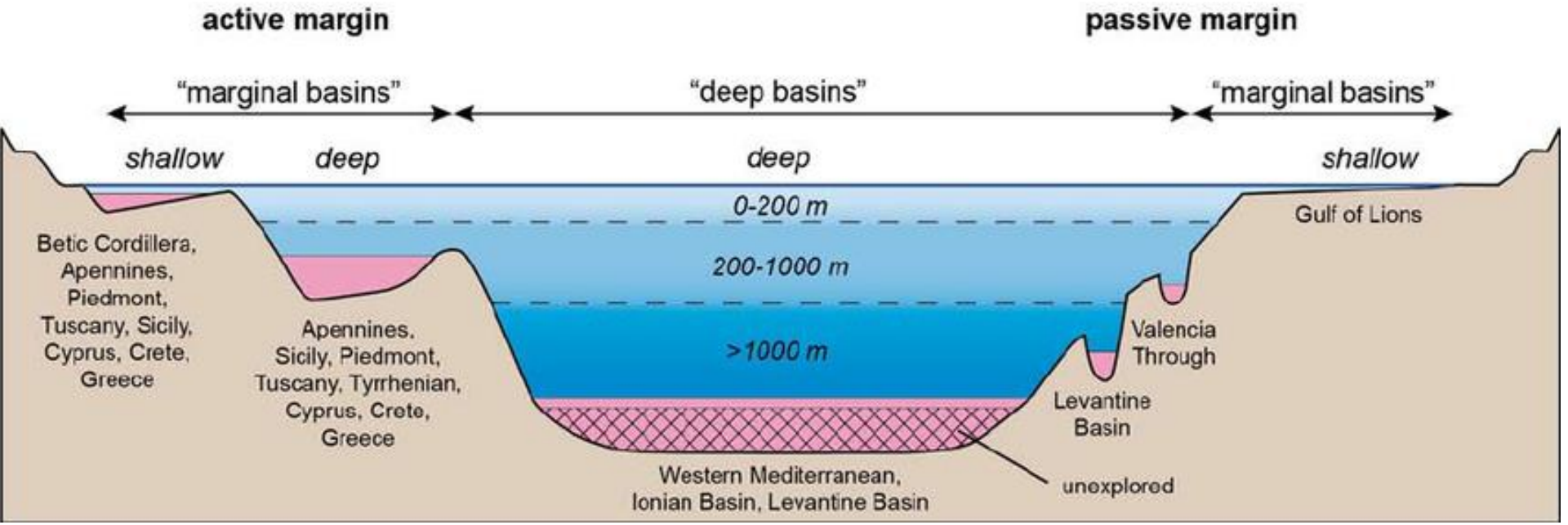

Conceptual scheme showing the distribution of Messinian marginal and deep basins in both tectonically passive and active margins; hatched area highlights the deep basin Messinian record still uncovered by cores.

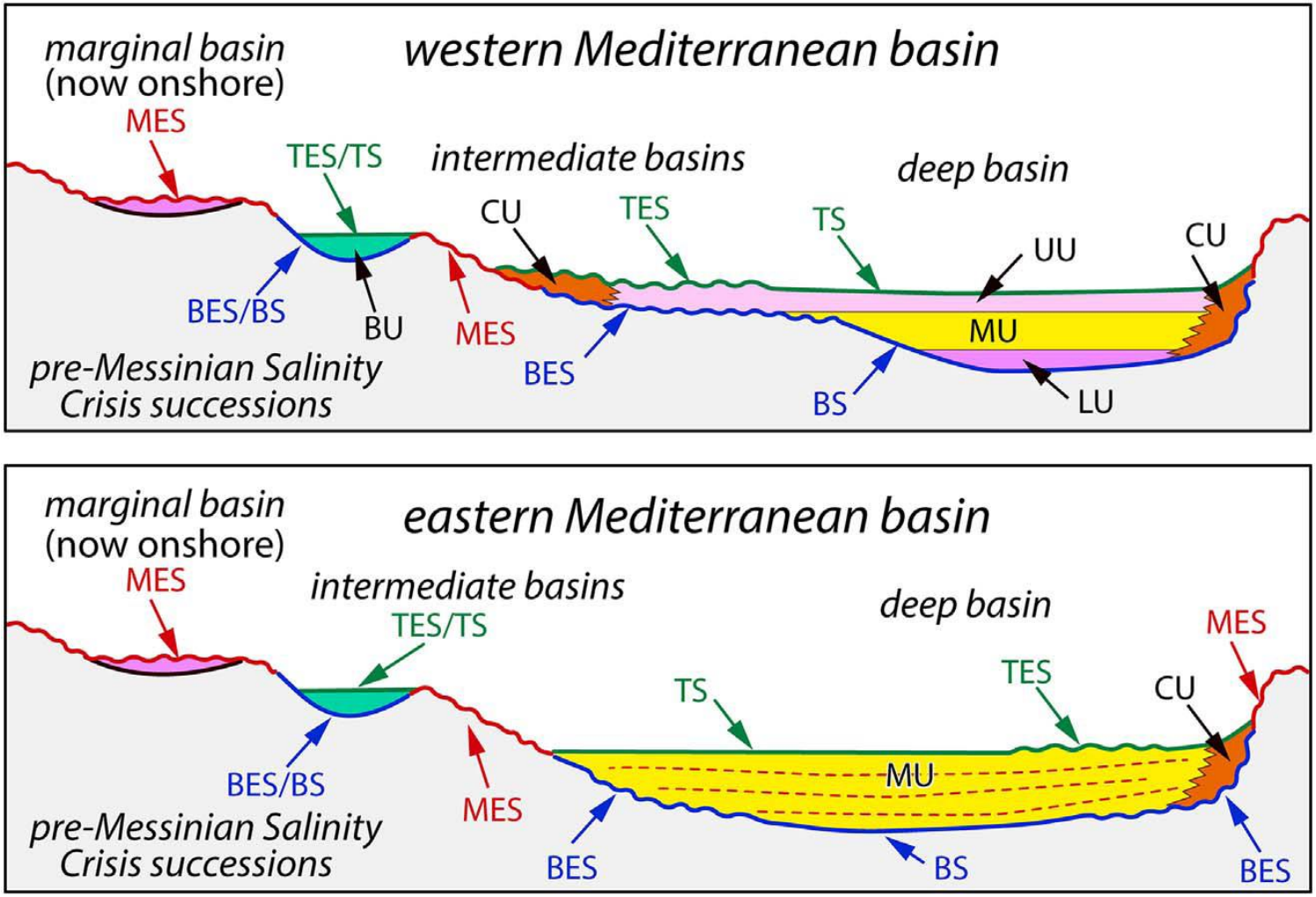

Fig. 3. Schematic drawing across the western and eastern Mediterranean basins, illustrating the Messinian Salinity Crisis seismic markers and units (from Roveri et al., 2014a, 2014b). *Onshore units*: PLG = Primary Lower Gypsum; H = halite; RLG = Resedimented Lower Gypsum; UG = Upper Gypsum; LM = Lago Mare; *Offshore units*: LE = Lower Evaporites; LU = Lower Unit; H = Messinian Salt; MU = Mobile Unit; UE = Upper Evaporites = UU. MES = Messinian erosional surface/marginal erosional surface. BS/BES = Bottom Surface/Bottom Erosional Surface (or N-reflector), TS/TES = Top Surface/Top Erosional Surface (or M-reflector). (For interpretation of the references to color in this figure legend, the reader is referred to the web version of this article.)

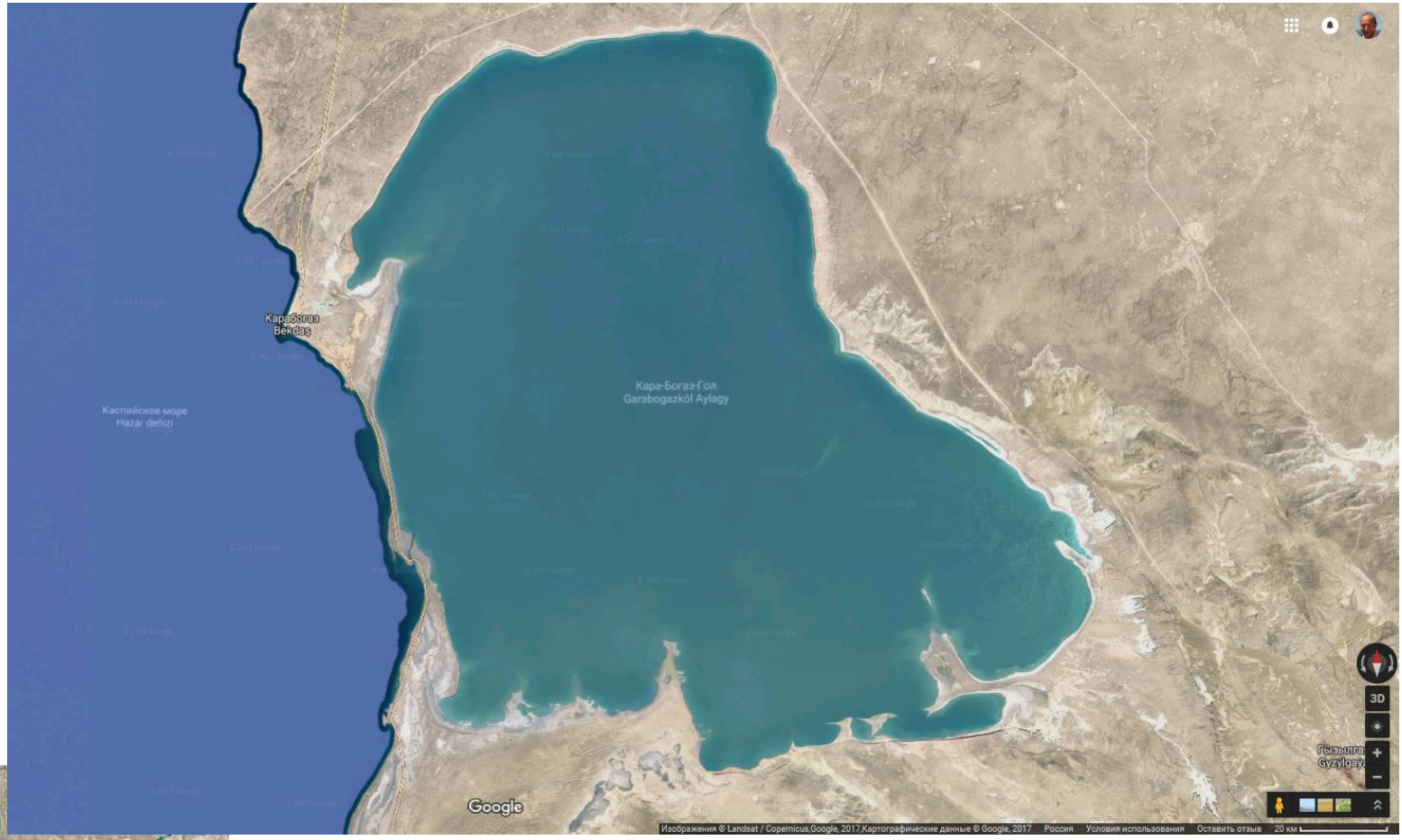

Залив Кара-Богаз-Гол

Мертвое море

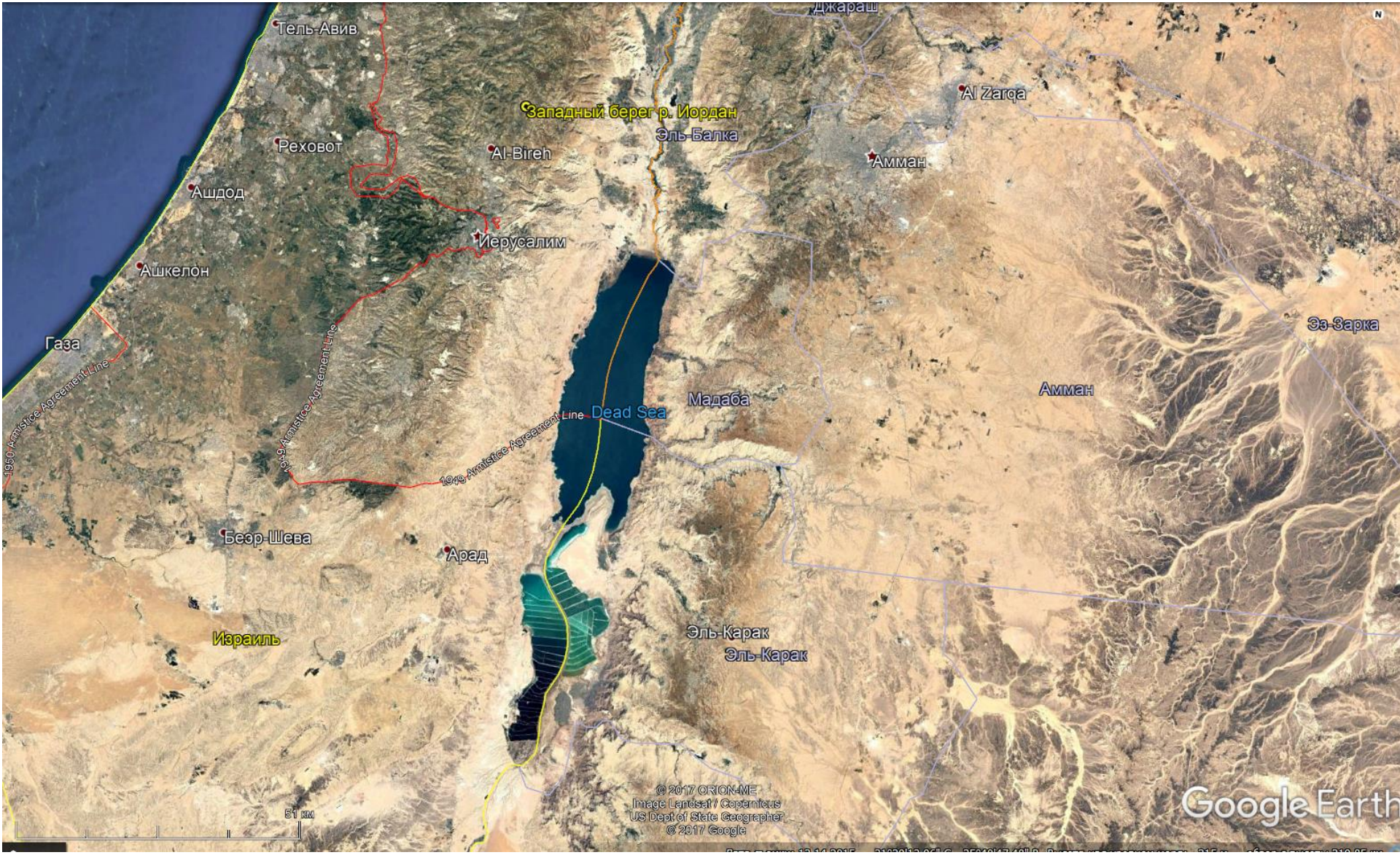

Sebkhat (or Sebkha) El Melah, Tunisia in 2001, mostly dry. Note rectangular industrial evaporite pans, probably for sea-salt production, upper right. Landsat 7 image.

Себха – прибрежные солончаки на суше

Coastal sabkhas – located in the upper intertidal to supratidal zone of arid coastlines and strongly influenced by water of a marine origin.
Continental sabkhas – occurring in inland areas of arid regions and influenced by ground water.
The accepted type locality for a coastal sabkha is at the southern coast of the Persian Gulf, in the United Arab Emirates

Секвентная стратиграфия и эвапориты

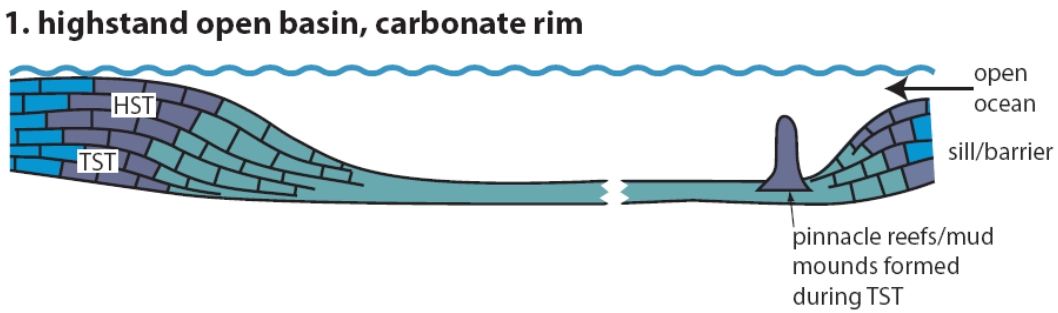

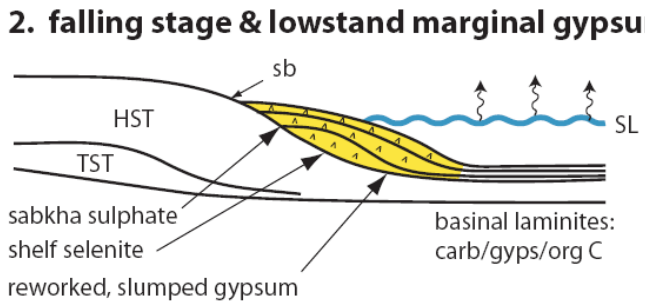

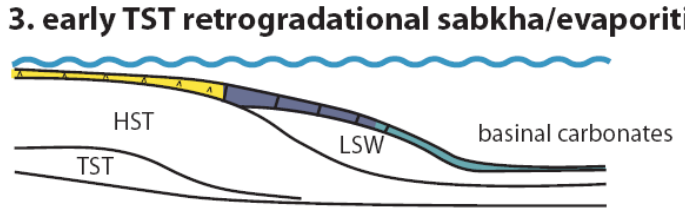

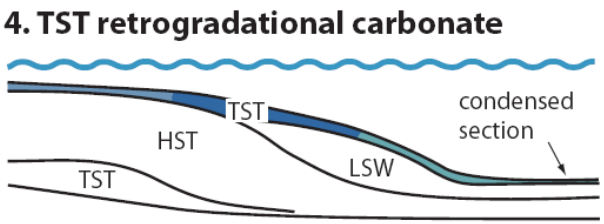

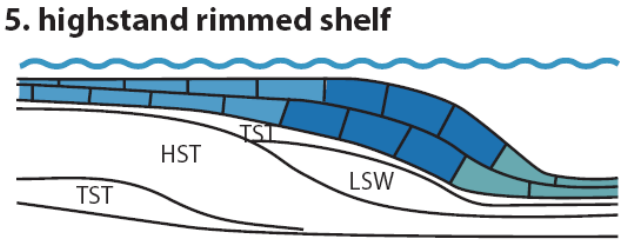

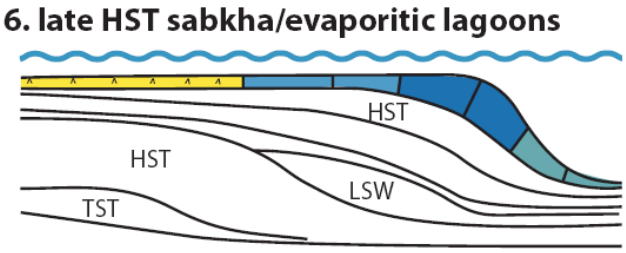

Fig. 44. Carbonate – evaporite intracratonic basins: sequence stratigraphic model for a basin with incomplete drawdown, leading to basin-margin gypsum wedges (from Tucker 1991).

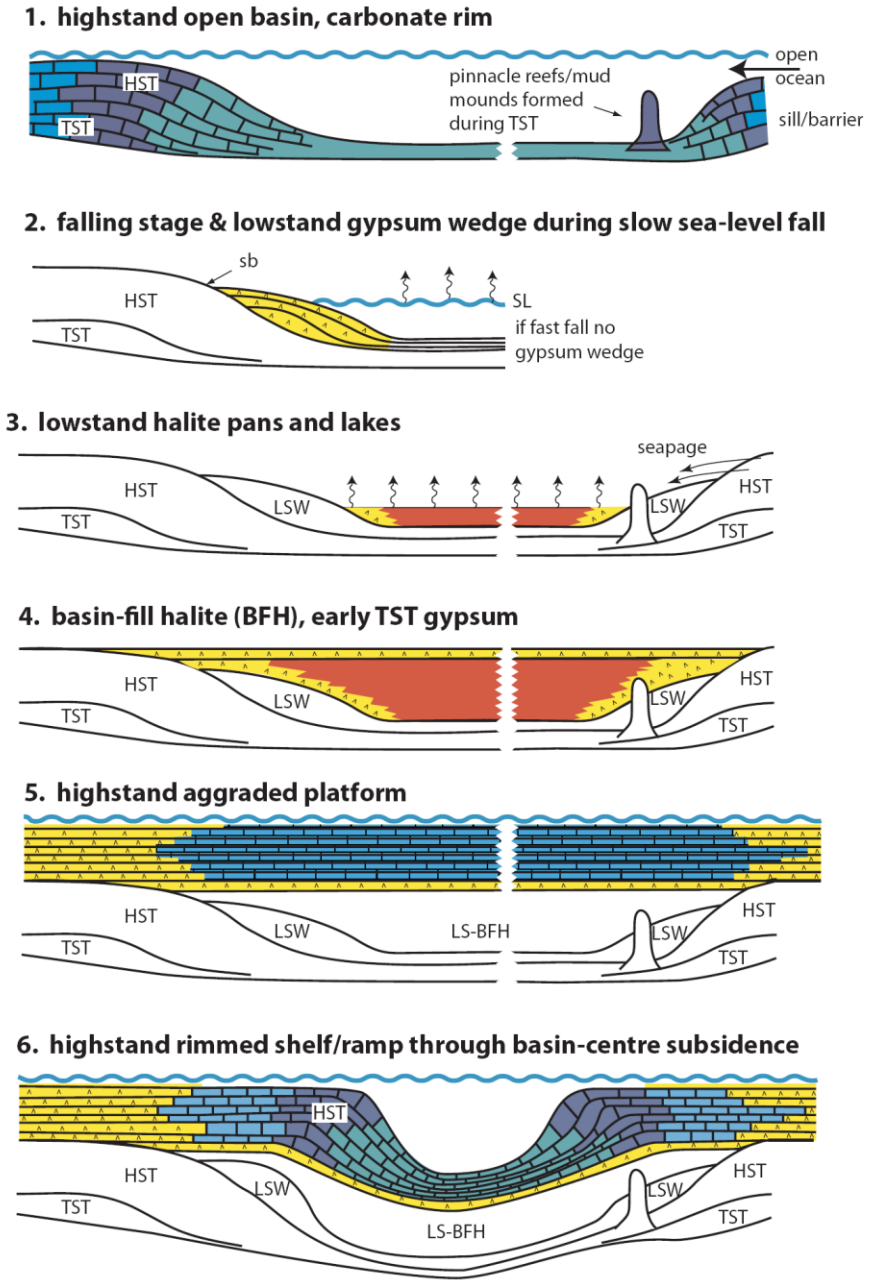

Fig. 45. Carbonate – evaporite intracratonic basins: sequence stratigraphic model for a basin with complete drawdown leading to basin-fill halite (from Tucker 1991).

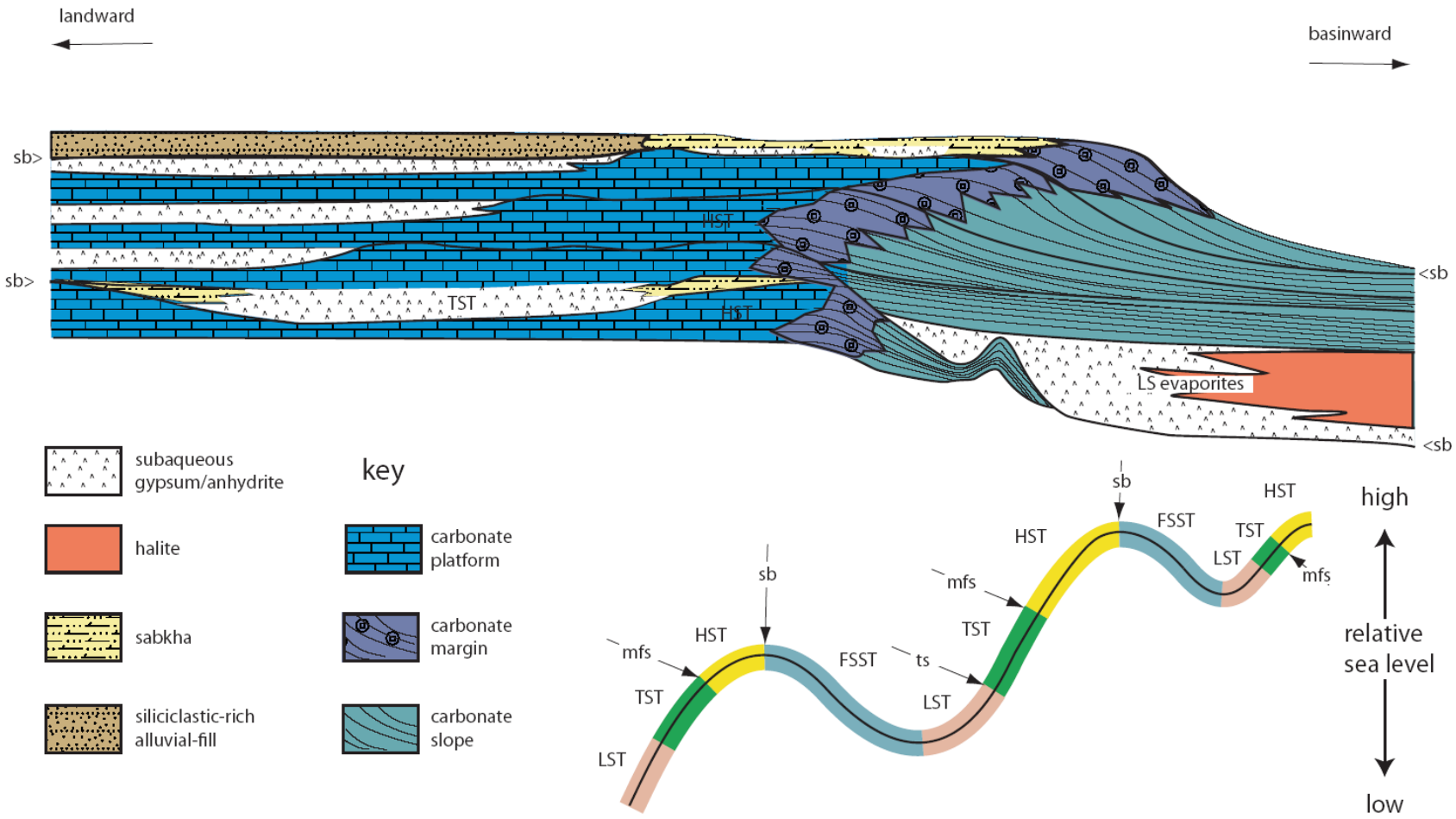

Fig. 46. Summary diagram of evaporite-carbonate lithofacies distribution in a sequence stratigraphic framework. Evaporites can occur within all systems tracts but are preferentially developed within the basin during falling-stage and lowstand systems tracts, and on the platform itself during early transgressive and late highstand to falling-stage systems tracts (after Sarg 2001). The designation of sequence boundary in this diagram conforms with Posamentier and Allen (1999).

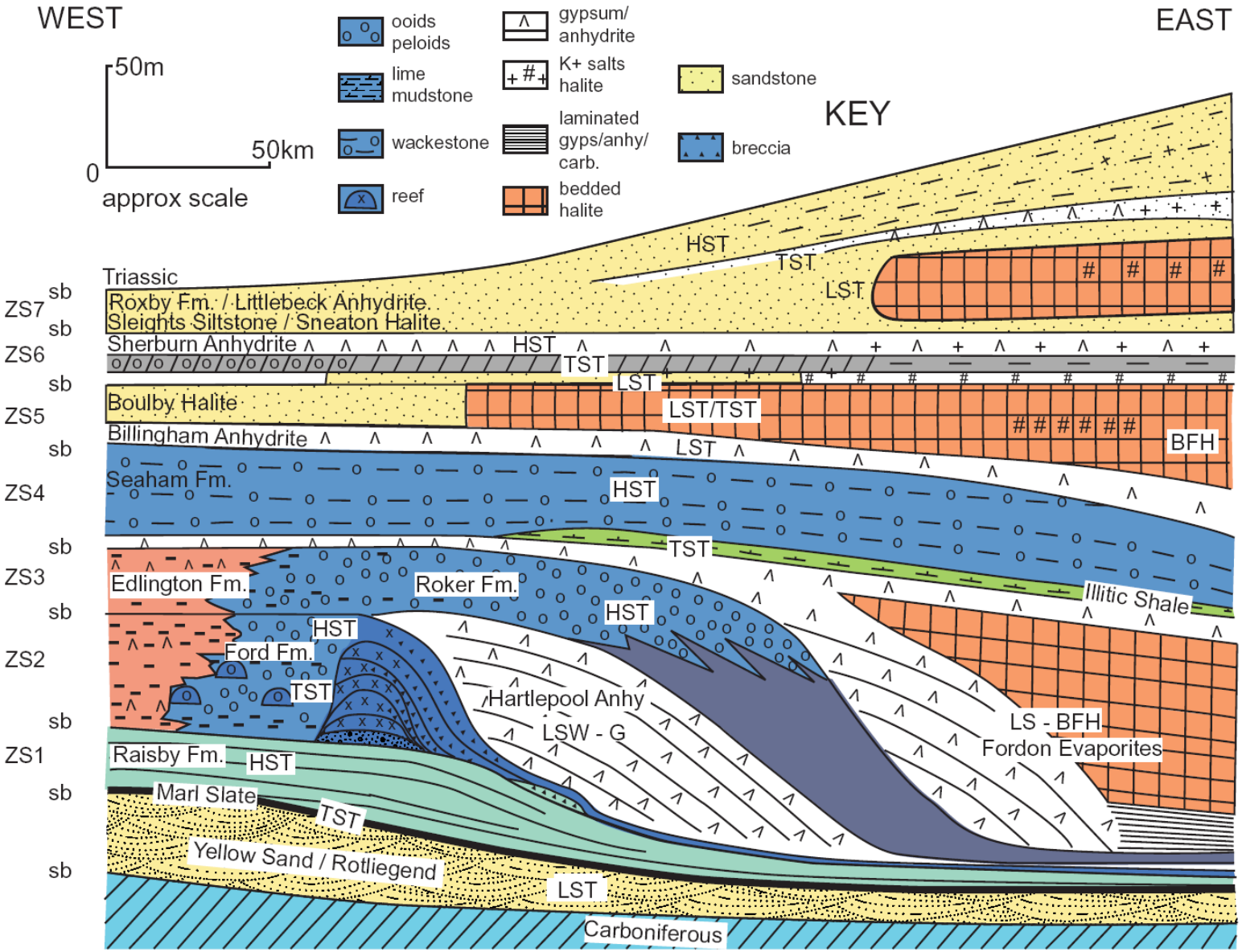

Fig. 47. Lithostratigraphy of the Upper Permian strata of NE England and North Sea, showing four major carbonate platforms (Raisby, Ford, Roker and Seaham formations), and two major evaporite successions (basin-margin Hartlepool Anhydrite and basin-fill Fordon evaporites) (from Tucker 1991).

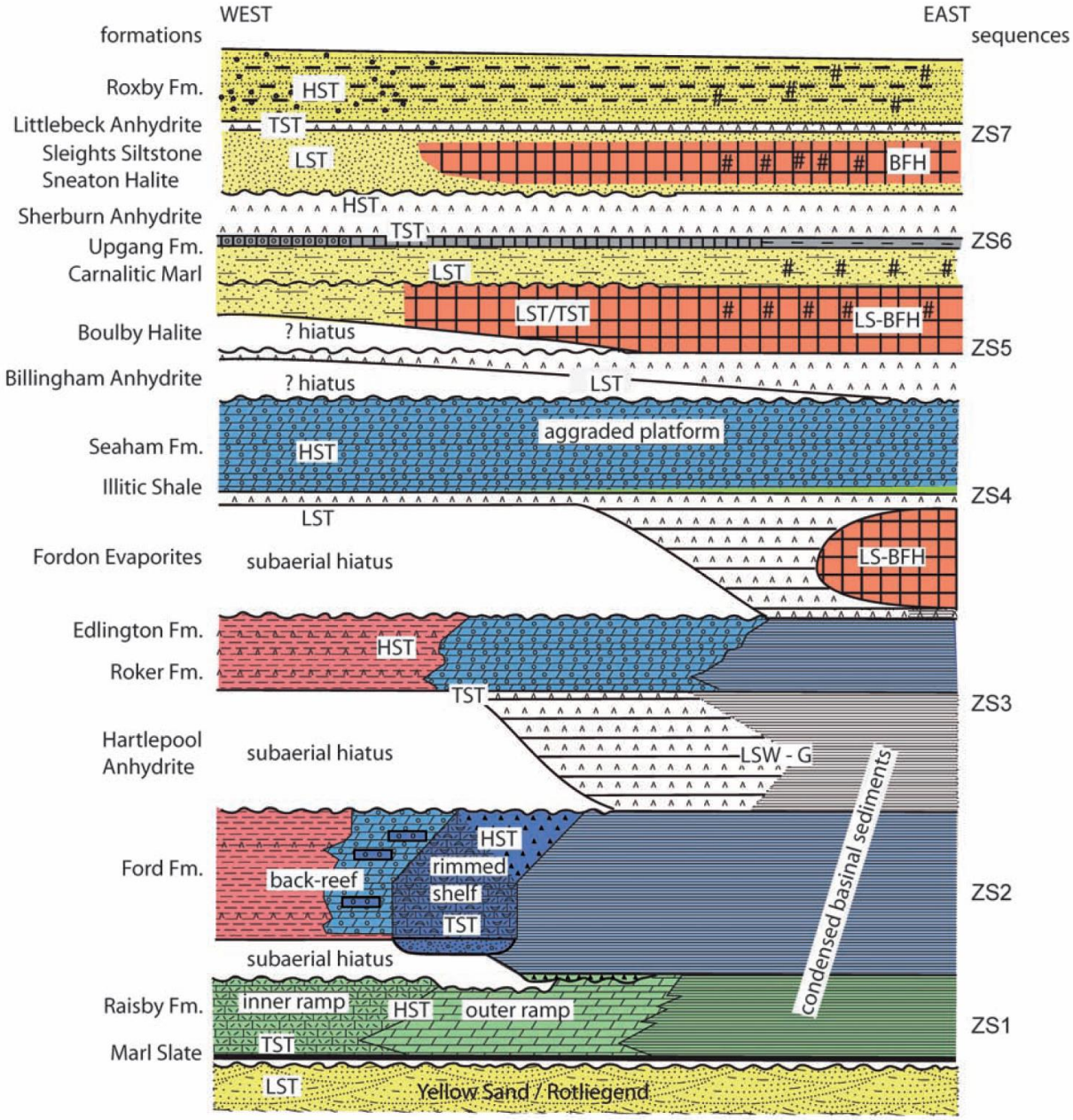

Fig. 48. Chronostratigraphy of the Permian Strata of NE England and the adjoining North Sea (from Tucker 1991).

Характерные морфологические типы соляных диапиров (Twiss, Moores, 1992). Диапиры образуются из слоя солей и затем всплывают в виде соляных подушек, соляных штоков или соляных стен. Соли могут достигать земной поверхности и образовывать соляные глетчеры.

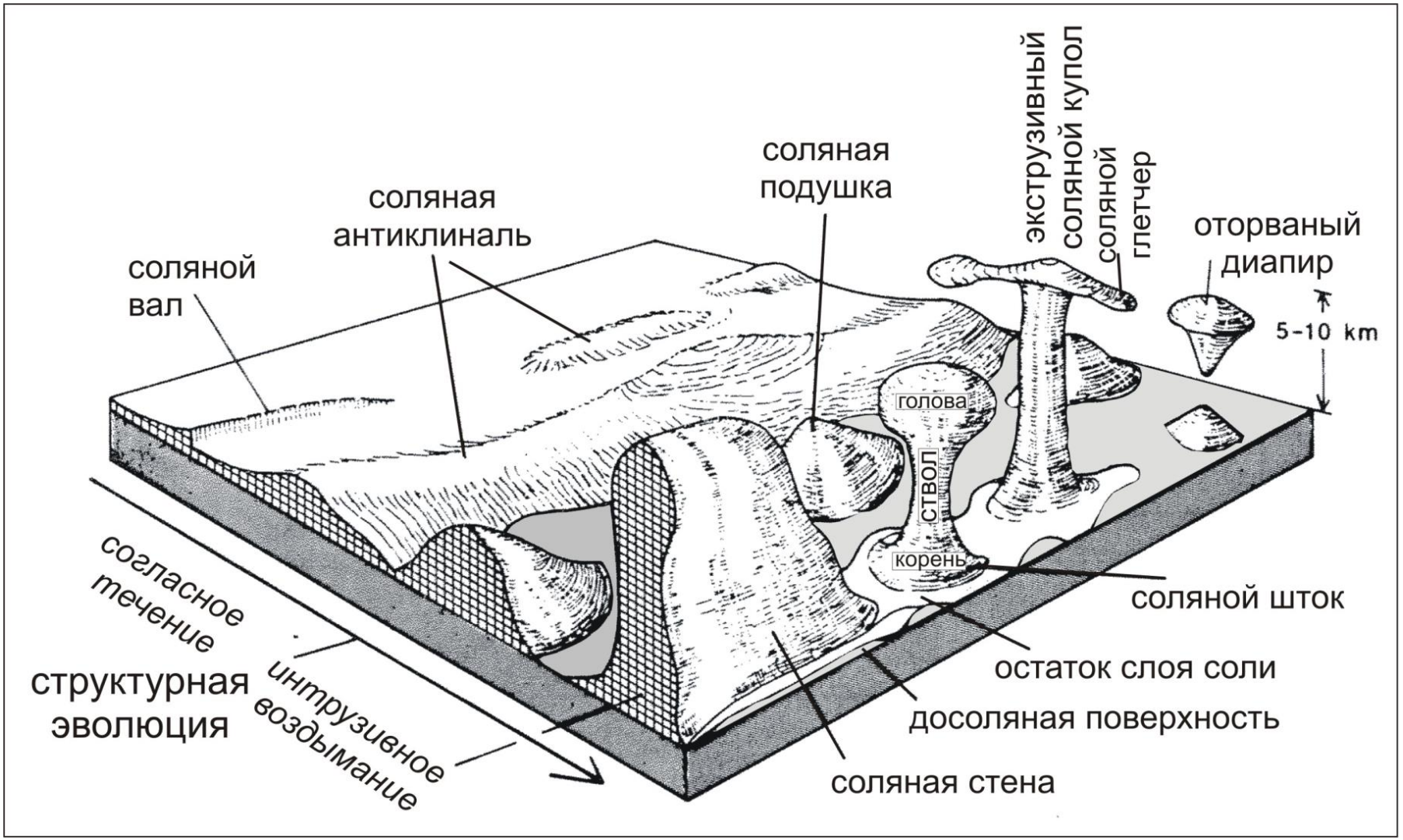

Схематическая модель развития диапиров.

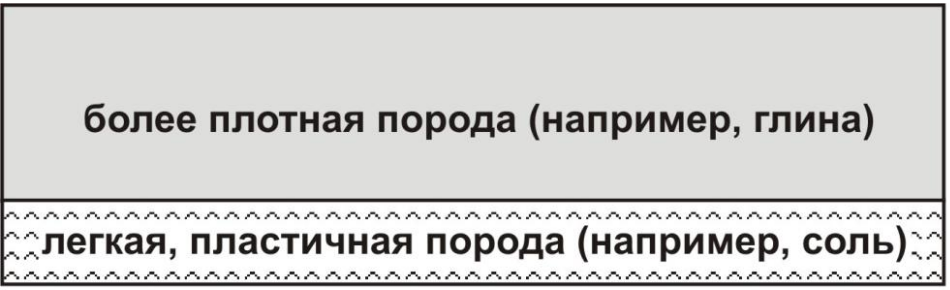

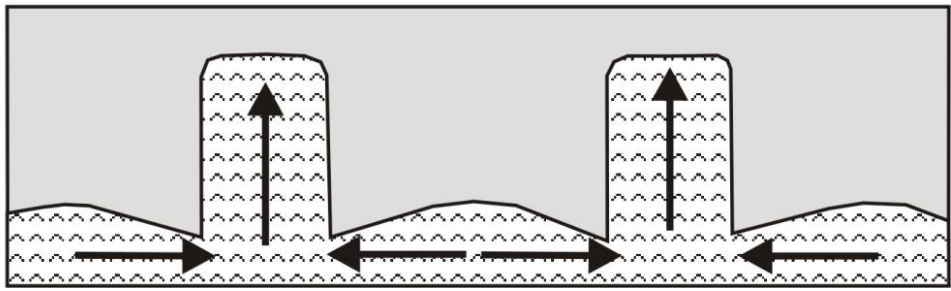

Модели строения соляной интрузии и соляной подушки.

А. Соляная интрузия

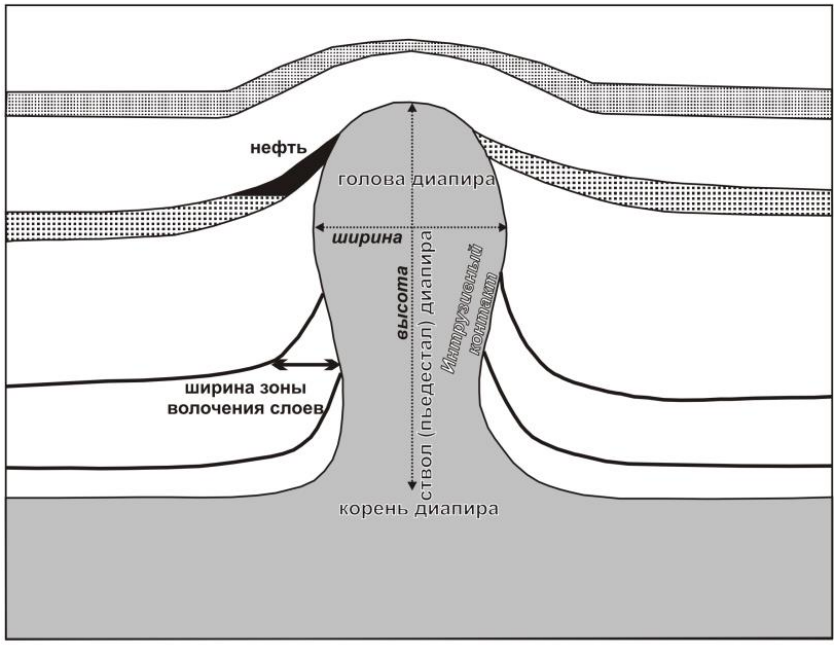

Б. Соляная подушка

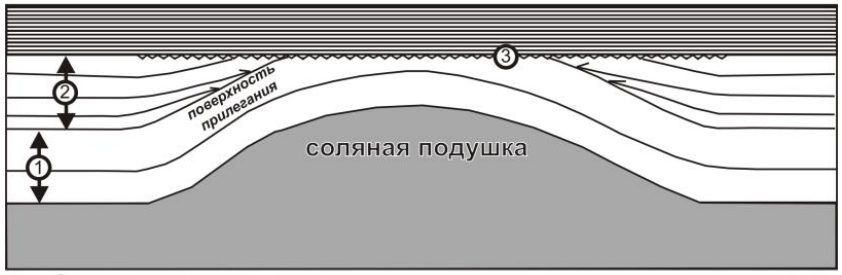

① осадки додиапировой покрышки солей
② осадки формировавшиеся синхронно с ростом диапира
③ несогласие маркирующие окончание роста диапира

Интерпретация сейсмического профиля для района соляного диапира в Северном море (Davison et al., 2000a). Над соляным диапиром видны системы сбросов. Внутримиоценовое несогласие соответствует фазе подъема диапира и конседиментационных деформаций.

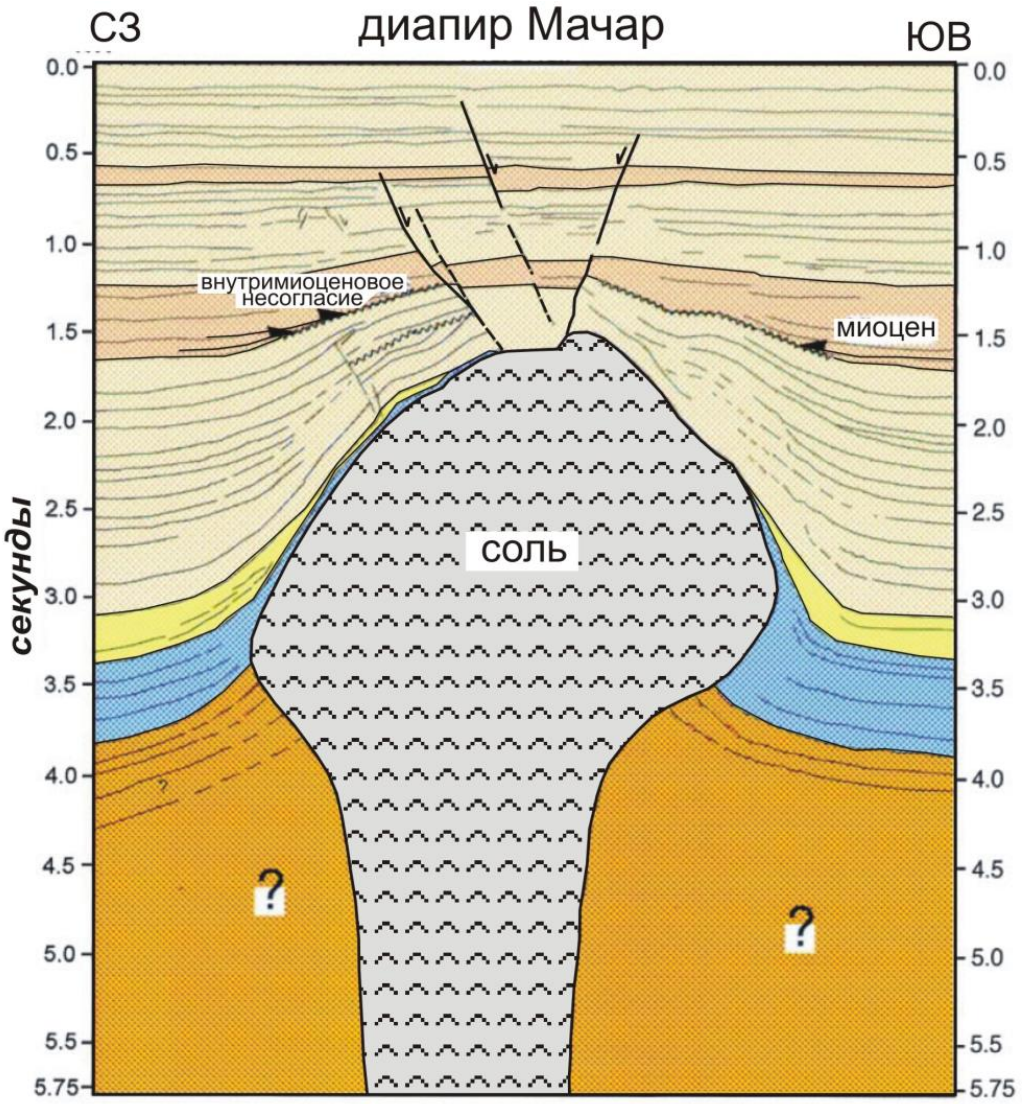

Пример строения верхней части соляного диапира и вмещающих пород в районе Северного моря (Davison et al., 2000b).

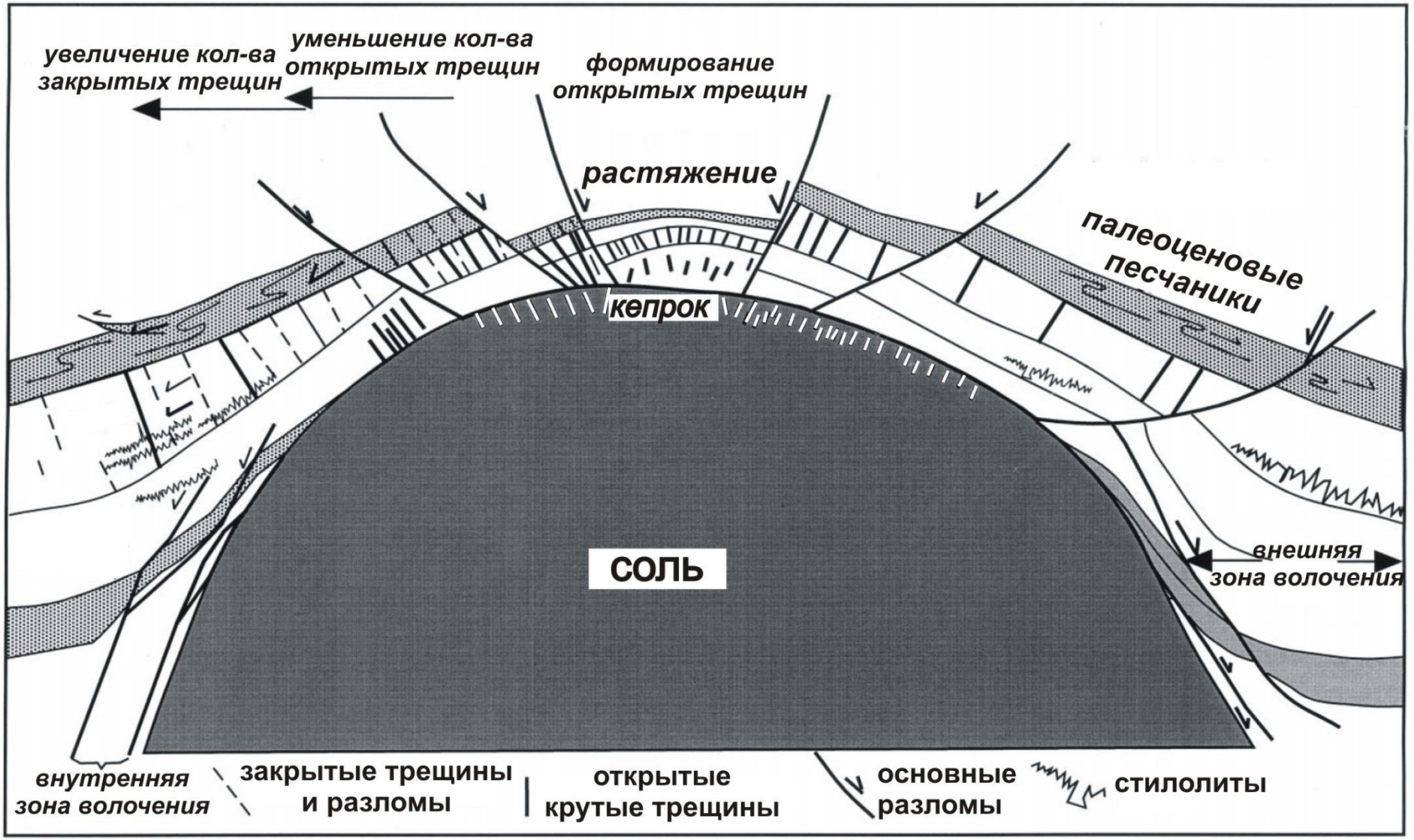

Примеры структурных карт для районов соляных диапиров в Северном море (Davison et al., 2000a). Изолинии проведены по горизонту в кровле палеоцена

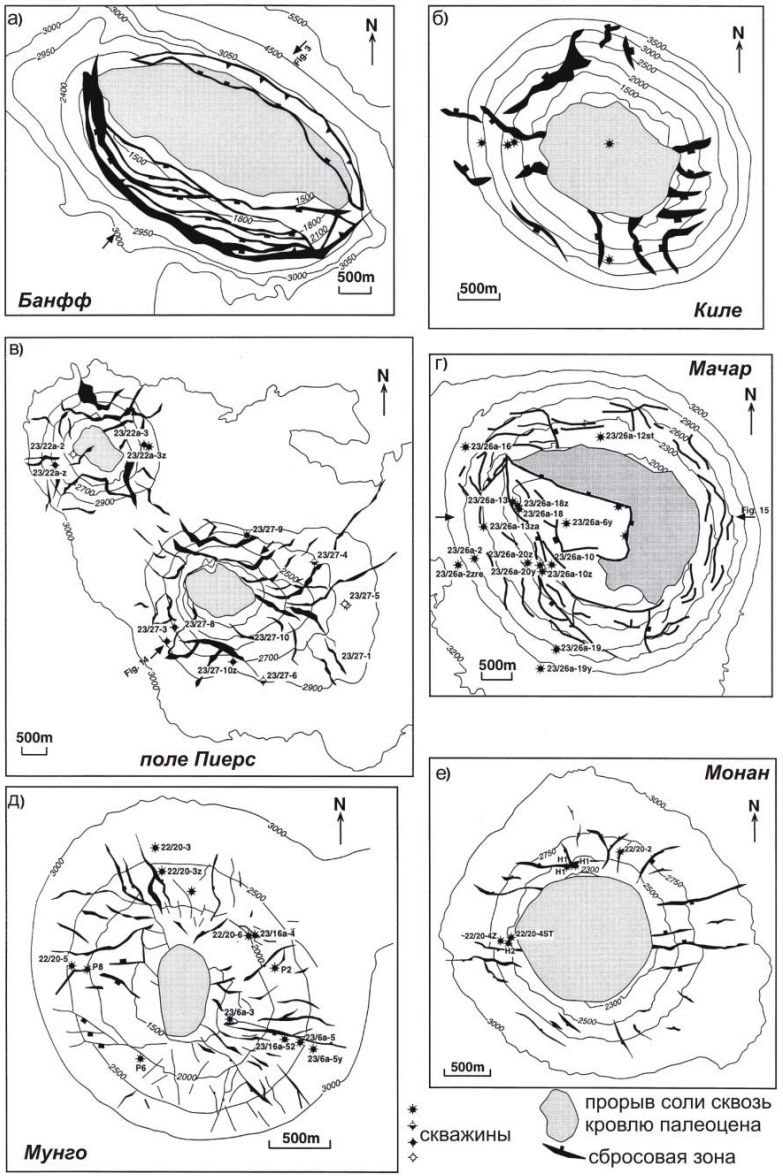

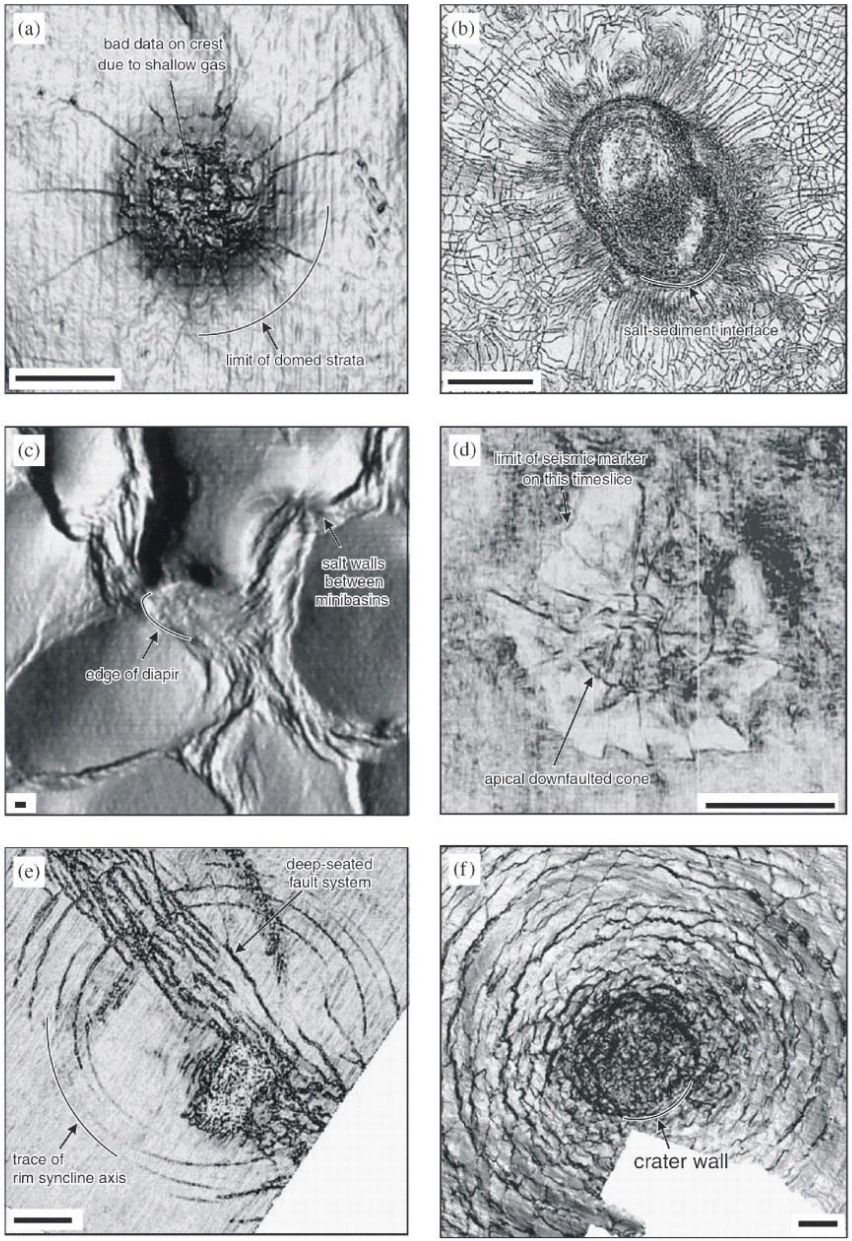

Radial and concentric faults mapped on various 3D seismic data attributes. All scale bars 1 km. (a) Radial faults in domed sediments above salt diapir, North Sea (dip magnitude of mapped surface shaded). (b) Radial faults adjacent to diapir in layer that shows far field polygonal faulting, example from a South Atlantic salt basin (coherence slice). (c) Sediment minibasins separated by salt walls, and extensional faults. Diapirs at wall intersections. Seabed shaded bathymetry, Gulf of Mexico, after Diegel et al. (1995). (d) Radial faults and crestal conic graben, North Sea, coherence slice. (e) Concentric faults around rim syncline associated with mud withdrawal, Caspian Sea (horizon parallel coherence). (f) Concentric faults around cylindrical void (crater), North Sea—analog for collapsed salt diapir conduit.

Интерпретация сейсмического профиля для соляного надвига в северной части Мексиканского залива (Hudec, Jackson, 2006). В подошве надвиговой пластины гравитационного происхождения имеются соли. По их подошве проходит основная надвиговая поверхность. Наличие рампов и флэтов в основании толщи слоев свидетельствует в пользу надвигового характера этой границы.

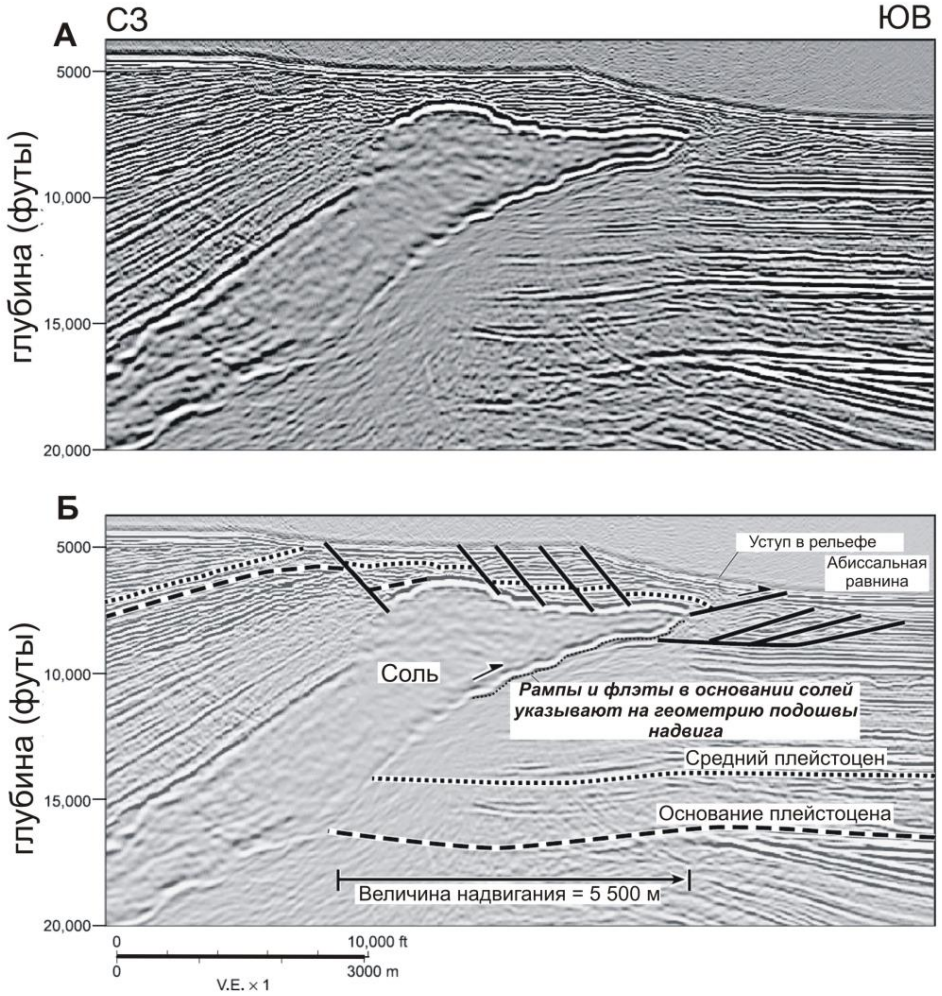

Сейсмический профиль и его интерпретация для района солянокупольной тектоники в Северном море в районе грабена Центральный (Davison et al., 2000a). ВК – основание мела.

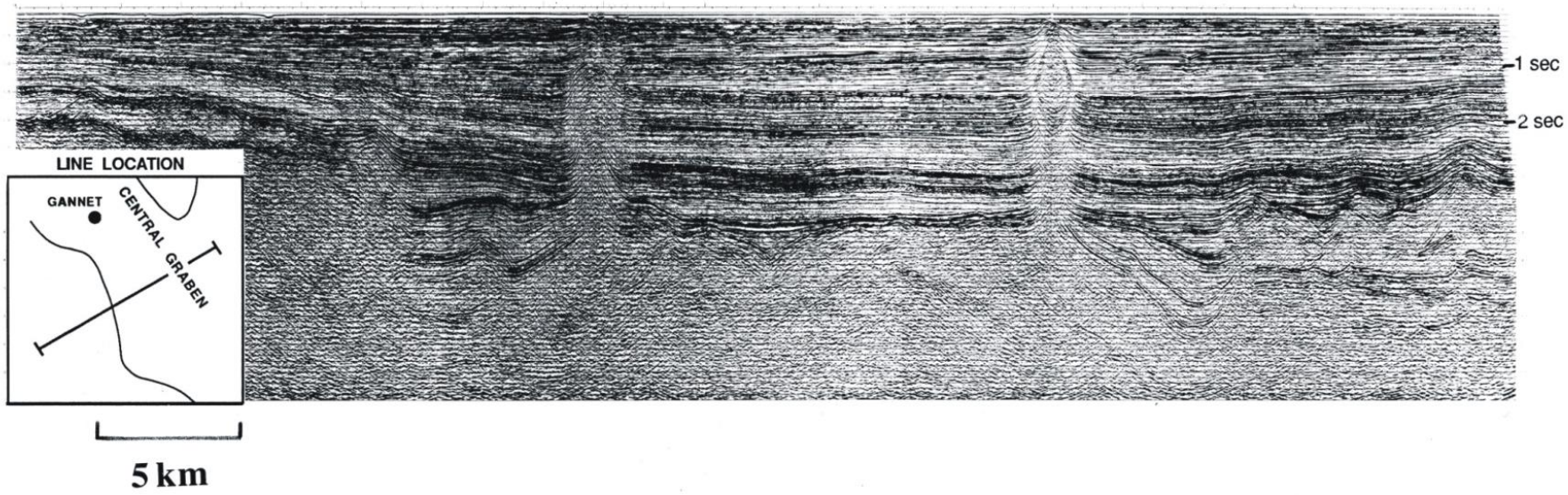

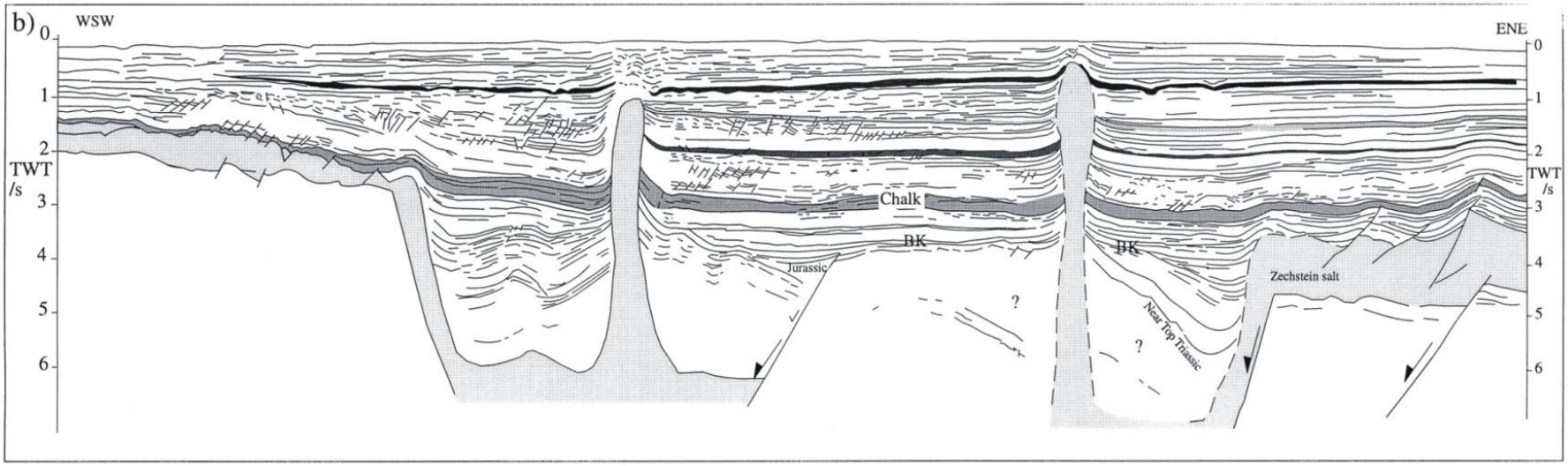

Сейсмический профиль и его интерпретация для района солянокупольной тектоники в Северном море (Stewart et al., 1996).

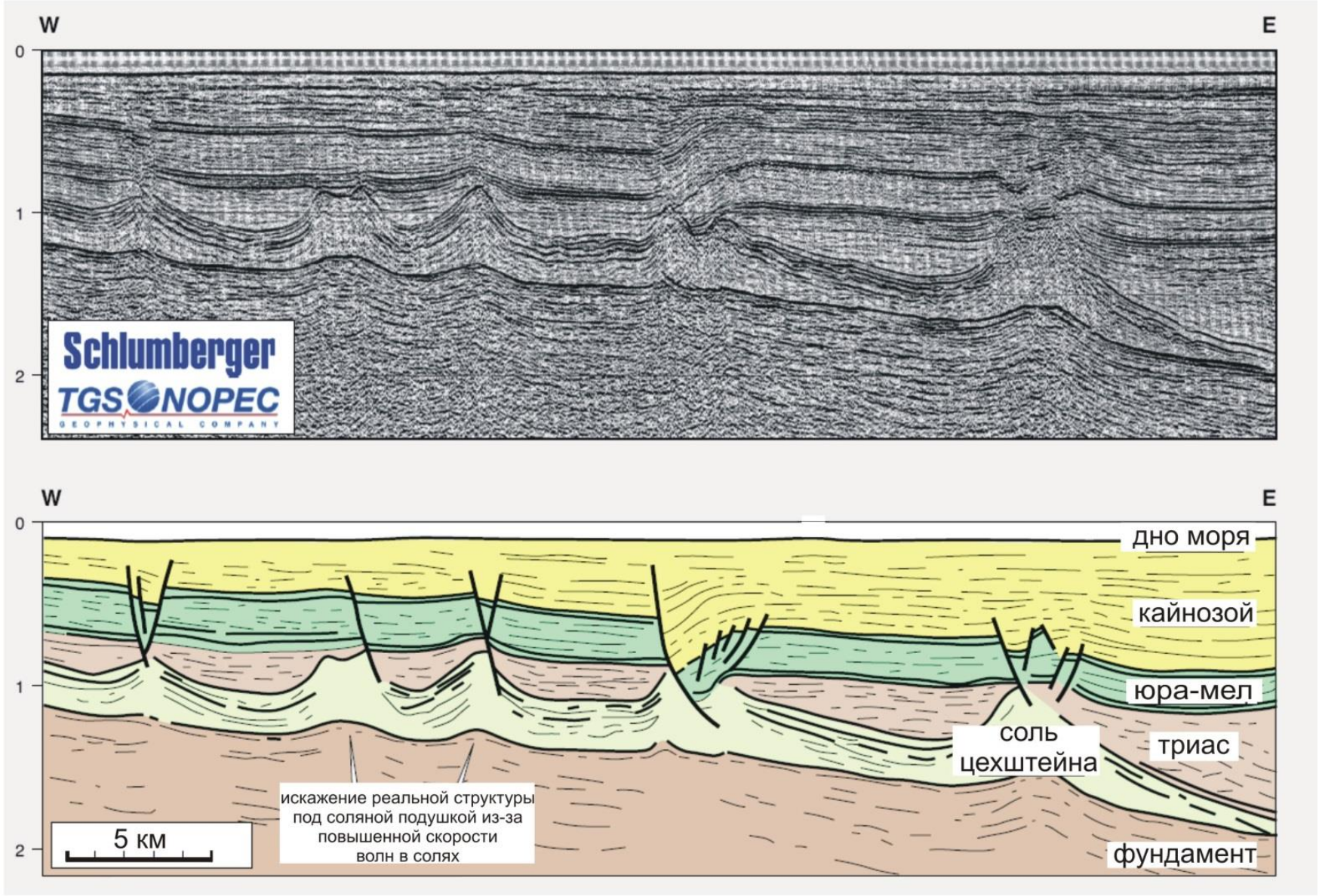

Примеры интерпретации сейсмических профилей для района соляного диапиризма на пассивной континентальной окраине Африке в районе Анголы (Cramez, Jackson, 2000). А, Б, В – разные случаи и нарастание глубины дна континентального склона. На разрезе "Б" отчетливо видна связь соляного диапиризма и развития надвигов

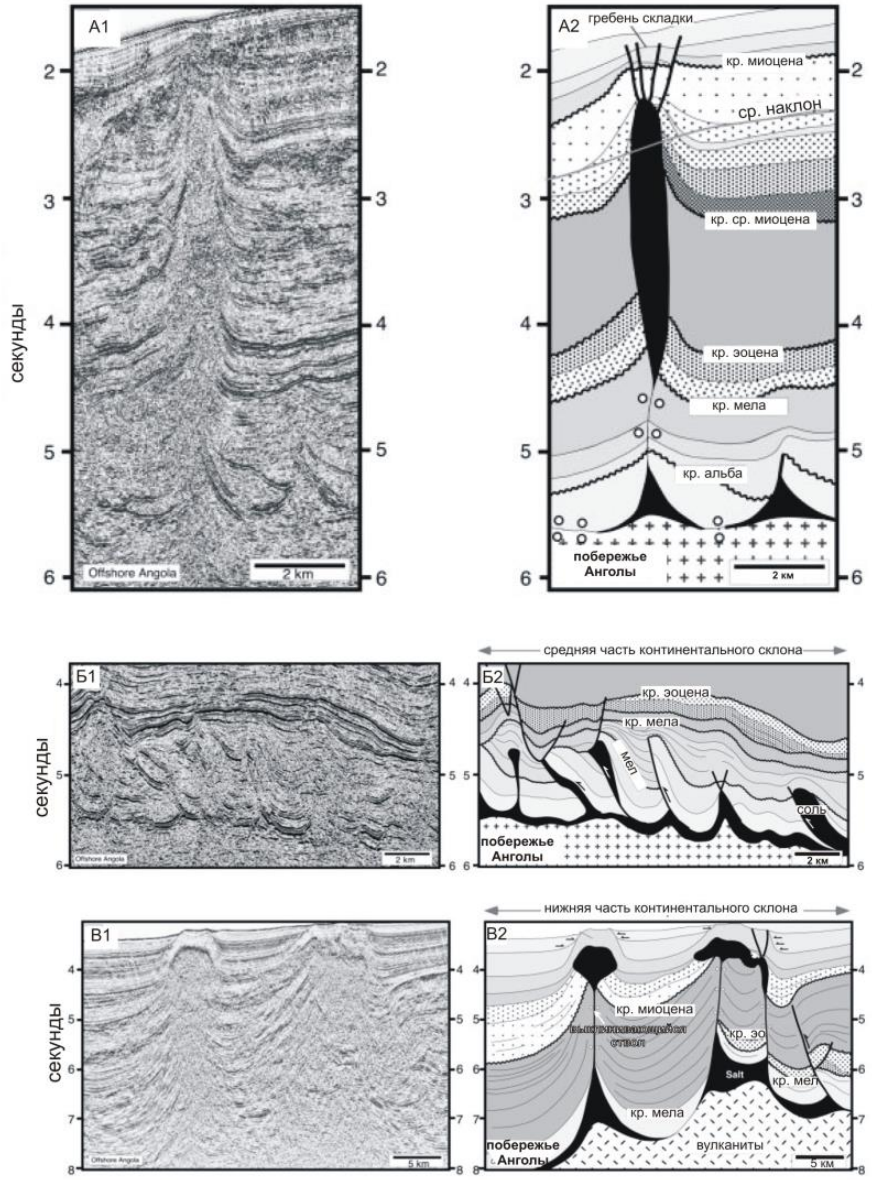

Интерпретация сейсмического профиля и данных бурения для Днепровского бассейна, разрез по линии Гупаливка-Гуты (район Полтавы) (Стовба…). Отчетливо выделяются крупные соляные диапиры разной геометрии. Соль позднедевонская.

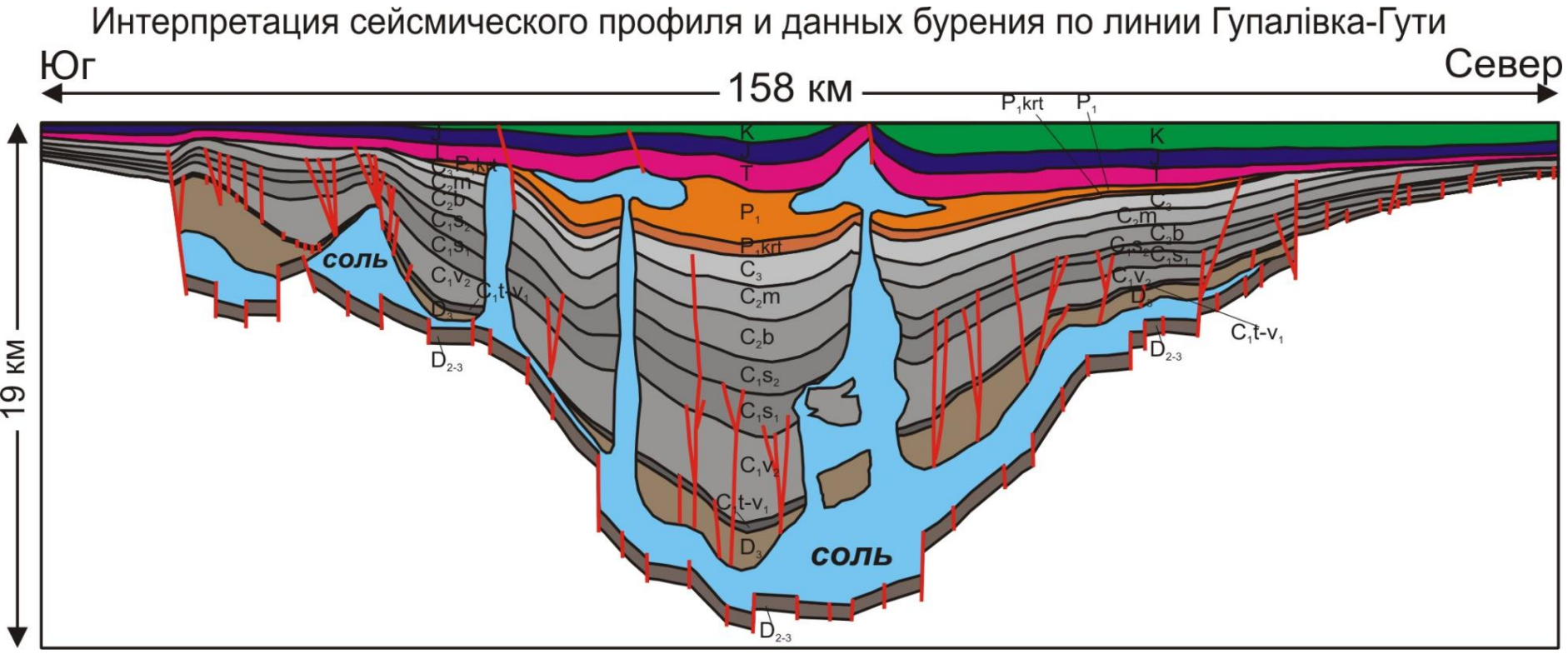

Structure map of kungurian salt

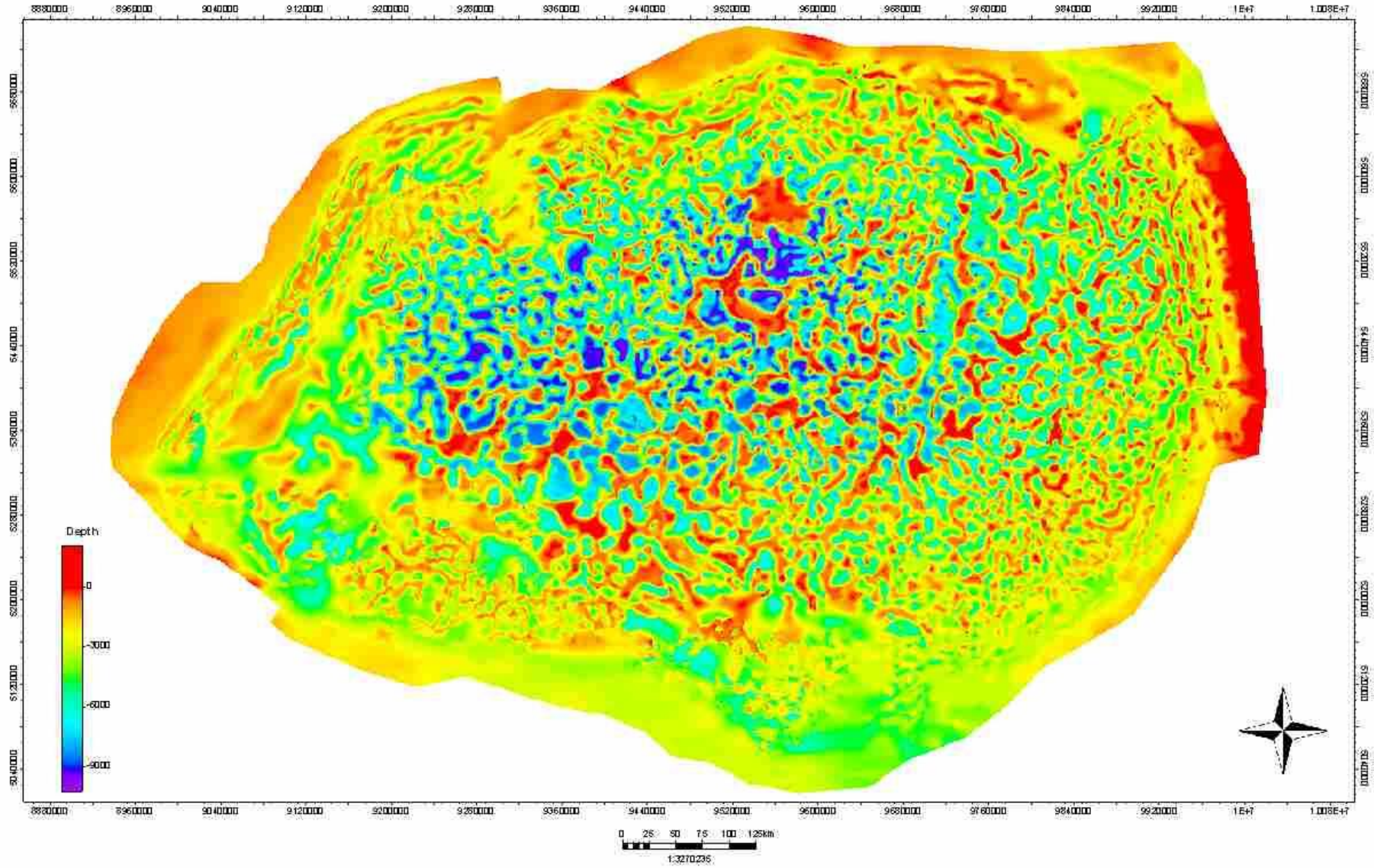

А.В. Ершов, М.А. Исаков и др., МГУ, 2010

Smooth thickness map of kungurian salt

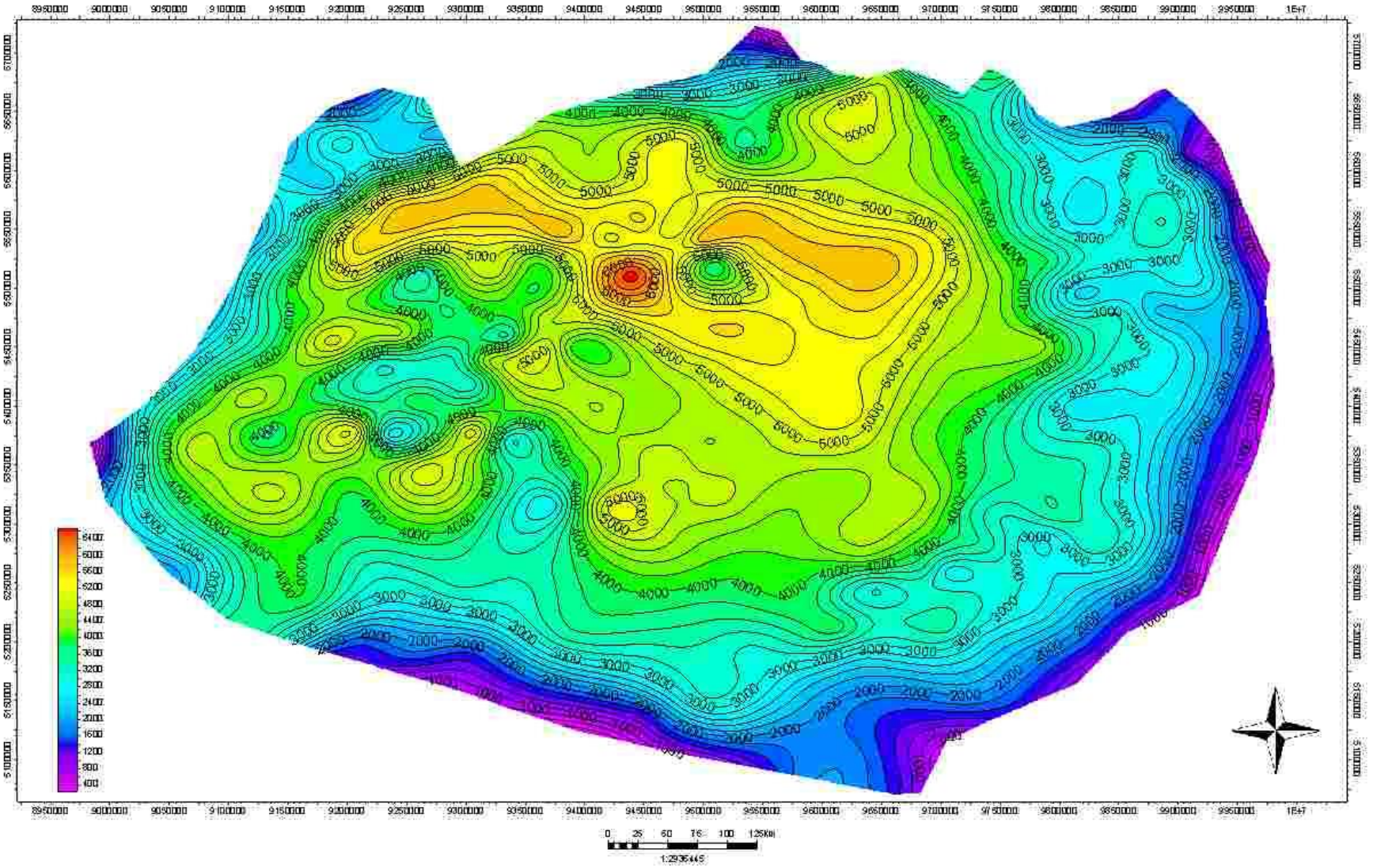

А.В. Ершов, М.А. Исаков и др., МГУ, 2010

Прикаспий

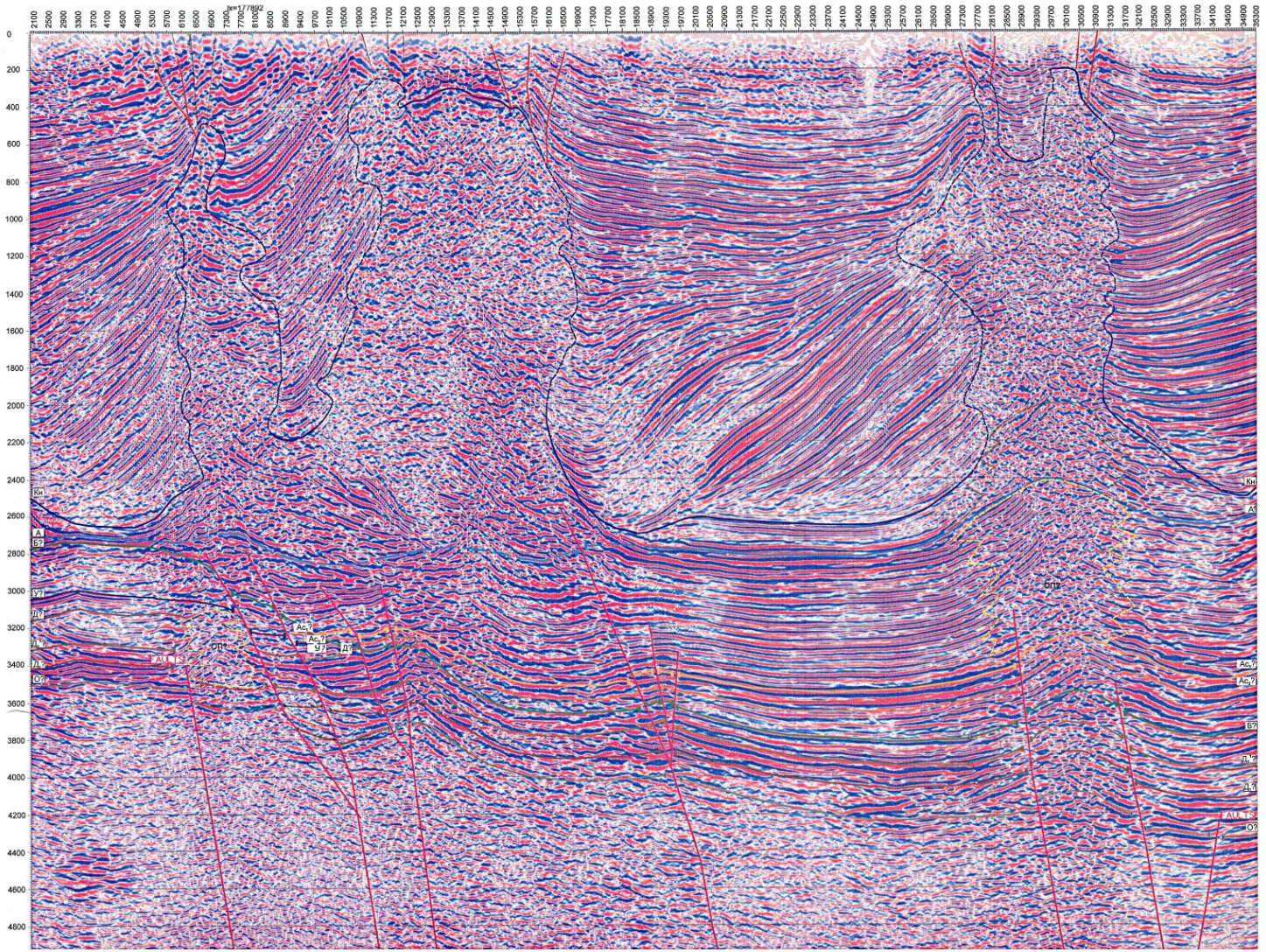

Прикаспий

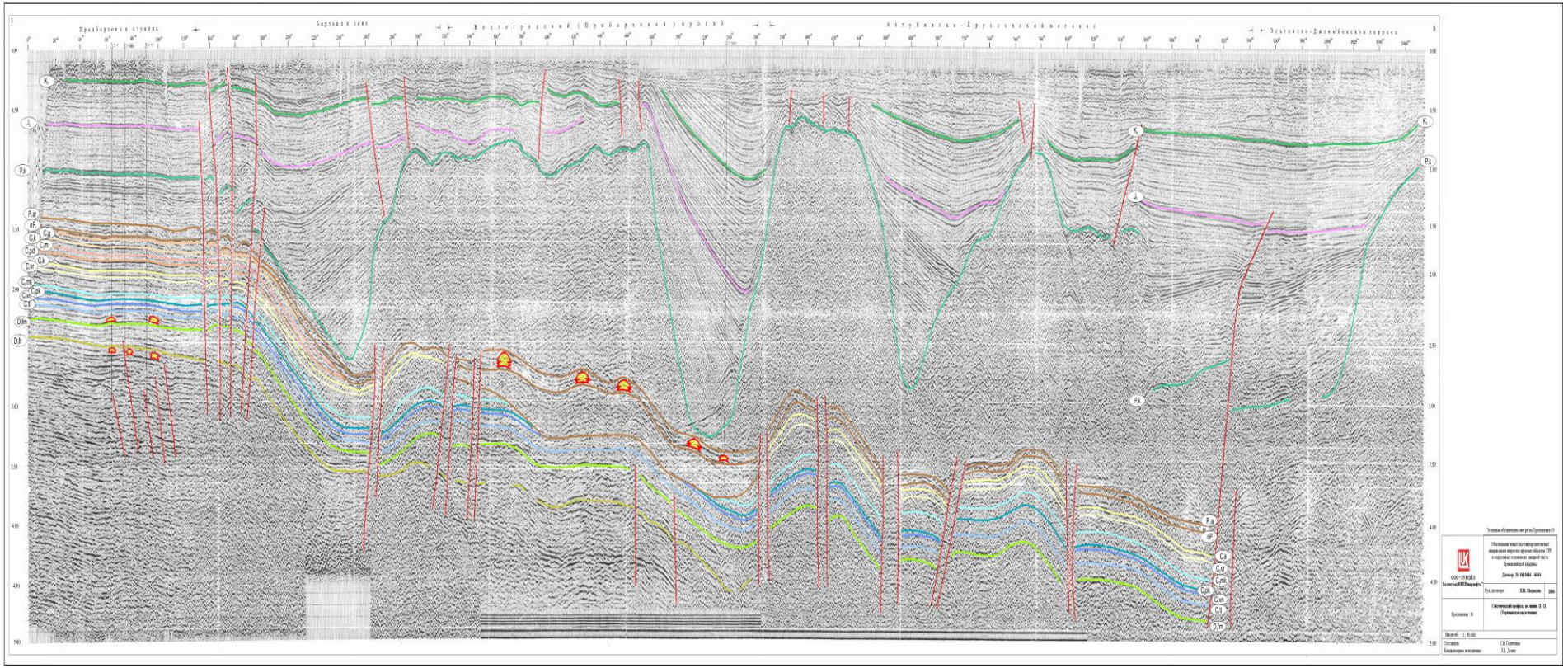

Прикаспий

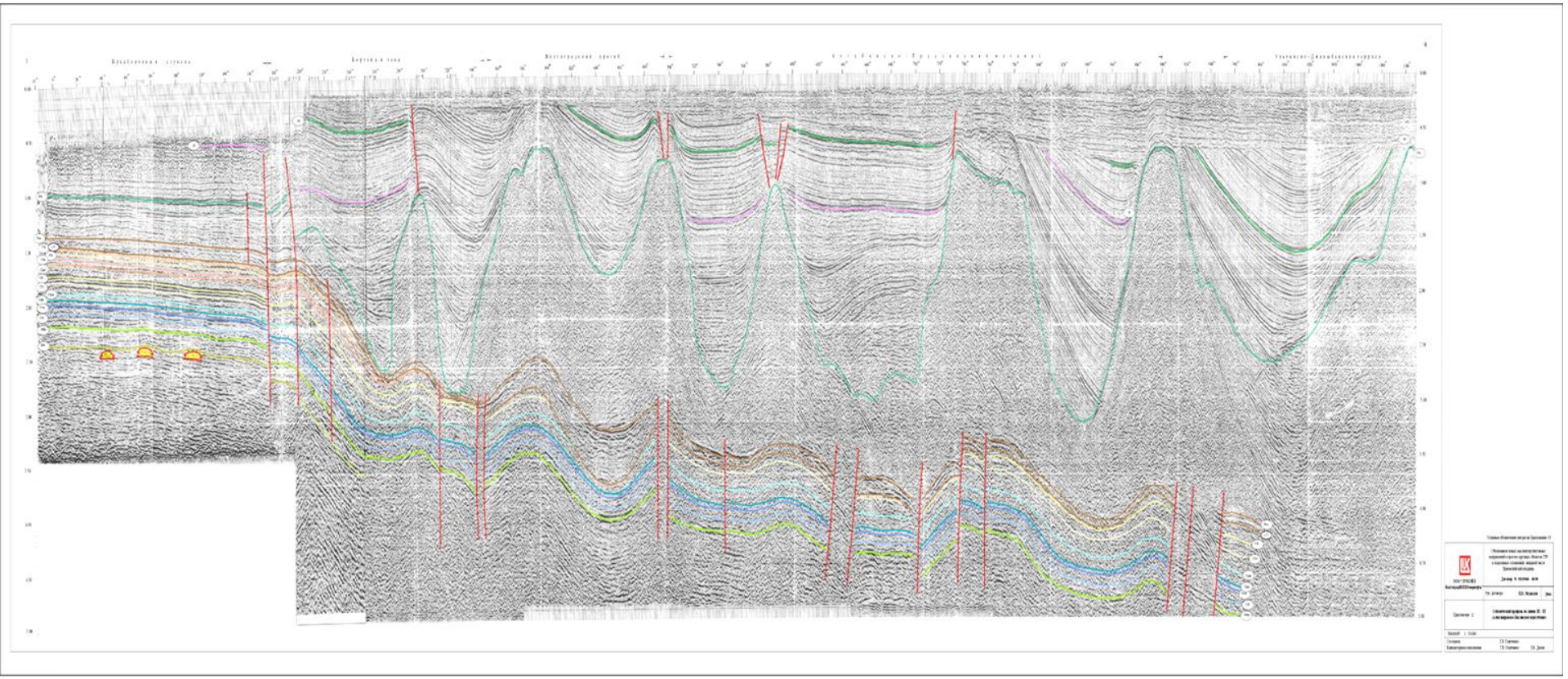

Северный Каспий

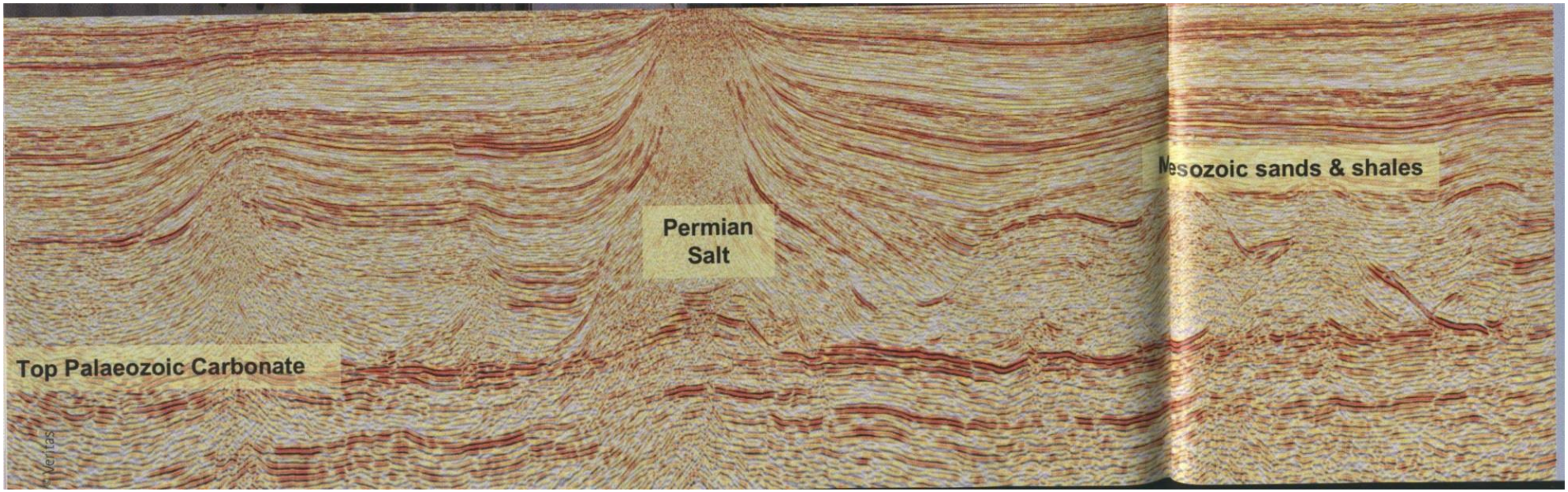

Вилюйский бассейн, Кемпендяйский палеорифт

Кемпендяйский купол

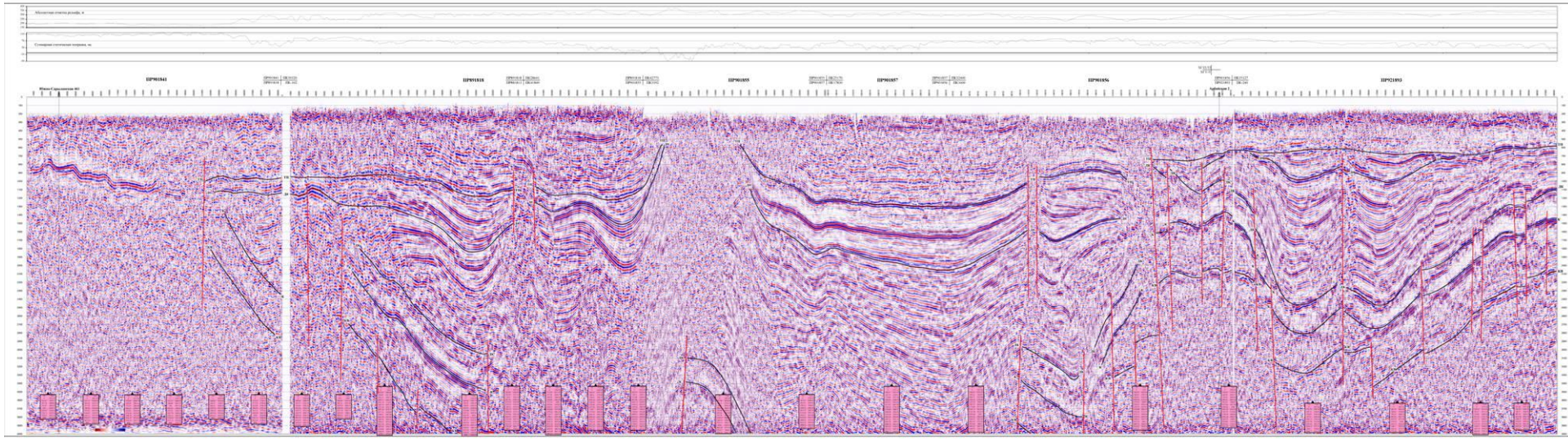

Block diagram showing schematic shapes of salt structures. Structural maturity and size increase toward the composite, coalesced structures in the background. (a) Elongated structures rising from line sources. (b) Structures rising from point sources. Simplified from Jackson and Talbot (1991).

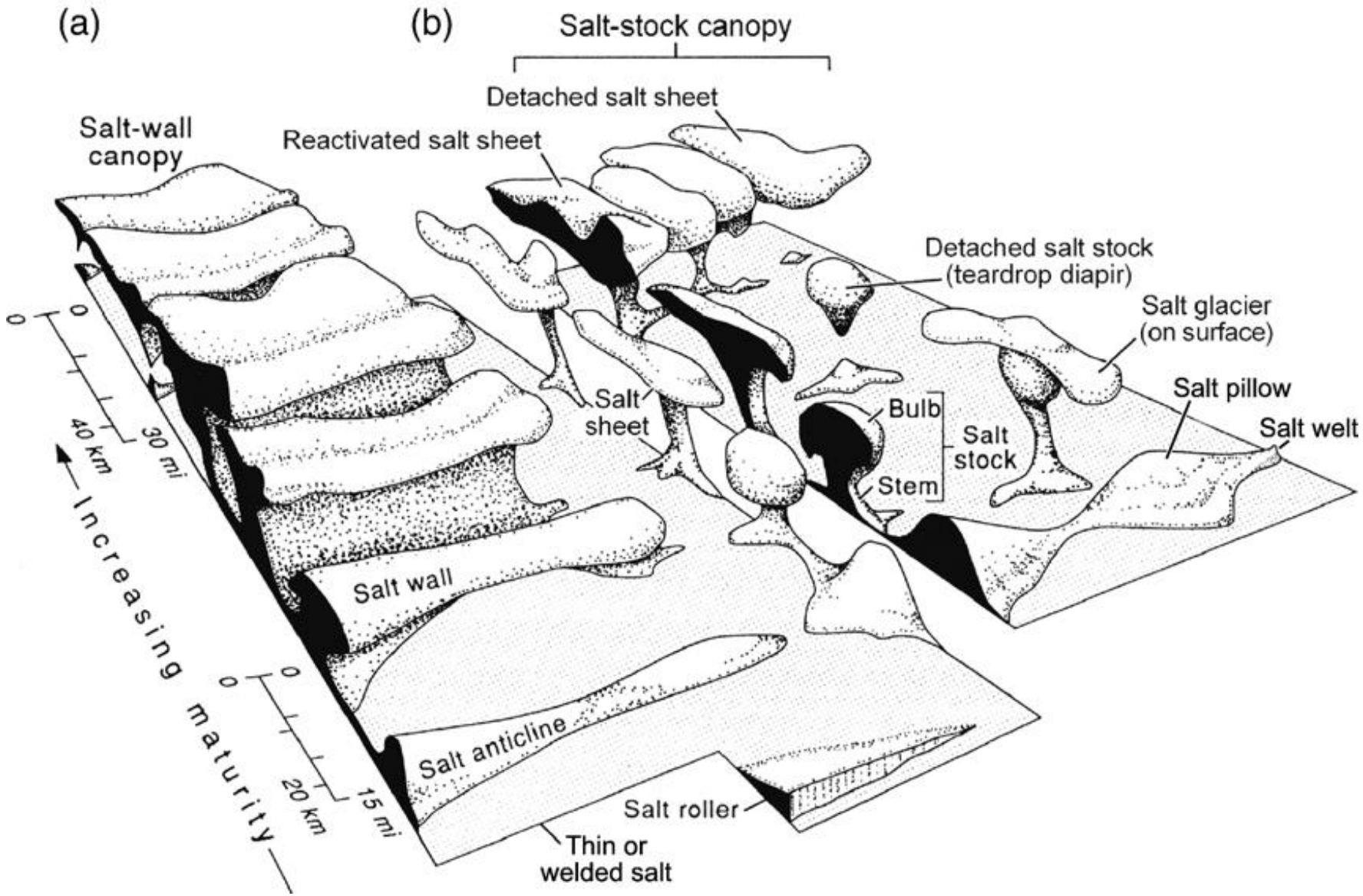

Examples of hydraulic head-gradient analysis in salt tectonics. (a) A laterally varying overburden thickness above a horizontal, tabular salt layer produces a pressure head gradient from Point 1 to Point 2 but no elevation head gradient. Salt will flow from left to right along the pressure head gradient. The load variation may be produced by sedimentation (e.g., a river delta) or deformation (a stack of thrust slices at the left end of the section) or by erosion. (b) A uniform overburden thickness above an inclined, tabular salt layer produces an elevation head gradient from Point 1 to Point 2 but no pressure head gradient. Salt will flow from left to right down the elevation head gradient. (c) A uniform overburden thickness above a flat-lying salt layer produces neither elevation nor head gradients, even though the salt thickness varies. Salt remains at rest because there is no hydraulic head gradient. Note that the shape of the base of the salt layer is not important for producing a head gradient (although it may influence the geometry of flow once it begins).

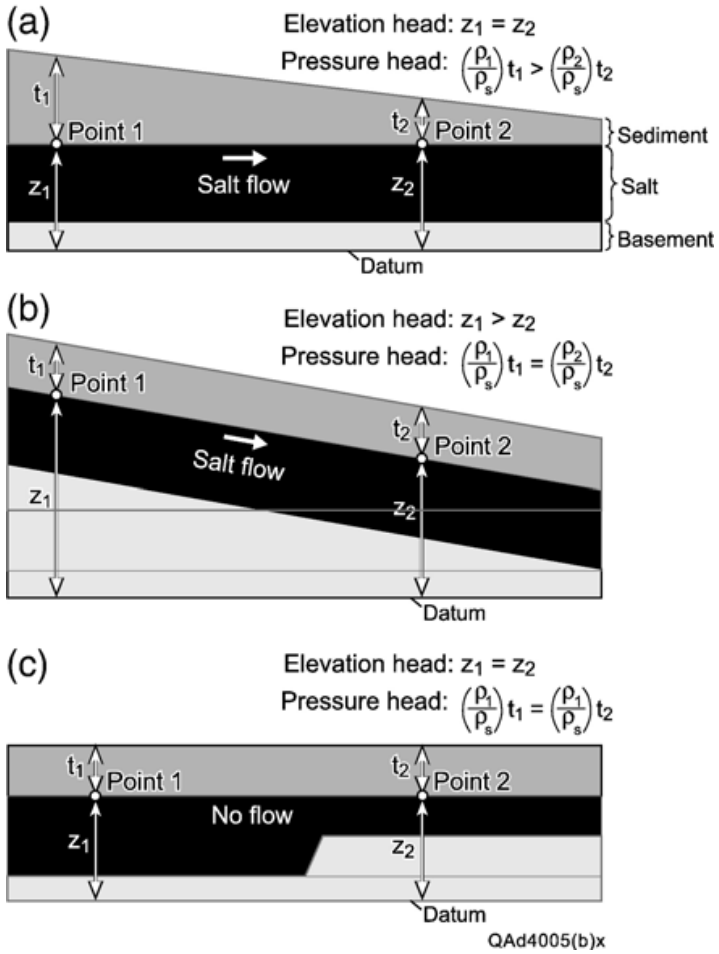

Schematic diagrams showing the effects of displacement loading on preexisting salt structures. (a) During shortening, salt is loaded horizontally by inward movement of one or both sidewalls. The horizontal displacement load then exceeds the vertical gravitational load, forcing salt to rise. In a natural example, the salt would flow out over the sediment surface rather than form a vertical column. (b) In extension, the salt is unloaded horizontally by outward movement of one or both sidewalls. The vertical gravitational load then exceeds the horizontal displacement load, so salt subsides.

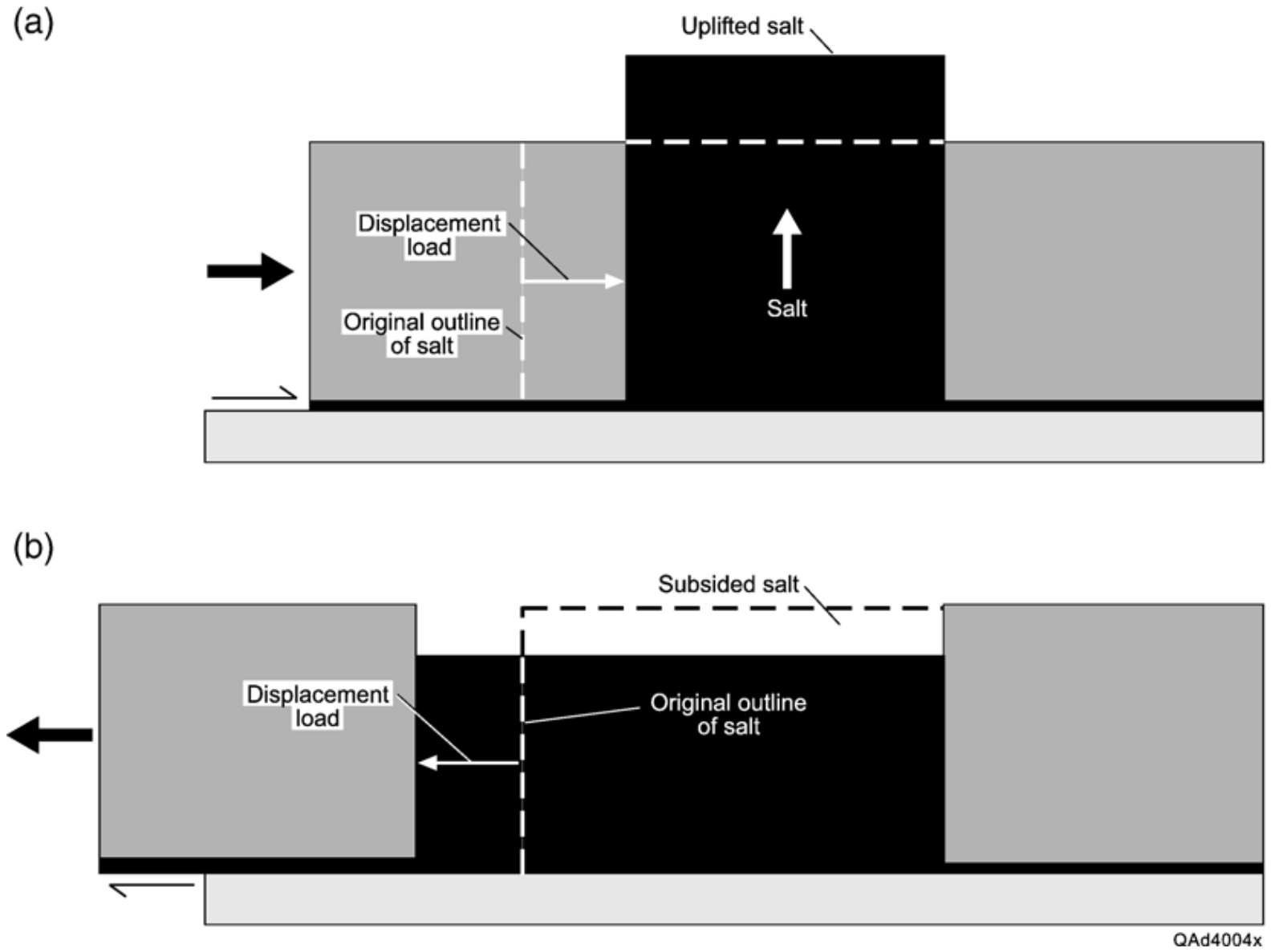

Sketch illustrating factors resisting salt flow. First, diapir rise requires deformation of the overlying roof. This deformation is easily
accomplished if the roof is thin and weak but becomes progressively more difficult as roof thickness increases. Second, salt is strongly sheared near
the edges of salt bodies during flow, which resists deformation. If a salt layer becomes too thin, flow is inhibited.

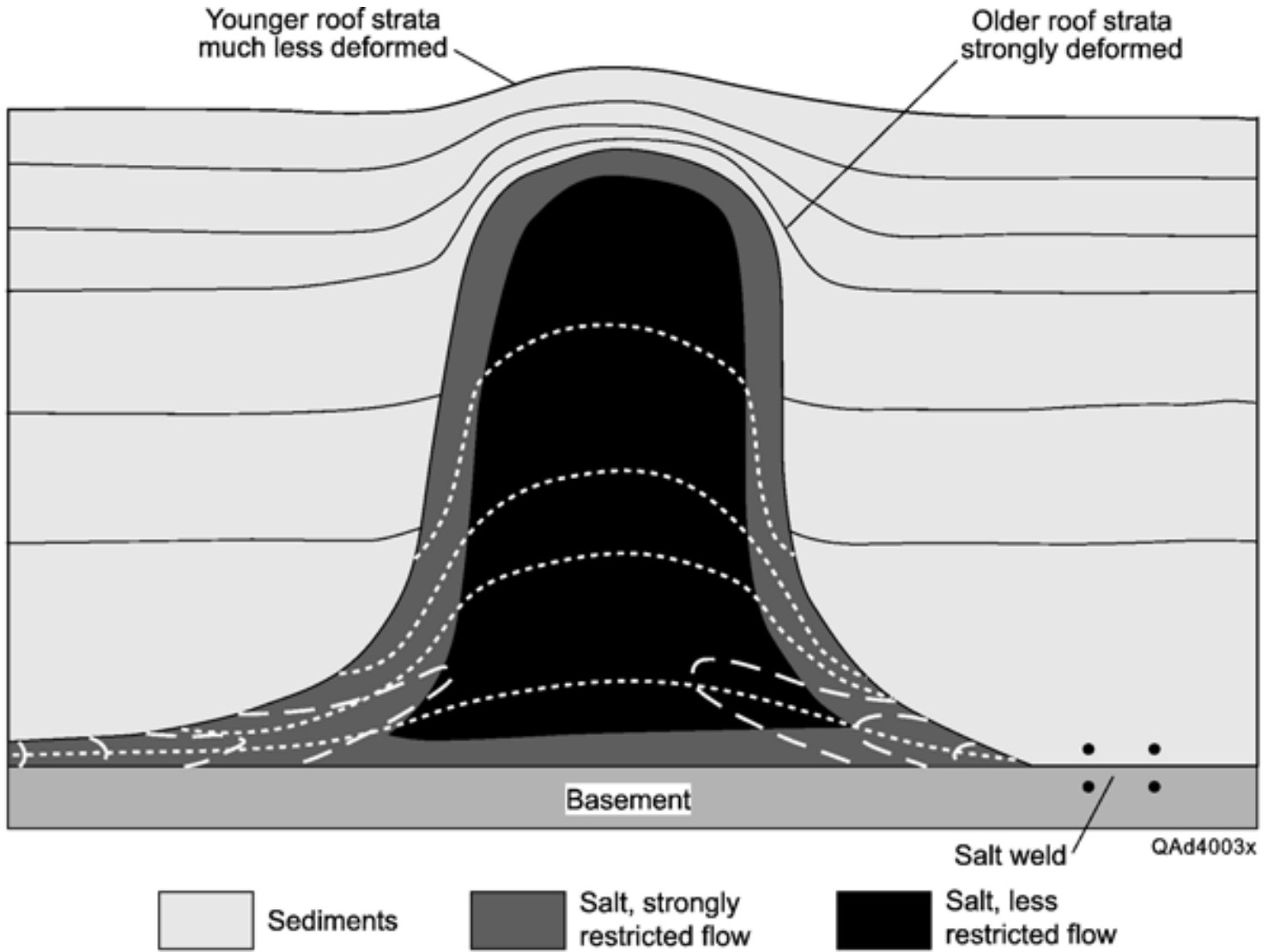

Modes of diapir piercement, shown in schematic cross sections. The overburden is brittle except in (e).

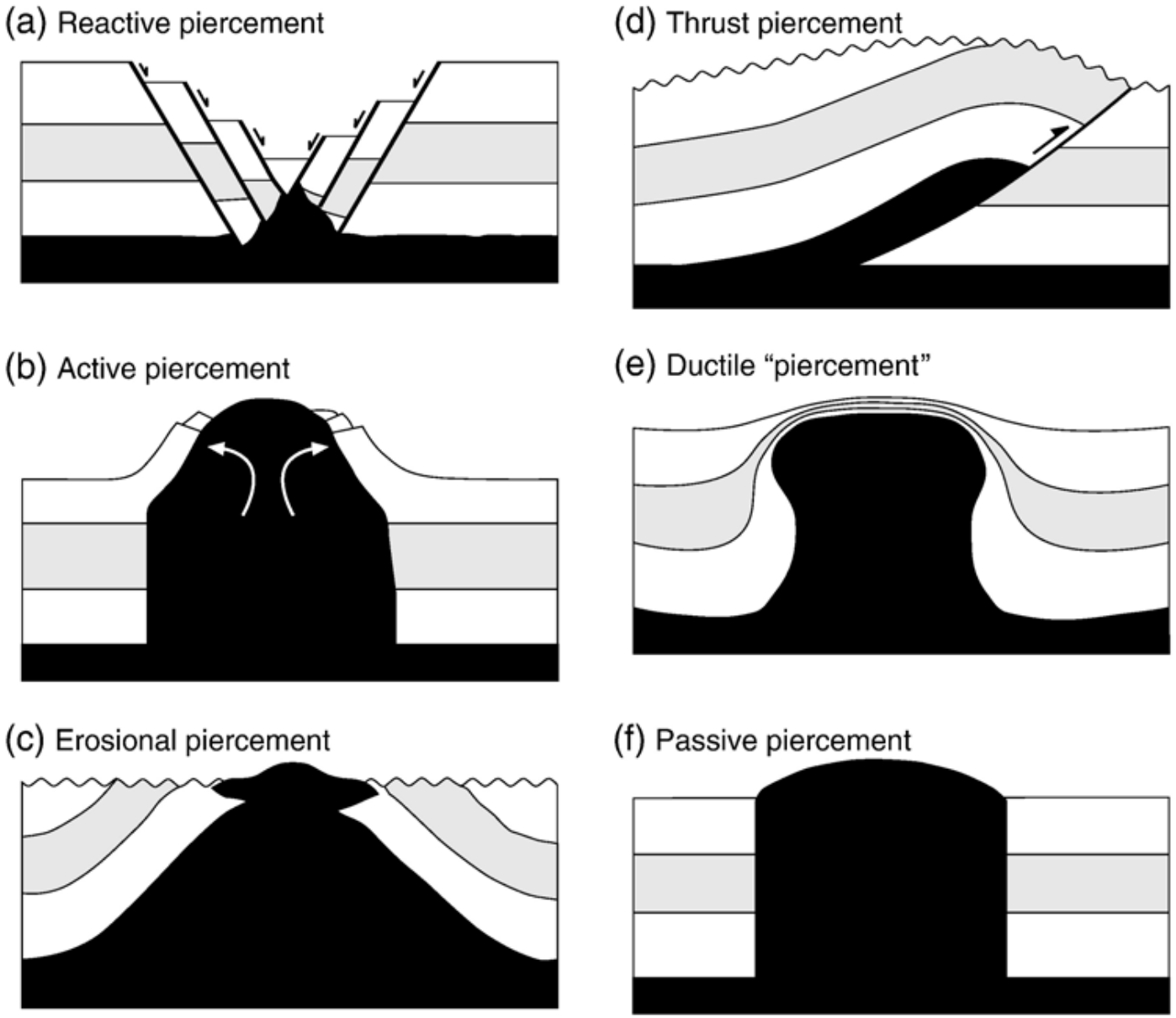

The cross-sectional shapes of passive diapirs are tied to the relative rates of net diapir rise (salt rise minus erosion and dissolution) and sediment aggradation. (a) Where diapir rise rate exceeds aggradation rate, diapirs widen upward and may ultimately form extrusive sheets. (b) Where diapir rise rate is equal to aggradation rate, diapirs have vertical walls. (c) Where diapir rise rate is less than aggradation rate, diapirs narrow upward and may ultimately become completely buried. Modified from Giles and Lawton (2002).

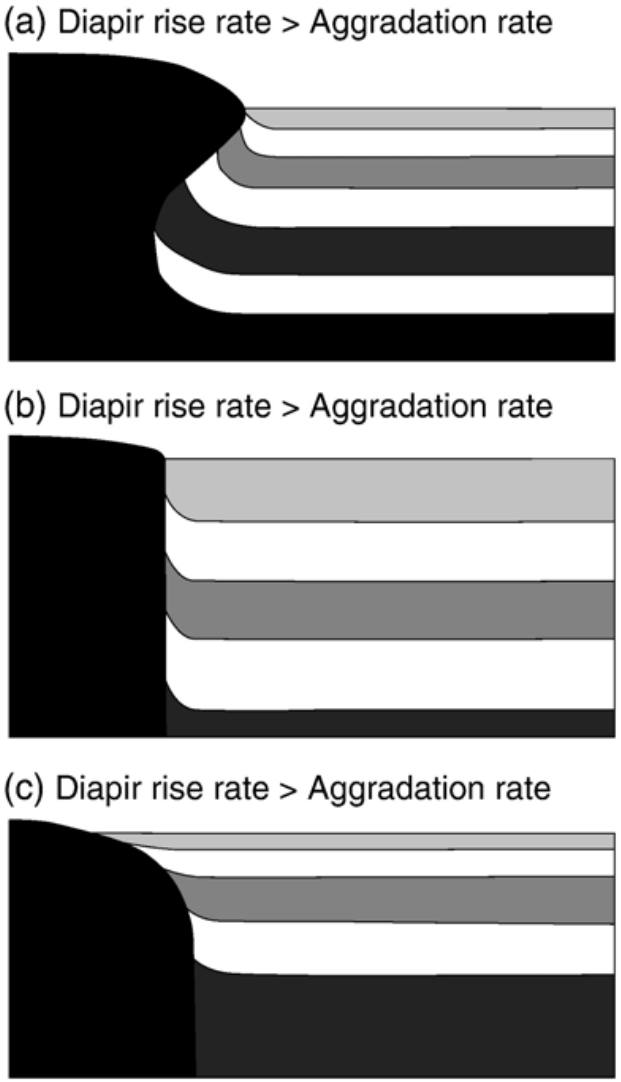

Diapir piercement during regional extension. Diapirs do not necessarily progress through all of these stages. The maturity of a given structure depends on availability of salt, total amount of extension, and relative rates of extension and sedimentation. Modified from Vendeville and Jackson (1992a).

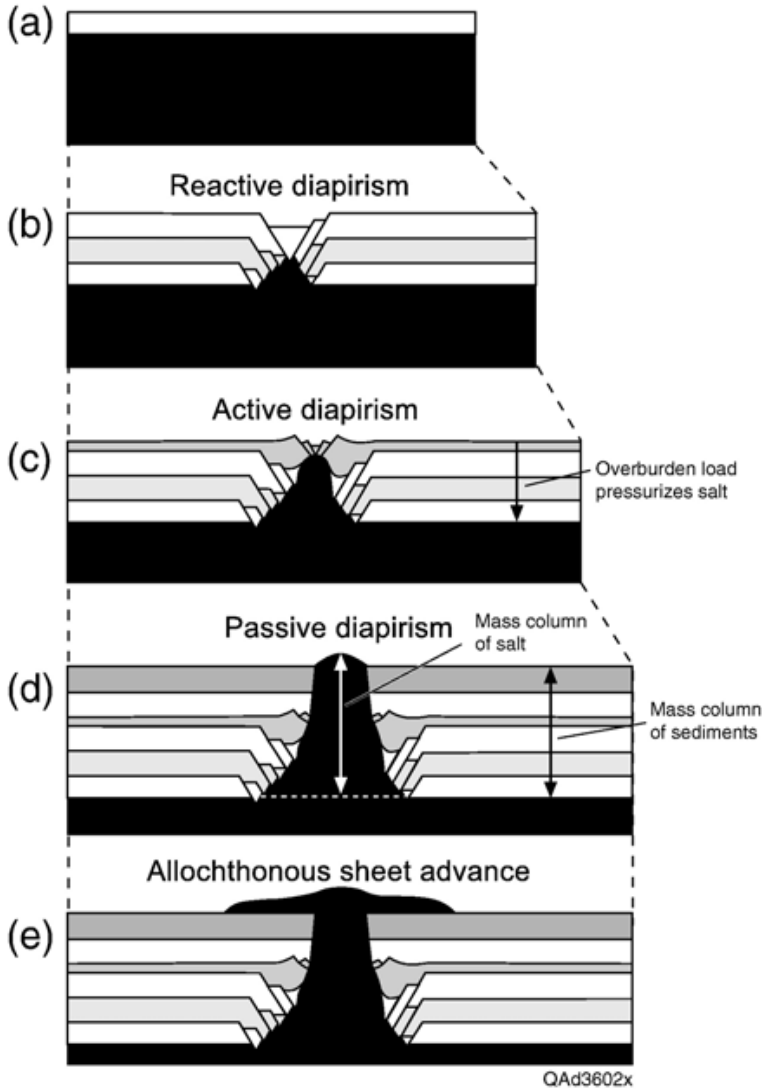

Photographs of cross sections from physical models showing stages of reactive piercement in extension, in the absence of synkinematic sedimentation. Numbers above fault tips refer to the order in which the faults formed. (a) Onset of extension. A small reactive diapir forms in the footwall of a normal fault. (b) Faulting steps inward to dissect the graben floor. Locus of reactive diapirism shifts inward to lie beneath the thinnest part of the graben. (c) Advanced stage of reactive diapirism. (d) After the roof thins to the point where pressure within the salt is sufficient for the diapir to actively force its way through to the surface, the diapir emerges and becomes passive. The former roof is preserved in steeply dipping flaps against the flank of the dome. Modified from Vendeville and Jackson (1992a).

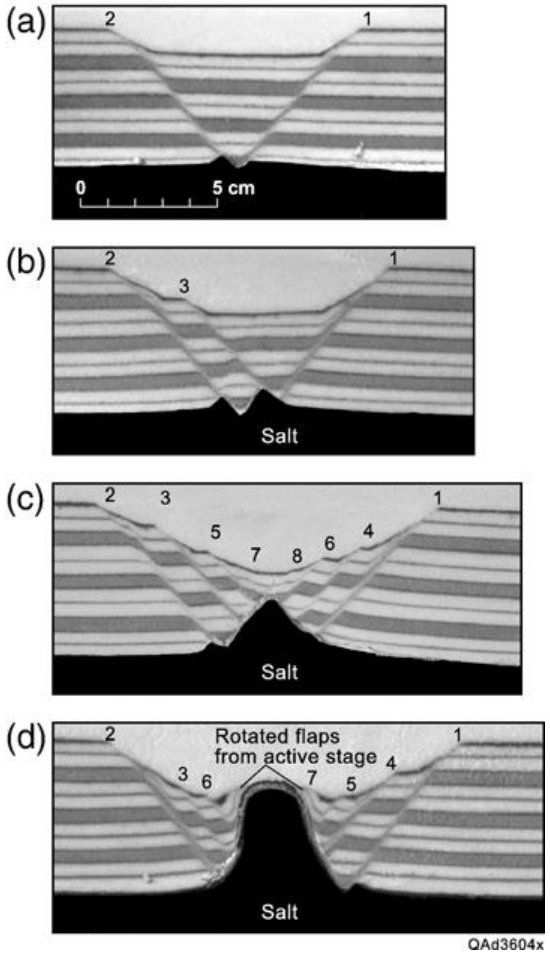

Seismic examples of salt diapirs. (a) Reactive diapir in the Gulf of Mexico. Modified from Rowan et al. (1999). Reprinted by permission of AAPG, whose permission is required for further use, AAPG©1999. (b) Formerly passive diapir from the Gulf of Mexico, now buried. Passive emplacement is inferred from the relatively undeformed reflectors abutting the diapir. The original image showed only half of the structure and has been mirrored for consistency with other images in this figure. Modified from Hale et al. (1992). Reprinted by permission of the SEG. (c) Formerly active diapir, Lower Congo Basin, Gabon. The active rise is recorded by the arched roof. Onlap of the crestal anticline indicates that uplift has ceased for now. Seismic section courtesy of Total Astrid Marin Gabon and partners. (d) Allochthonous salt sheet, Gulf of Mexico. The feeder has either been pinched off or is not on this line of section. Modified from Hodgkins and O'Brien (1994). Reprinted by permission of the SEG.

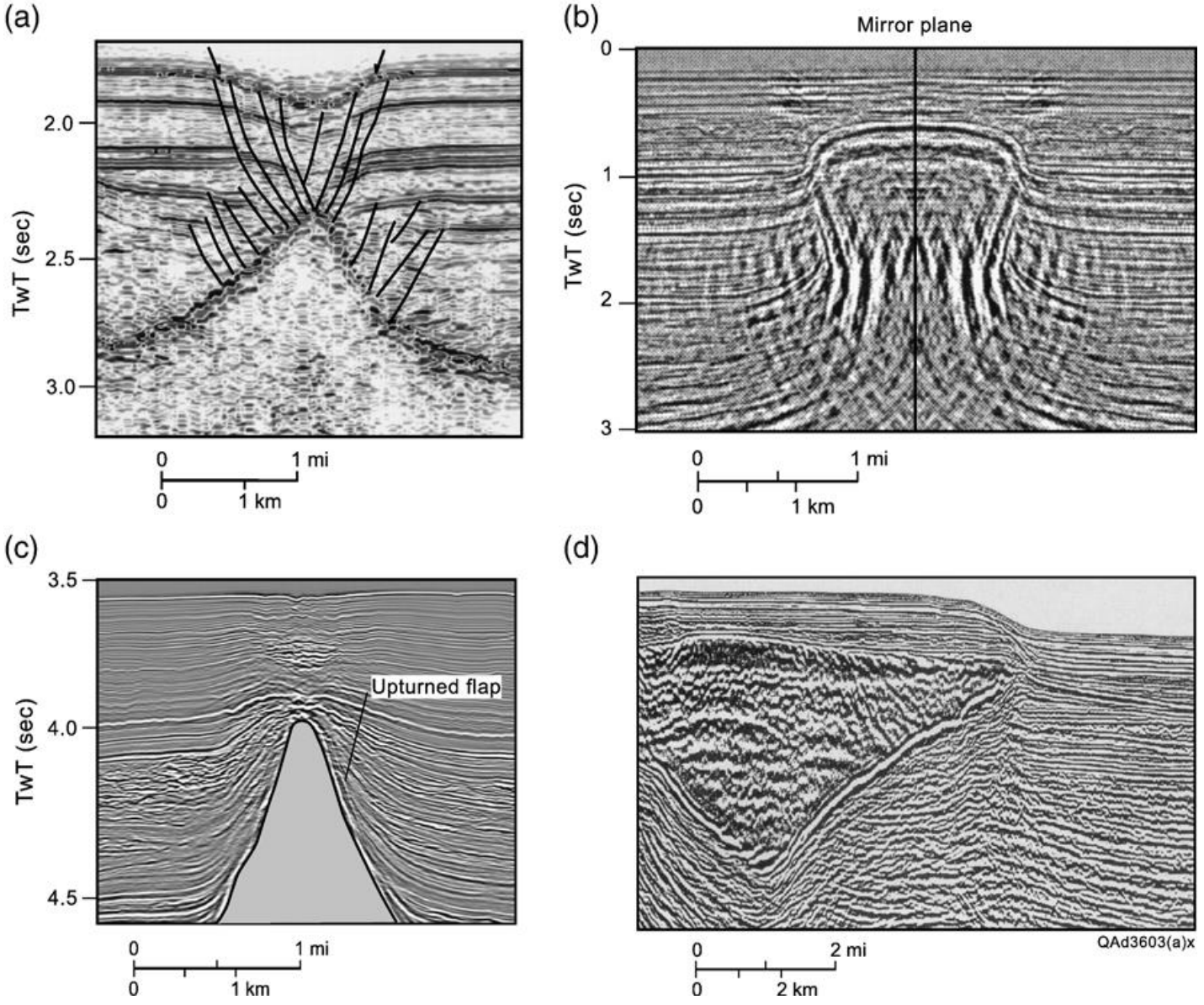

Serial sections of a diapiric wall formed in an extensional physical model. The northern section intersects a symmetric reactive diapir. In the southern section, this diapir evolved further to form a passive diapir. The inward-dipping array of normal faults above the diapir's pedestal reveals this structure's extensional origin. Modified from Vendeville and Jackson (1992a).

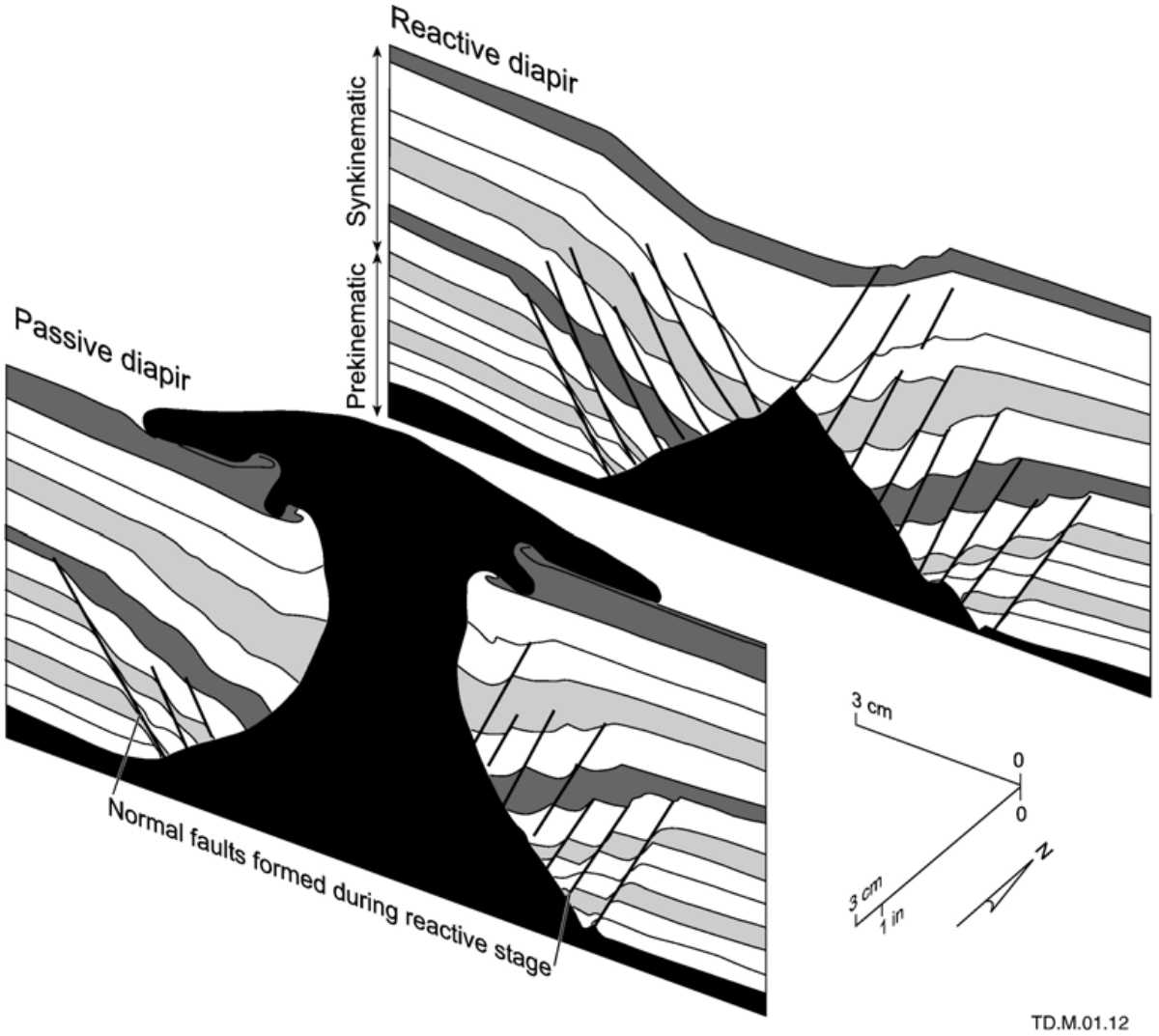

(a) Uninterpreted and (b) interpreted versions of a 3-D seismic section across a teardrop diapir in the northern Lower Congo Basin, offshore Gabon. The welded feeder has been reactivated as a thrust. Sediments adjacent to the salt have velocities comparable to salt, so the image is minimally affected by velocity pullup. Image courtesy of Total Astrid Marin Gabon.

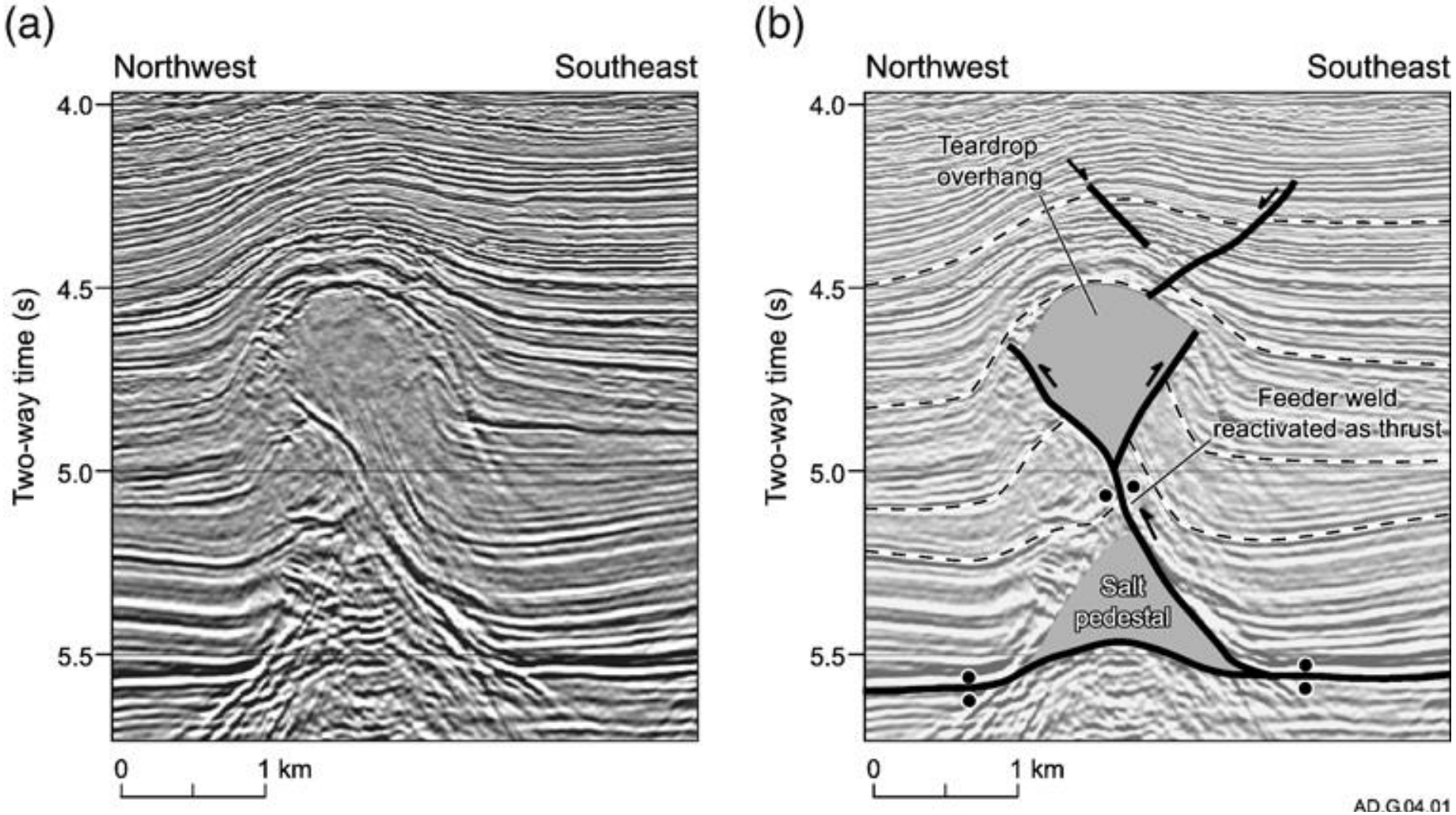

Four schematic models for salt-sheet advance. White lines within the salt represent selected deformed markers from an originally rectangular grid. The original grid was drawn at an arbitrary earlier time in sheet evolution, so the deformed grid represents incremental, not finite, strain. Modified from Hudec and Jackson (2006).

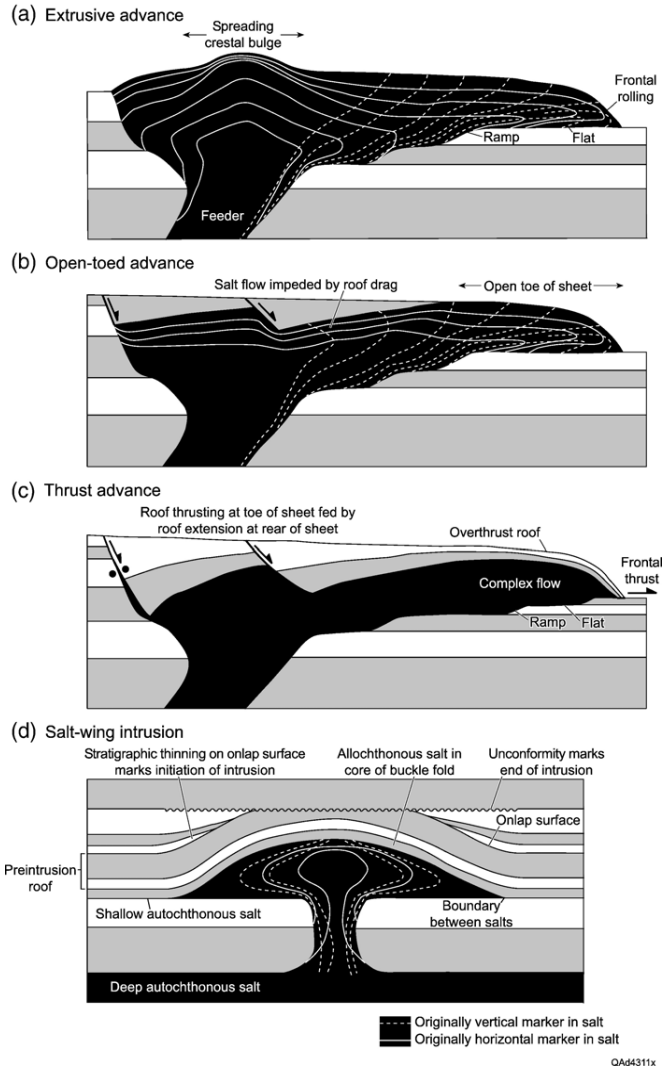

Satellite image of the Garmsar salt nappe, an open-toed extrusive sheet in northern Iran. Eocene salt has been carried up to the surface in
frontal thrusts of the Alborz Mountains. Erosion at the leading edge of this thrust complex has exposed the salt, allowing it to extrude as an open-toed
sheet. This sheet is carrying and rotating rafts detached from the leading edge of the roof.

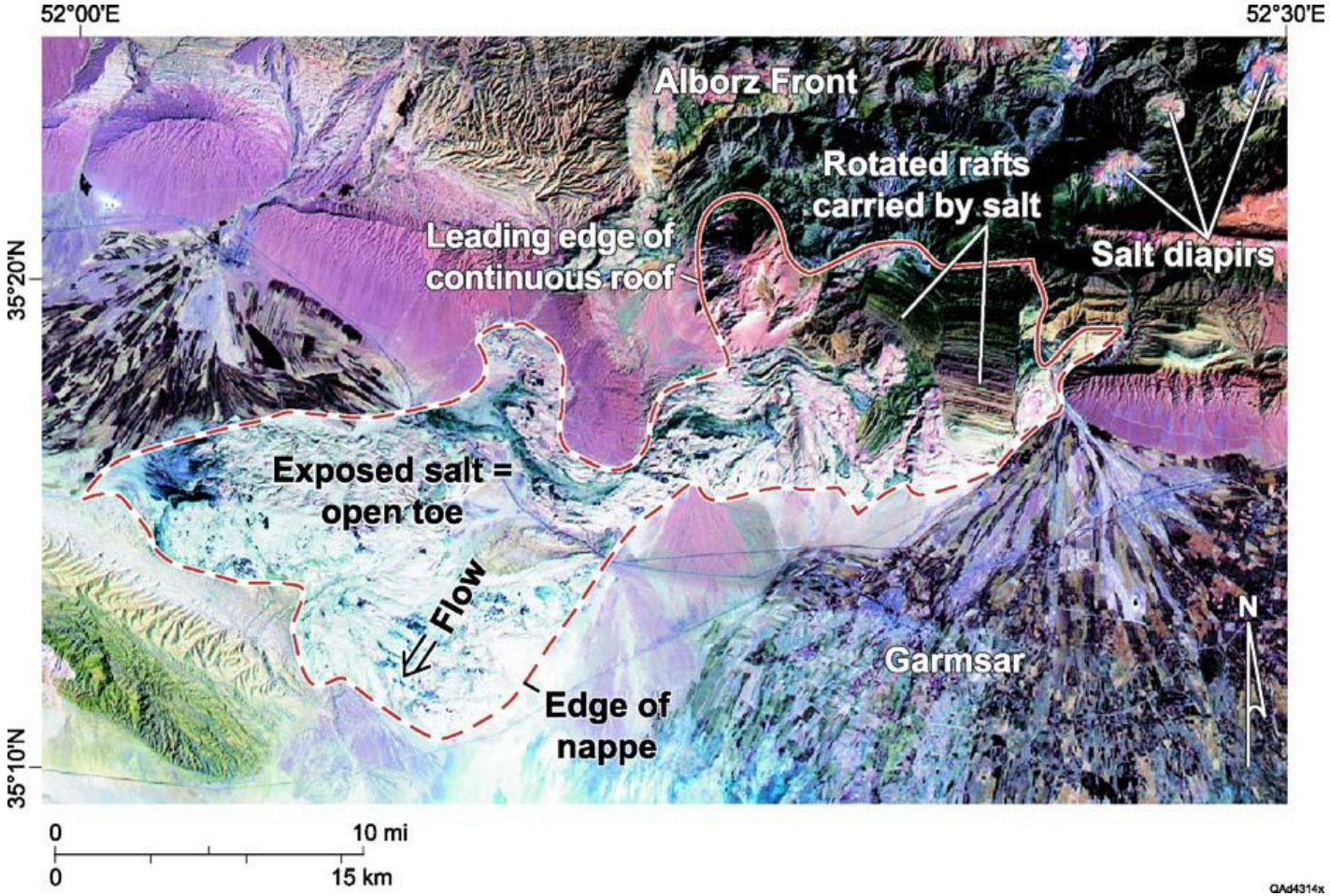

Schematic forward models of salt tectonics during regional extension, constructed using Geosec-2D.

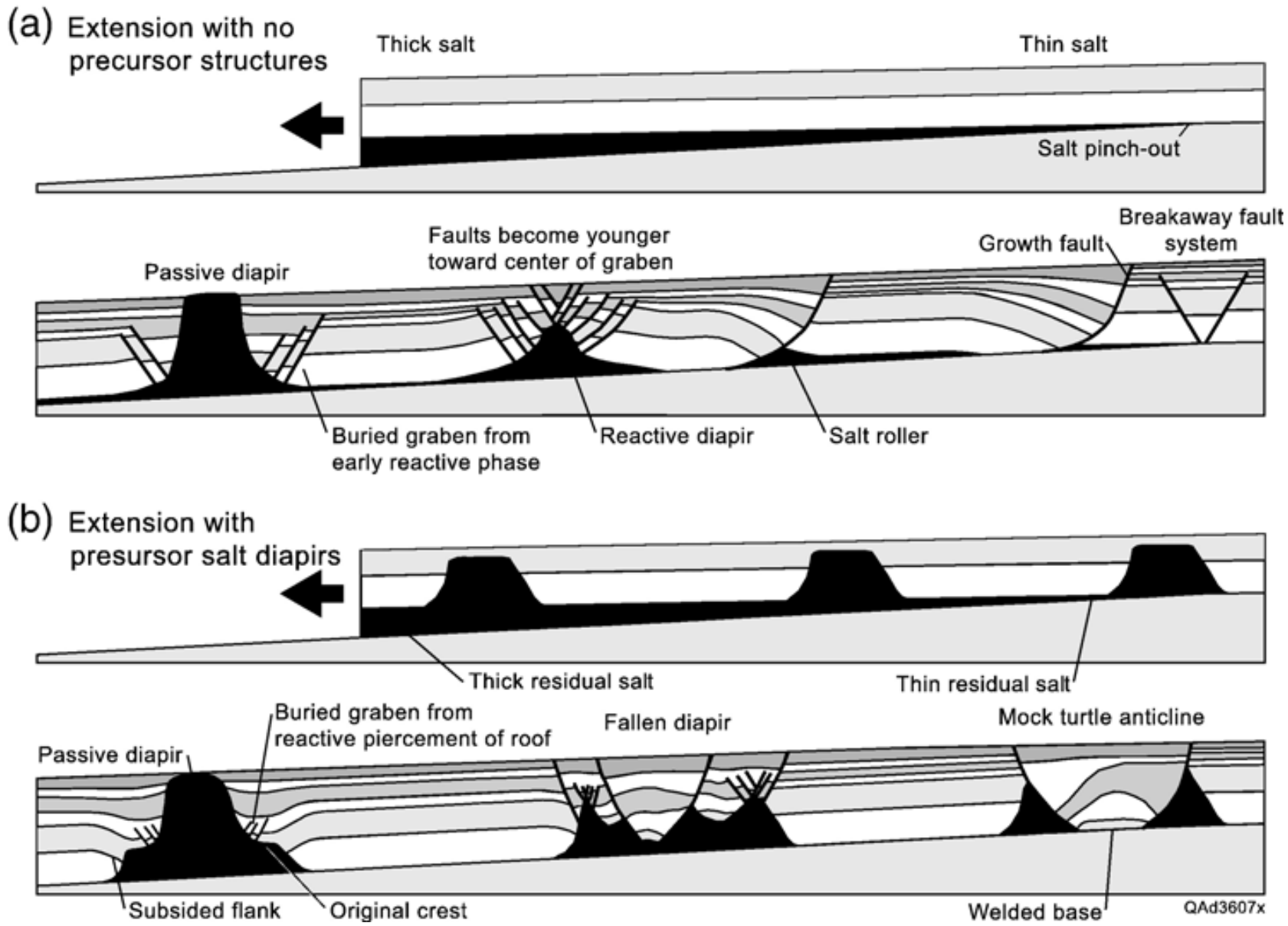

Schematic forward models of salt tectonics during regional shortening, constructed using Geosec-2D.

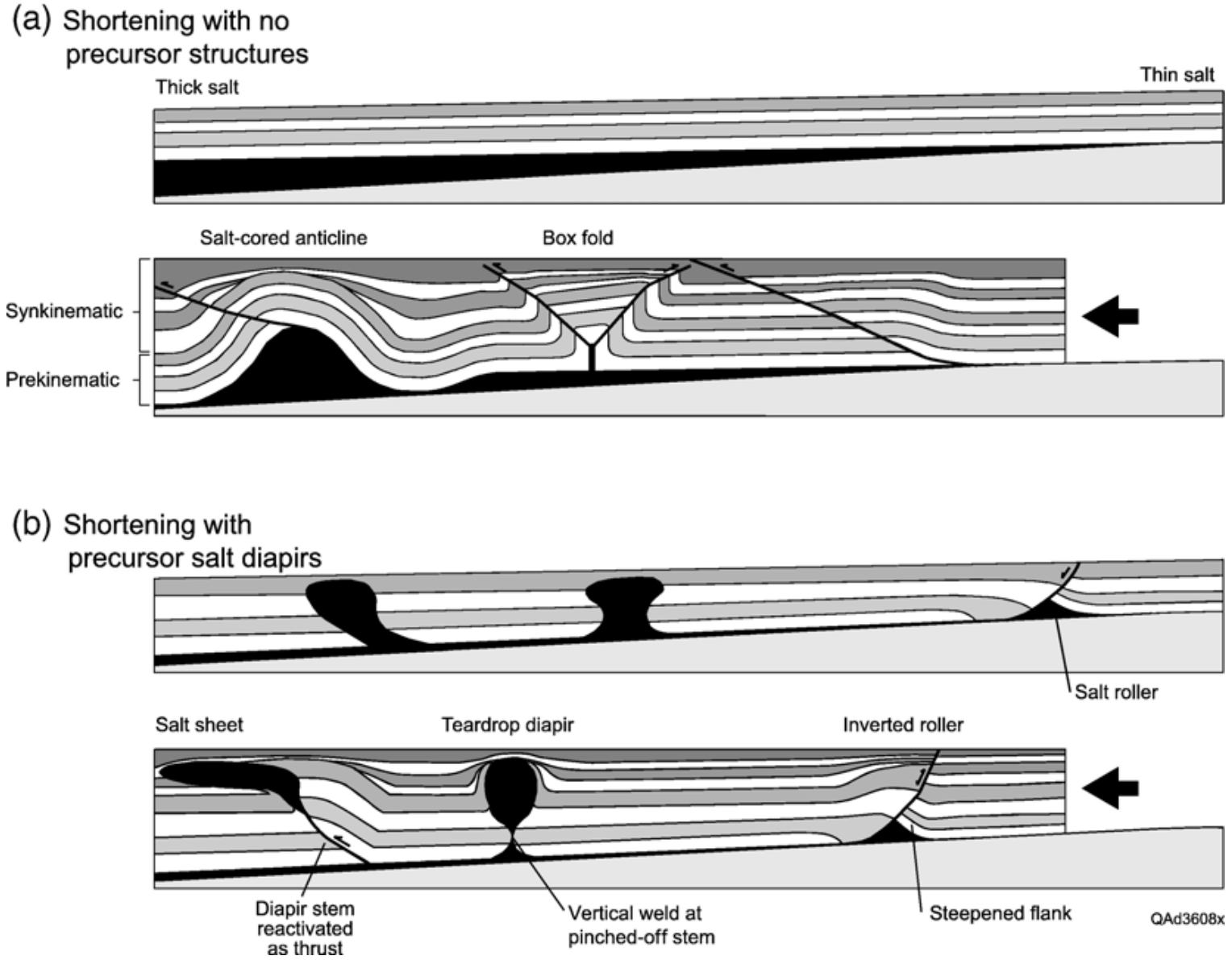

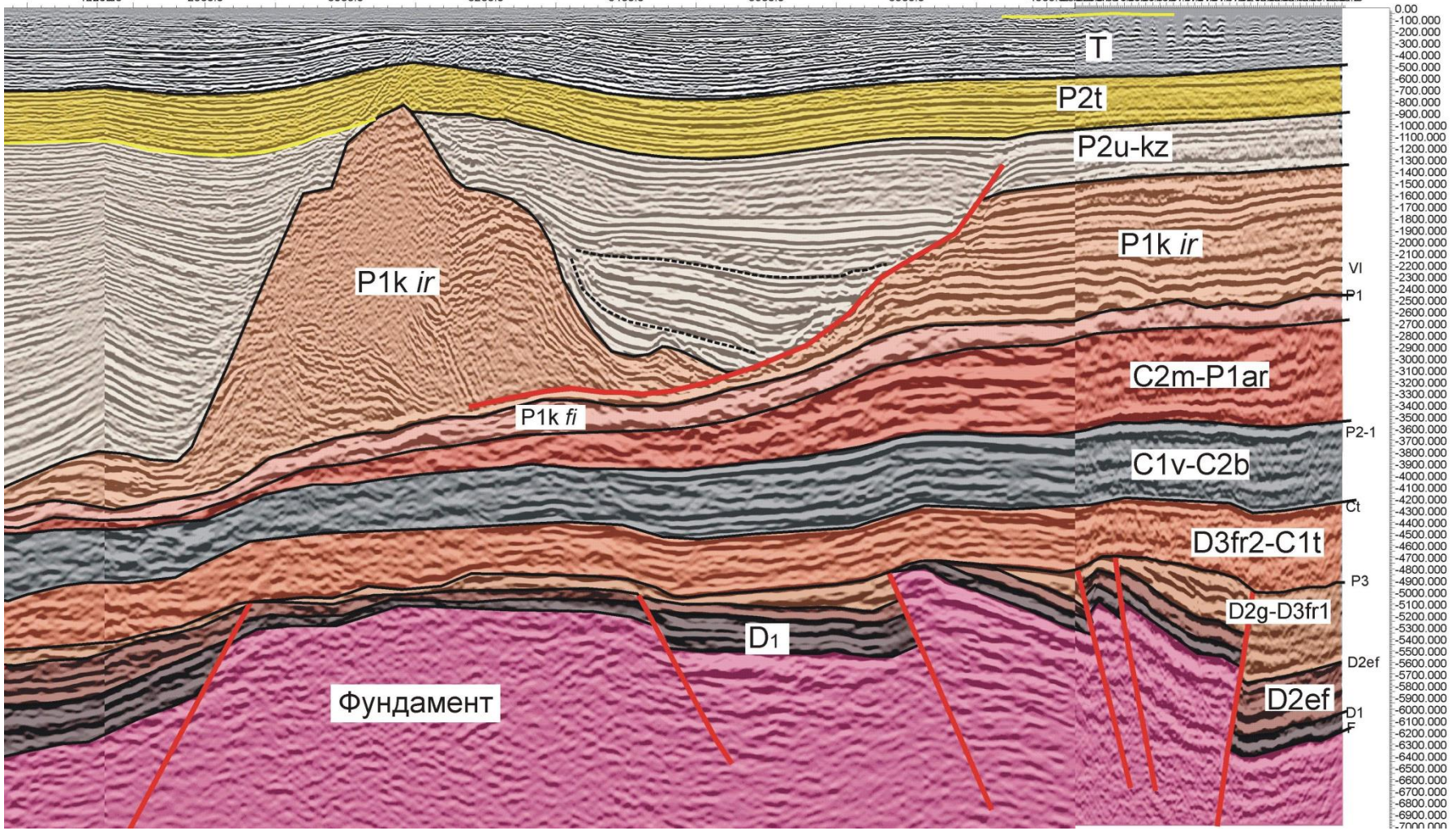

О. Альмендингер, А. Никишин

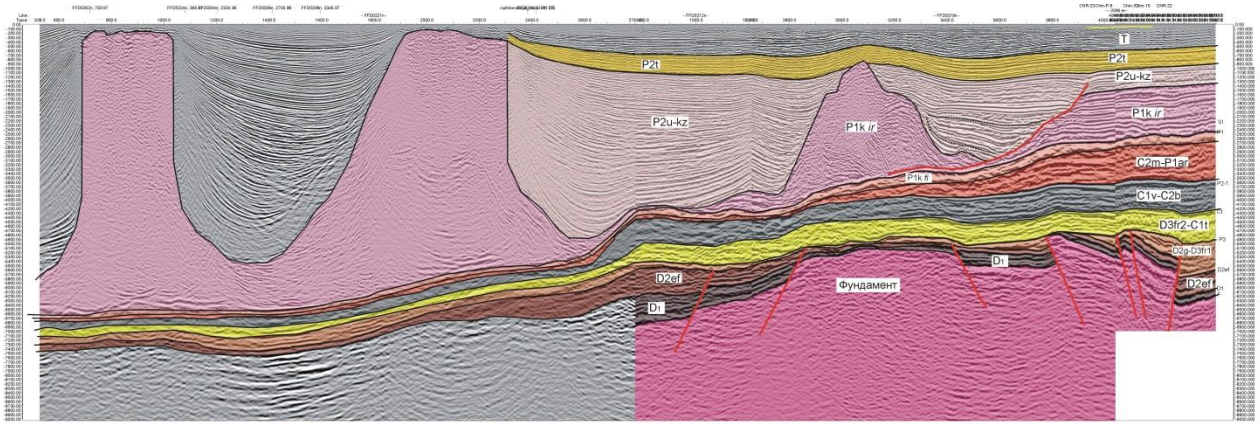

Рожковское поднятие

Чинаревский выступ

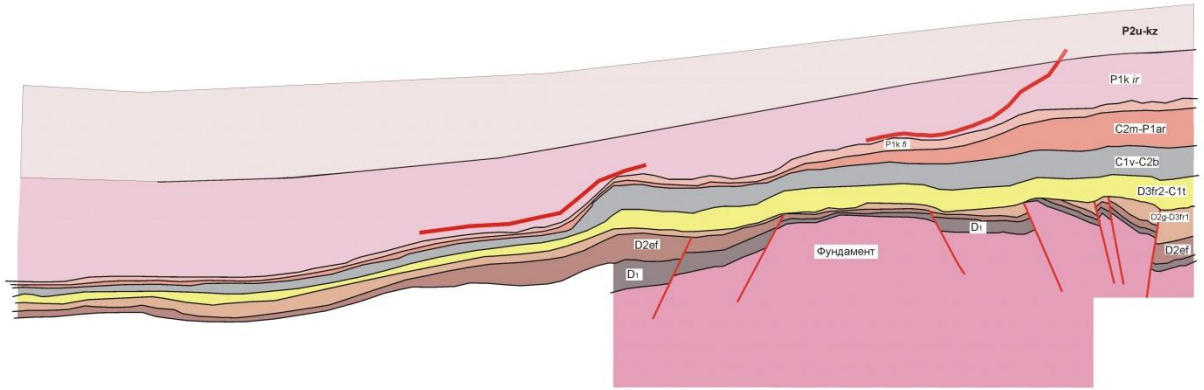

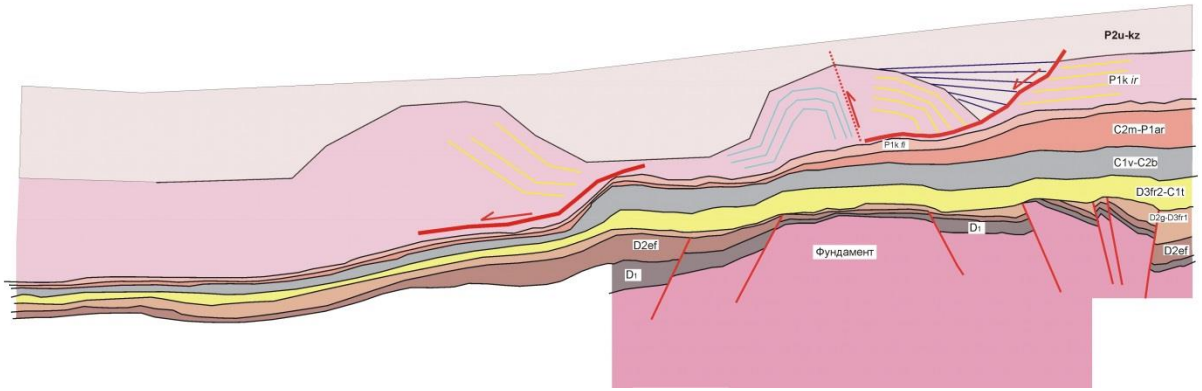

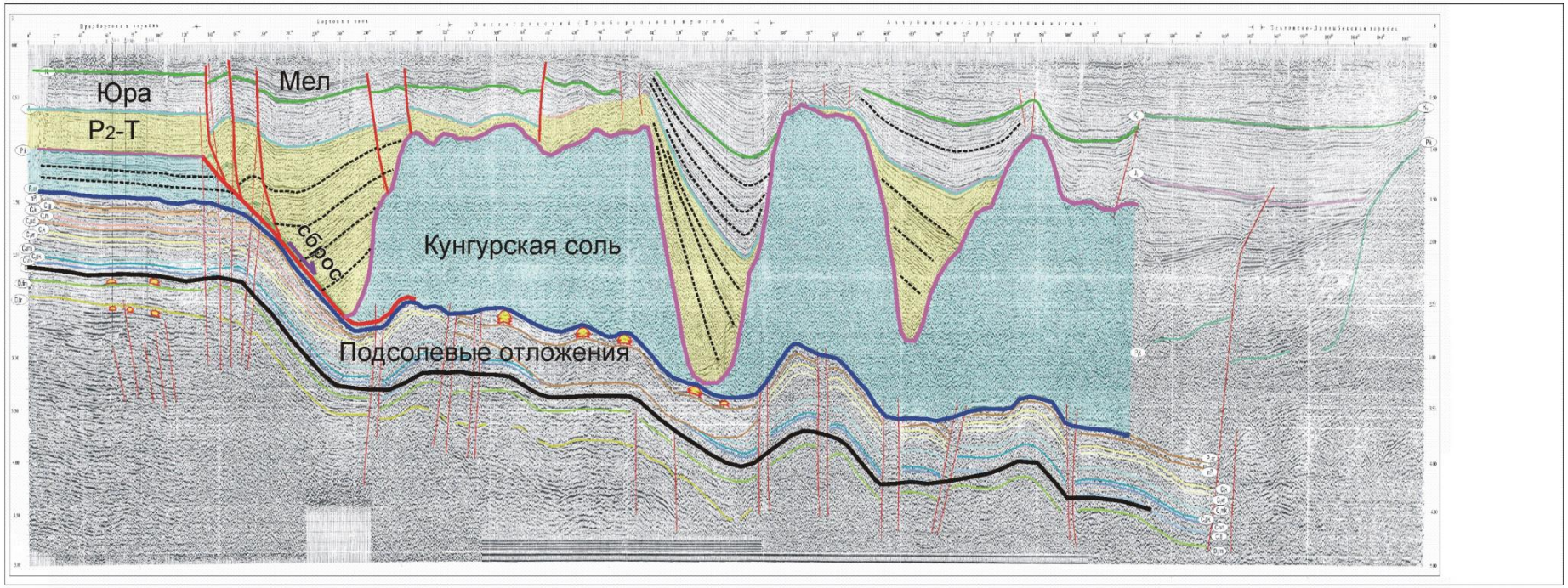
Юра
Мел
P2-T
сброс
Кунгурская соль
Подсолевые отложения


United States of America
Spindletop
HOUSTON
Mississippi – Alabama Shelf
De Soto Canyon
Texas Louisiana Shelf
Coulomb
Spiderman
Thunder Horse
Mississippi Canyon
West Florida Shelf
Texas Louisiana Slope
Neptune
Florida Escarpment
Baha #2
Sigsbee Salt sheet
Mad Dog
Cascade
Chinook
St. Malo
Mississippi Fan
Sigsbee Escarpment
Perdido Foldbelt
Florida Keys
MEXICO
Sigsbee Abyssal Plain
Campeche Escarpment
CUBA
Mexican Ridges
Yucatan Peninsula
Wells mentioned in text
©KPA/Masaoki Adachi

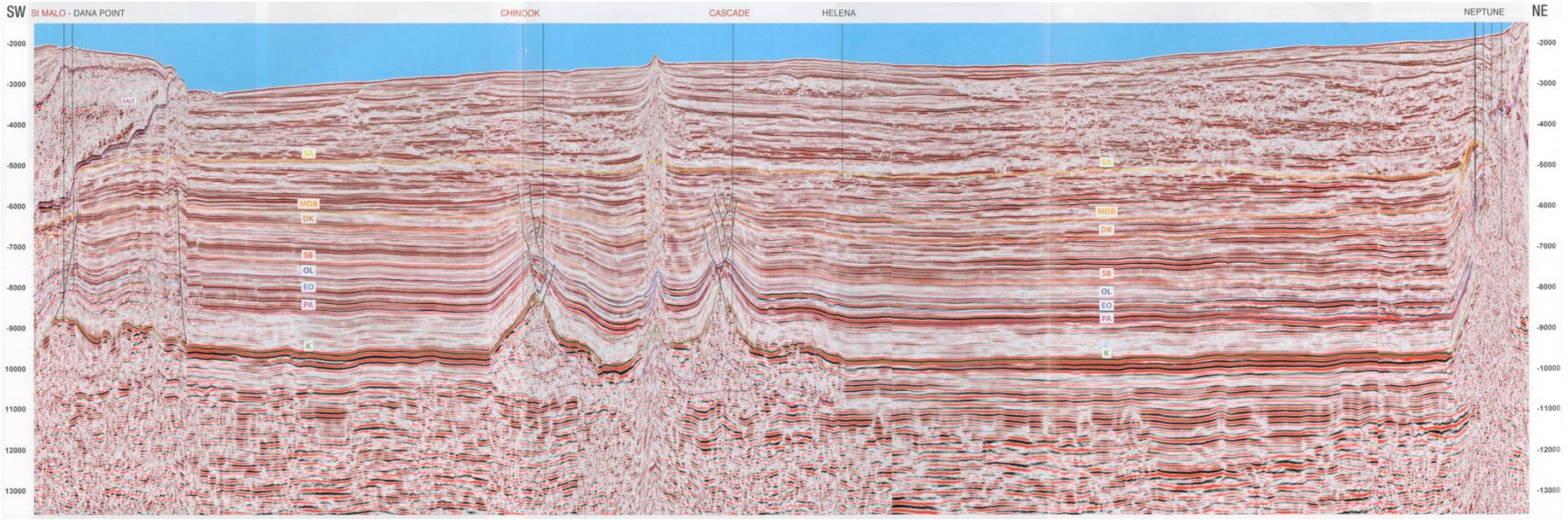
SW
St MALO - DANA POINT
CHINOOK
CASCADE
HELENA
NEPTUNE
NE
SEAFLOOR
SA
MDB
DK
SB
OL
EO
PA
K
-2000
-3000
-4000
-5000
-6000
-7000
-8000
-9000
10000
11000
12000
13000

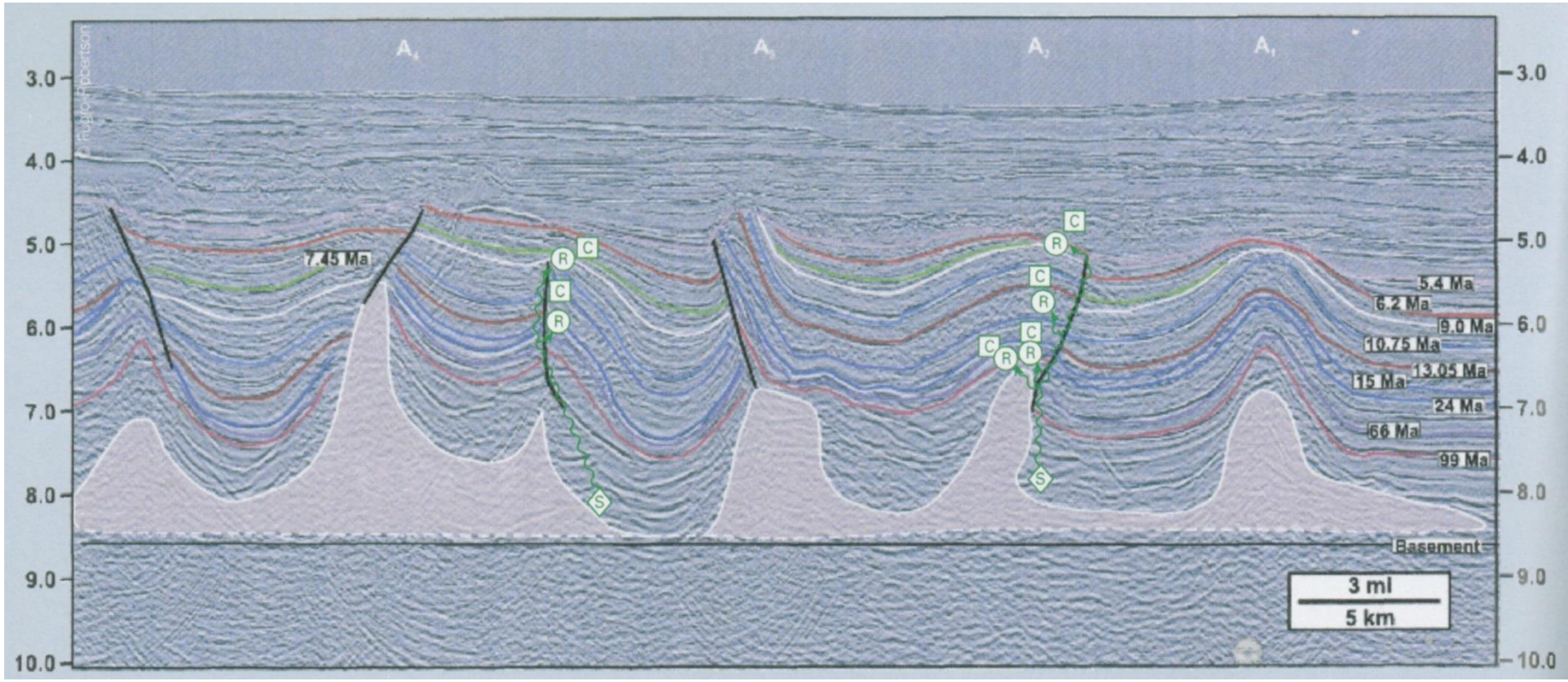
A4
A3
A2
A1
7.45 Ma
5.4 Ma
6.2 Ma
9.0 Ma
10.75 Ma
13.05 Ma
15 Ma
24 Ma
66 Ma
99 Ma
Basement
C
R
S
3 mi
5 km
3.0
4.0
5.0
6.0
7.0
8.0
9.0
10.0

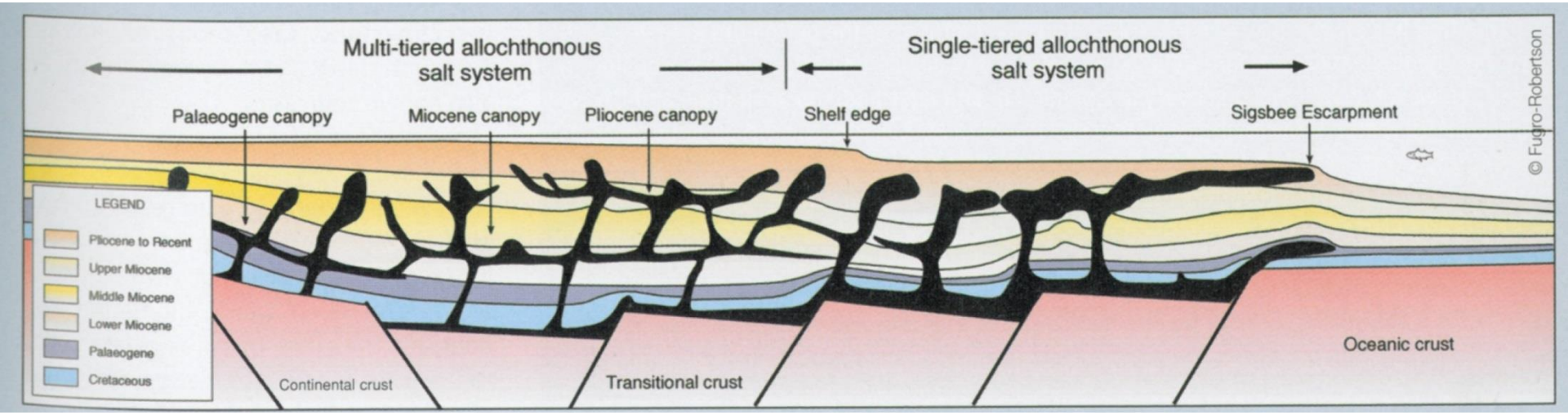
Multi-tiered allochthonous salt system
Single-tiered allochthonous salt system
Palaeogene canopy
Miocene canopy
Pliocene canopy
Shelf edge
Sigsbee Escarpment
LEGEND
Pliocene to Recent
Upper Miocene
Middle Miocene
Lower Miocene
Palaeogene
Cretaceous
Continental crust
Transitional crust
Oceanic crust
© Fugro-Robertson

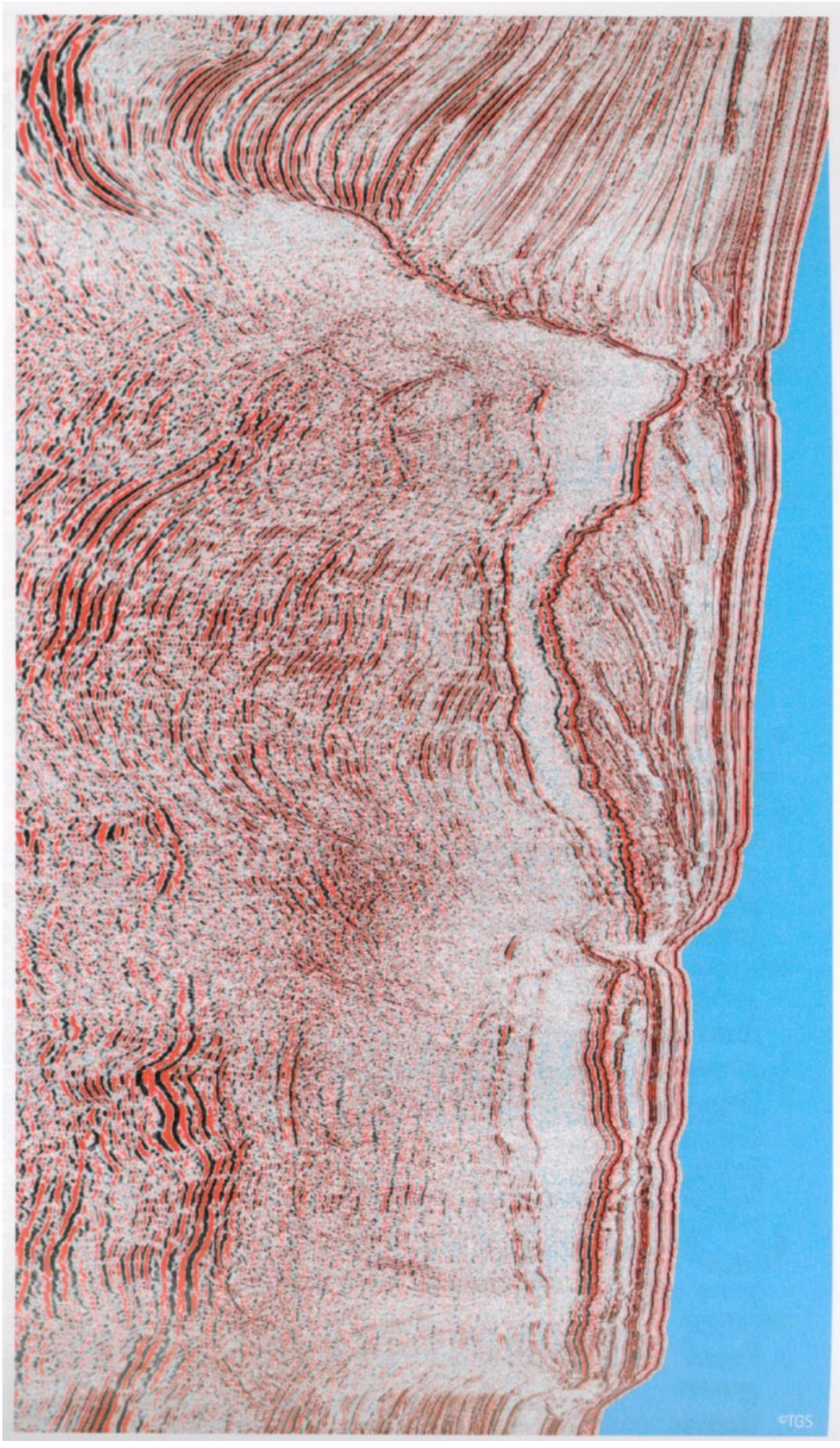
©TGS

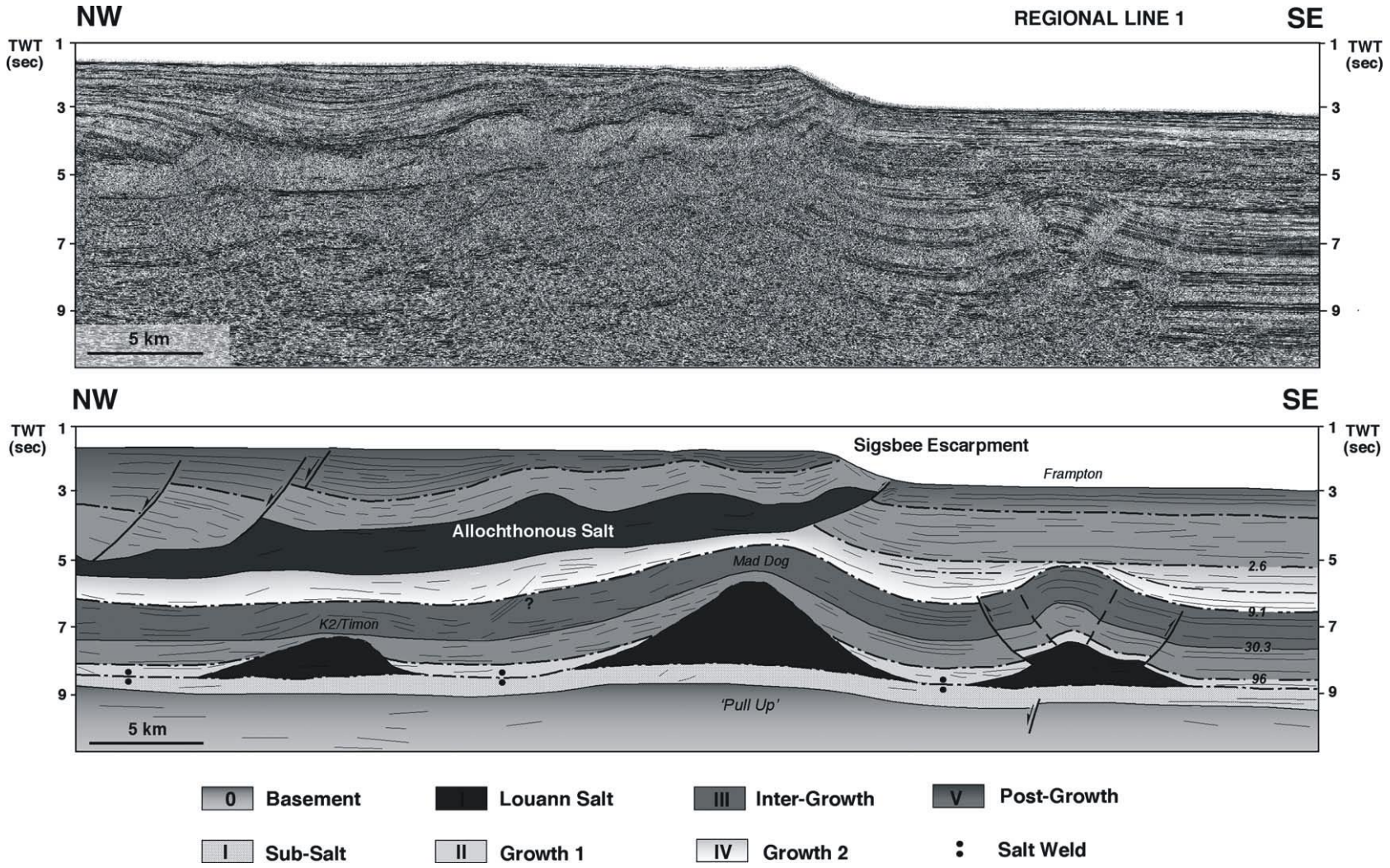

Regional NW–SE seismic profile across the Atwater Valley fold belt, showing the eastern geometries of K2/Timon, Mad Dog and Frampton detachment folds. Notice the shape of the Frampton anticline on its eastern part: a box fold with well-imaged kink bands on the fold limbs. The Sigsbee allochthonous salt sheet over-rides the landward portion of the folds, partially masking their seismic expression (location of line shown in Fig. 2).

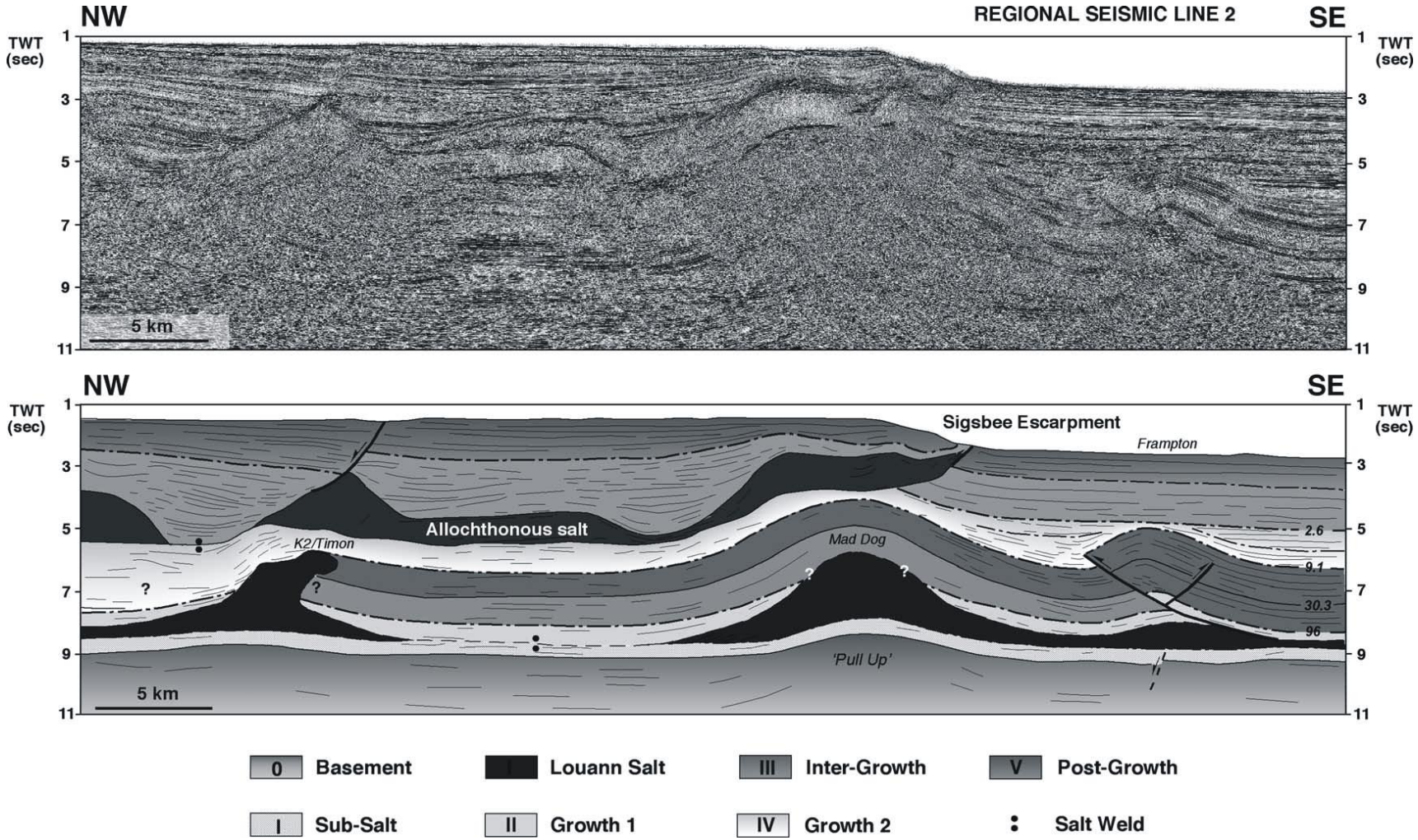

Regional NW–SE seismic profile across the Atwater Valley fold belt, showing the western geometries of K2/Timon, Mad Dog and Frampton detachment frontal folds close to the Green Knoll diapir. Frampton anticline to the west is a breached detachment fold characterised by a NW vergent thrust fault (location of line shown in Fig. 2).

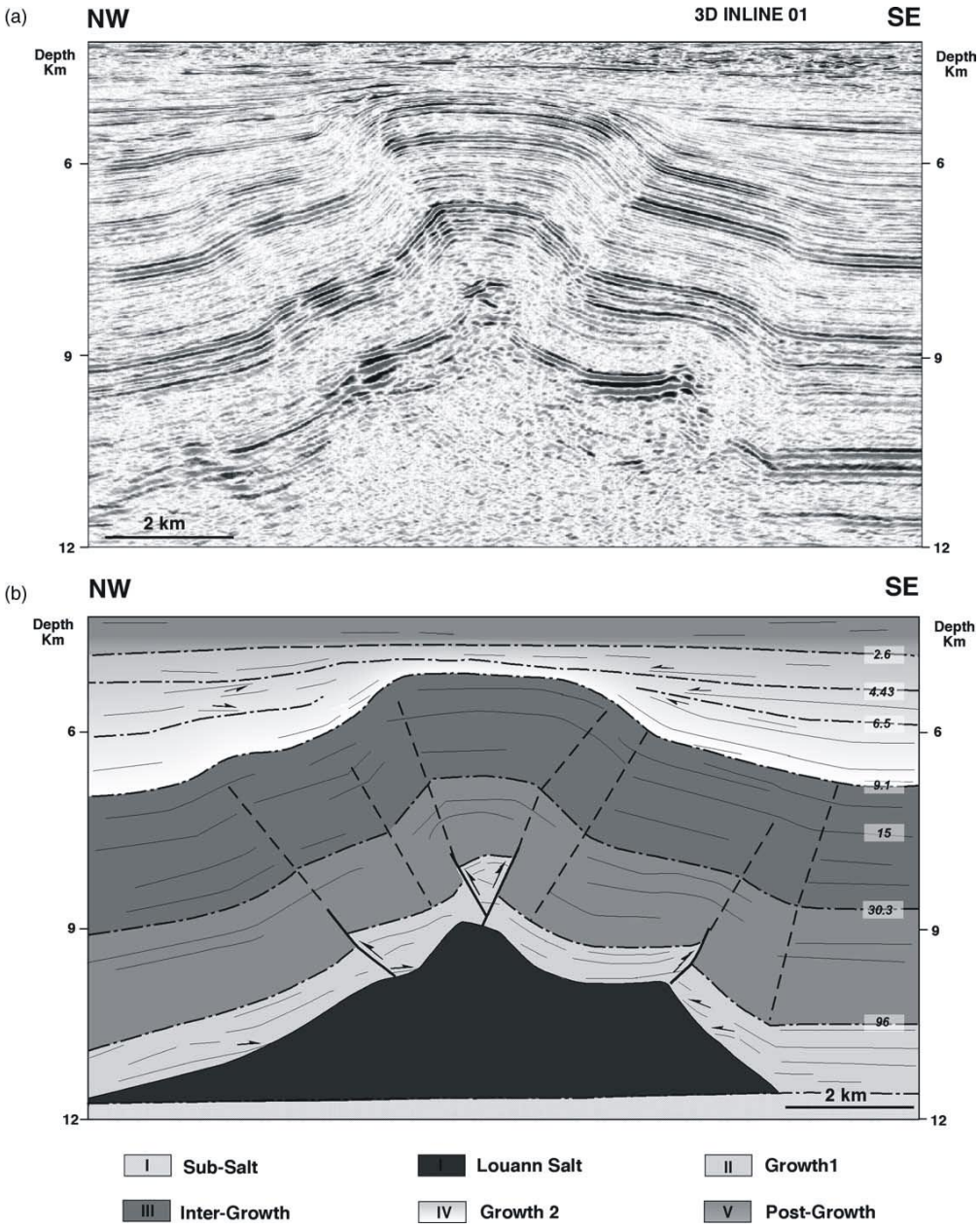

a) NW–SE trending seismic profile from the Frampton 3D survey showing the symmetric detachment box-fold in the eastern part of the area. A wellimaged, constant- width kink-band geometries developed in the pre-growth sequence. (b) Line diagram interpretation of the seismic profile showing the major megasequences. Small arrows indicate onlap and truncation geometry of stratal terminations on fold limbs.

M.G. Rowan, B.C. Vendeville / Marine and Petroleum Geology 23 (2006) 871–891

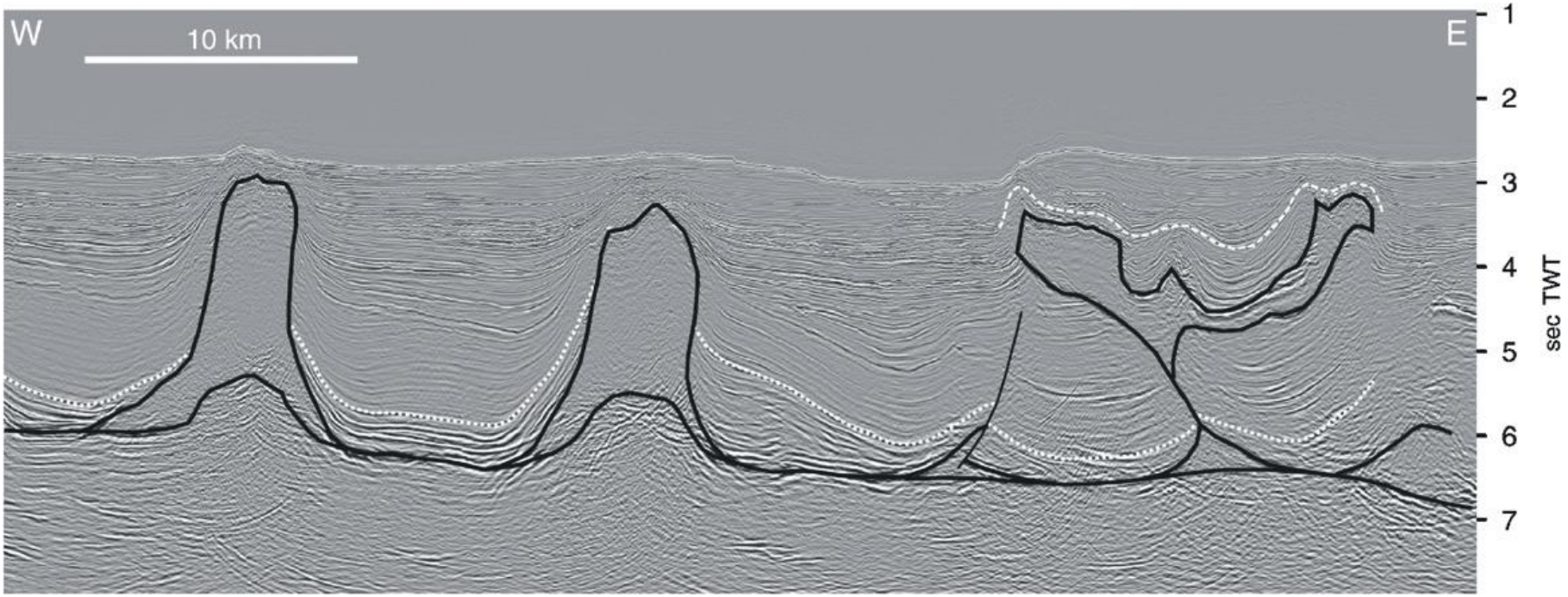

3-D, time-migrated seismic profile from the deepwater Espirito Santo Basin of Brazil. The Aptian salt and its allochthonous equivalent is in black, the near-top Albian carbonates are in short white dashes, and an undated shallow horizon is in medium white dashes. Shortening at the basal detachment level has a regular wavelength and is accommodated by the squeezing of diapirs and by folding and thrusting. Shortening above the allochthonous salt is accommodated by smaller-wavelength folding because of the thinner section being deformed. Data courtesy of CGG Americas.

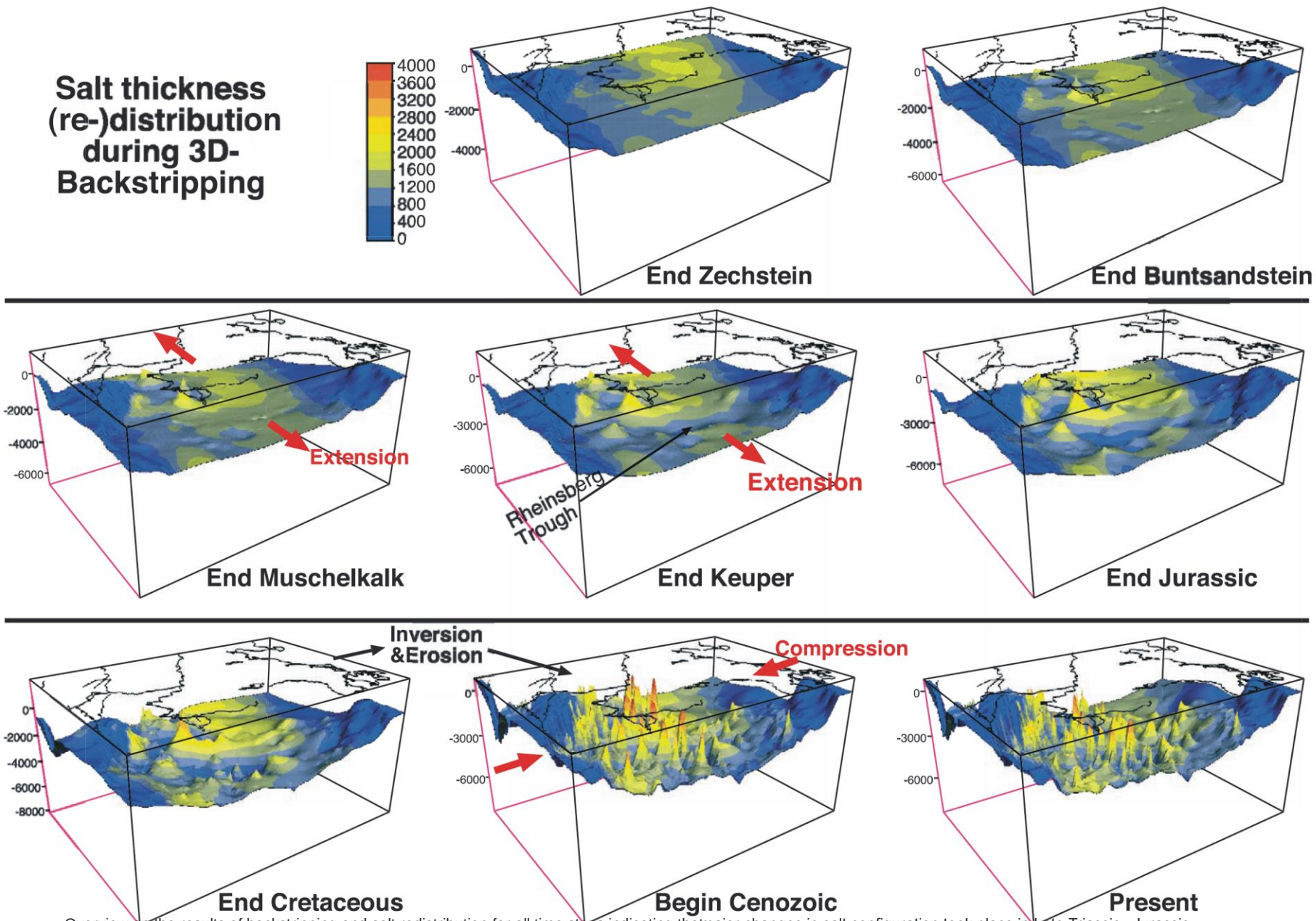

Overview on the results of backstripping and salt redistribution for all time steps indicating that major changes in salt configuration took place in Late Triassic –Jurassic extension and during Late Cretaceous inversion. The deformation intensity is largest during Late Cretaceous inversion.

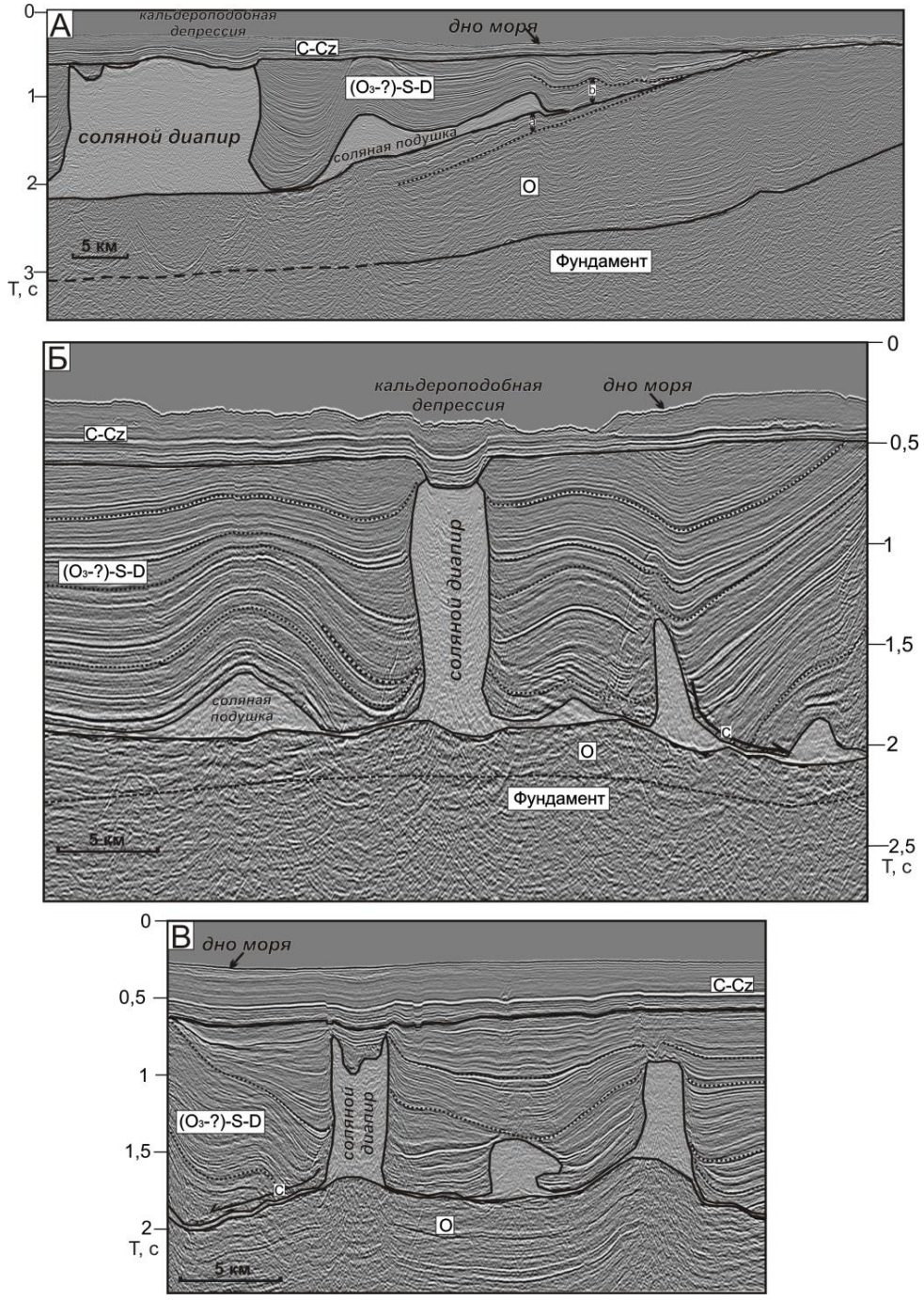
А
кальдероподобная депрессия
дно моря
C-Cz
(O₃-?)-S-D
соляной диапир
соляная подушка
O
Фундамент
5 км
0
1
2
3
T, с
Б
кальдероподобная депрессия
дно моря
C-Cz
(O₃-?)-S-D
соляной диапир
соляная подушка
O
Фундамент
5 км
0
0,5
1
1,5
2
2,5
T, с
В
дно моря
C-Cz
(O₃-?)-S-D
соляной диапир
O
5 км
0
0,5
1
1,5
2
T, с

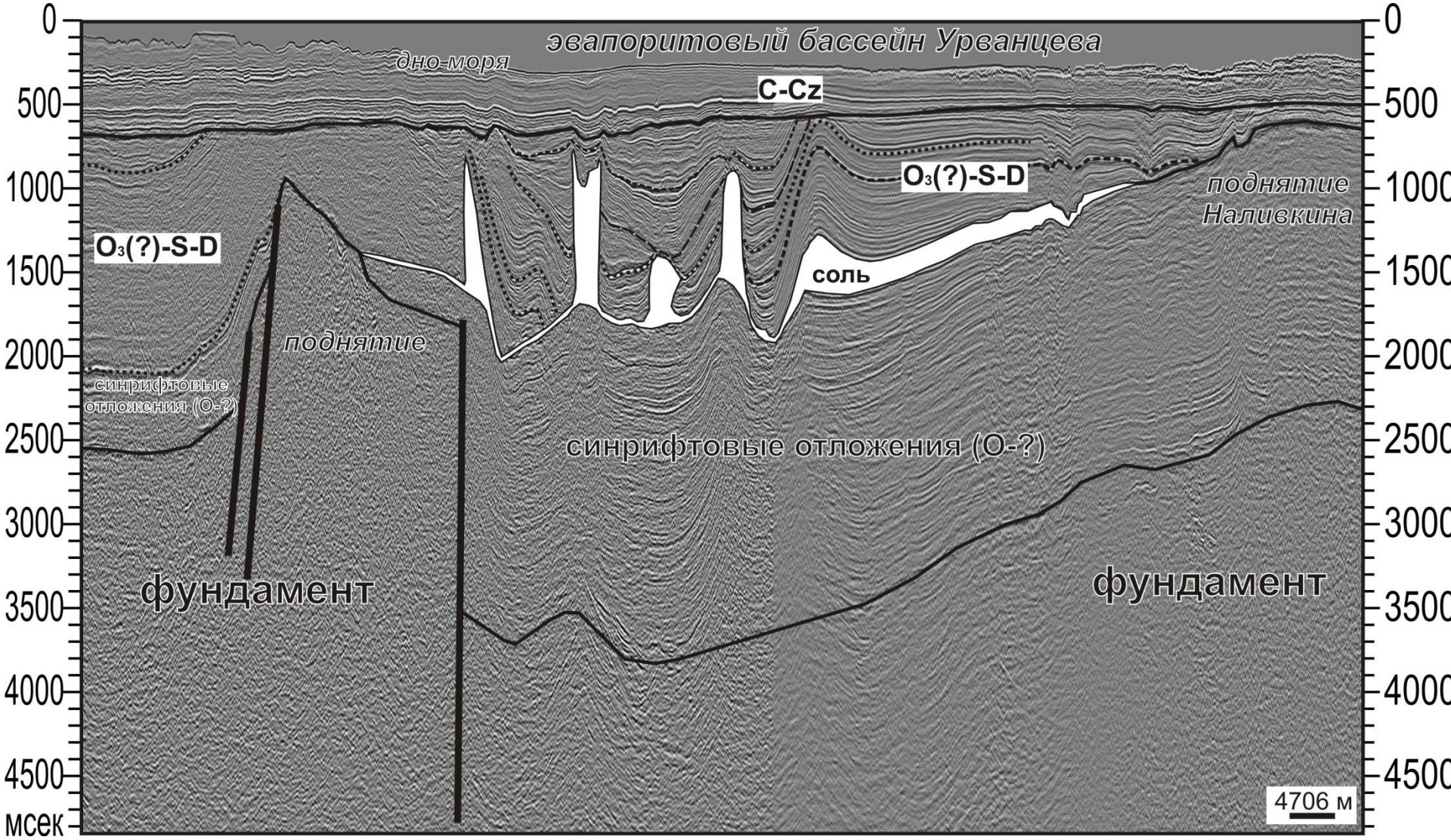
эвапоритовый бассейн Урванцева
дно-моря
C-Cz
O₃(?)-S-D
O₃(?)-S-D
поднятие Наливкина
соль
поднятие
синрифтовые отложения (O-?)
синрифтовые отложения (O-?)
фундамент
фундамент
4706 м
0
500
1000
1500
2000
2500
3000
3500
4000
4500
мсек

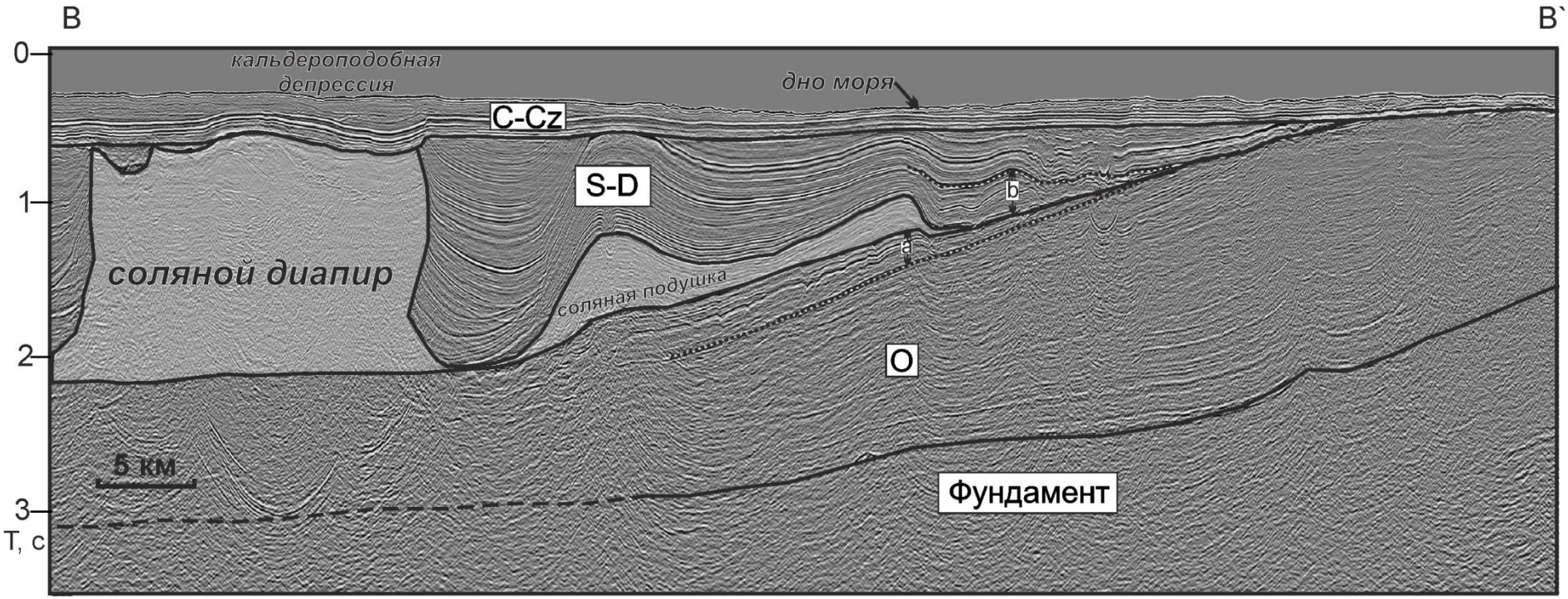
B
B`
0
1
2
3
T, c
кальдероподобная депрессия
дно моря
C-Cz
S-D
соляной диапир
соляная подушка
O
Фундамент
5 км
a
b

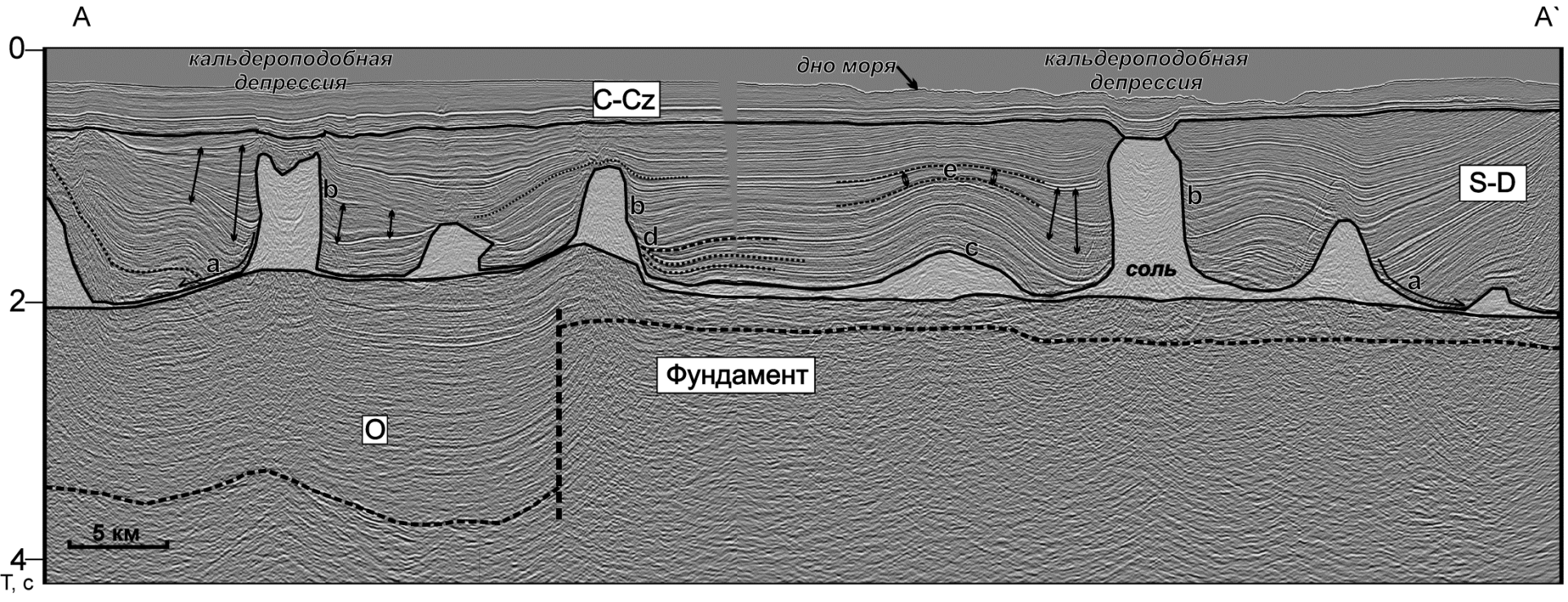
A
A`
0
2
4
T, c
кальдероподобная депрессия
дно моря
кальдероподобная депрессия
C-Cz
S-D
O
Фундамент
соль
a
b
b
d
c
e
b
a
5 км

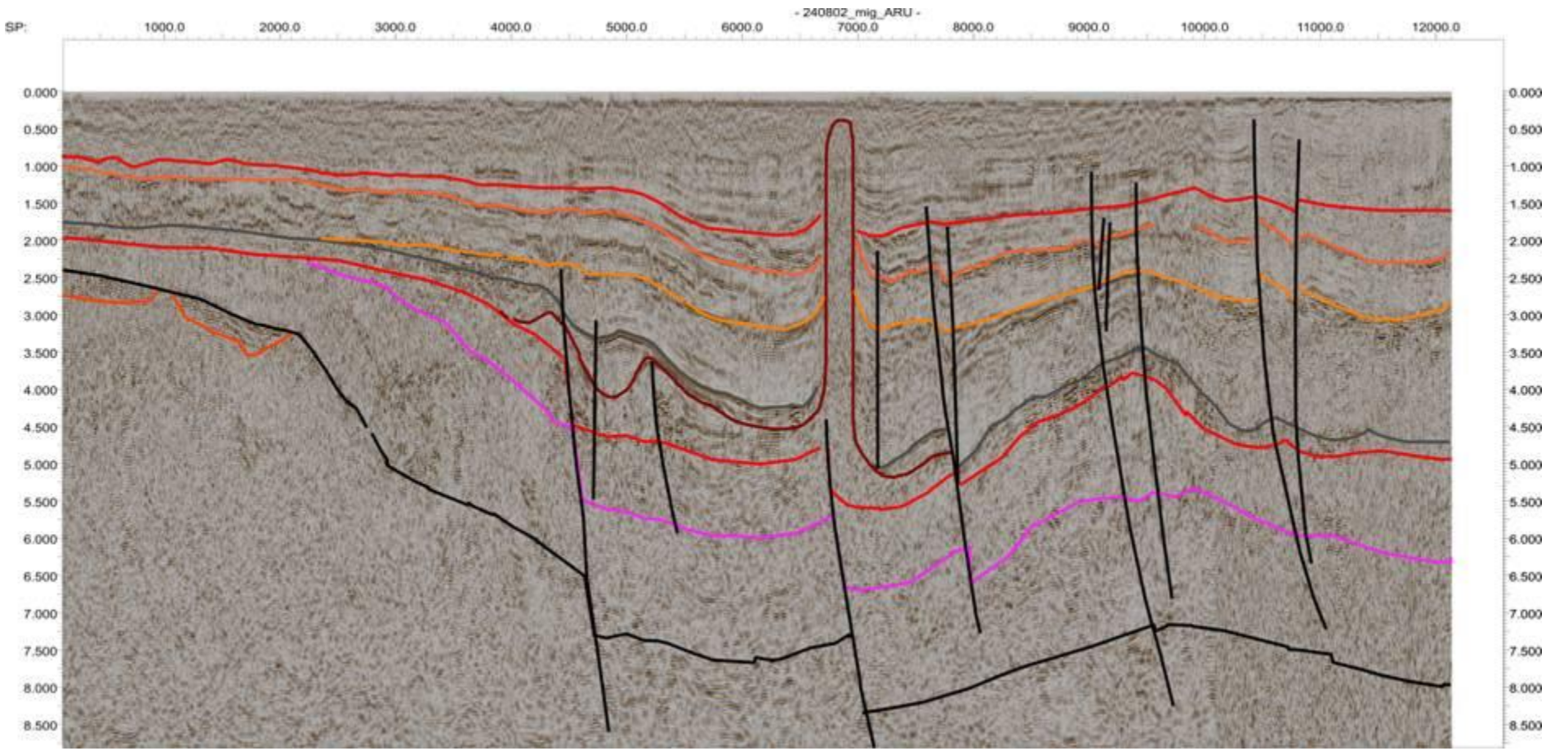
- 240802_mig_ARU -
SP:
1000.0
2000.0
3000.0
4000.0
5000.0
6000.0
7000.0
8000.0
9000.0
10000.0
11000.0
12000.0
0.000
0.500
1.000
1.500
2.000
2.500
3.000
3.500
4.000
4.500
5.000
5.500
6.000
6.500
7.000
7.500
8.000
8.500

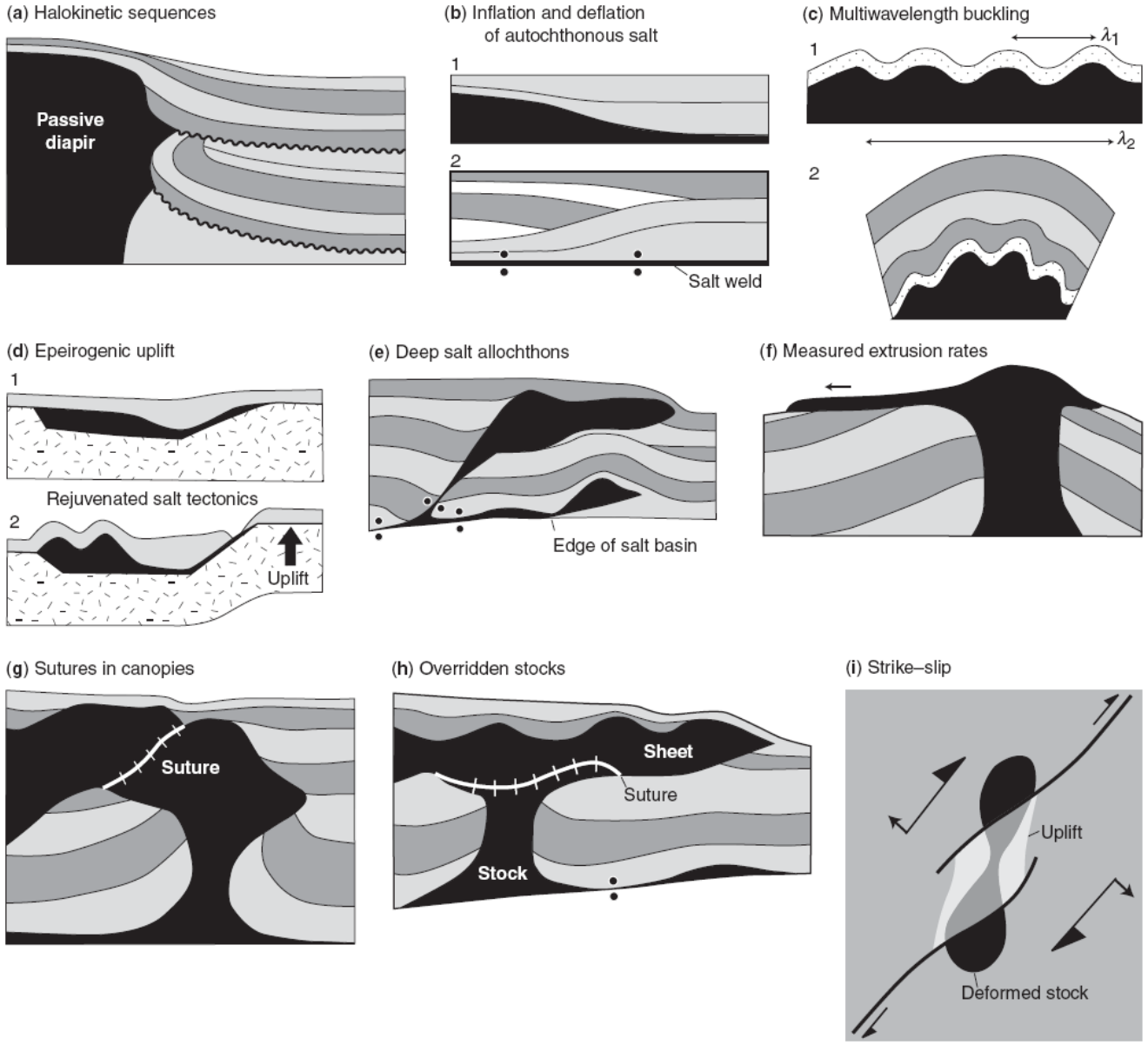

Fig. 1. Some concepts in salt tectonics recently discovered or improved: (**a**) halokinetic sequences around passive diapirs; (**b**) inflation and deflation of autochthonous salt layers; (**c**) multiwavelength (λ_1 and λ_2) compressional folding in thickening strata; (**d**) epeirogenic crustal uplift rejuvenating salt tectonics on passive margins; (**e**) emplacement of deep, old, allochthonous fringes; (**f**) directly measured rates of subaerial salt extrusion; (**g**) salt sutures; (**h**) surging salt canopies overriding small stocks; and (**i**) strike-slip (here transtensional) enhancing or retarding salt diapirism.

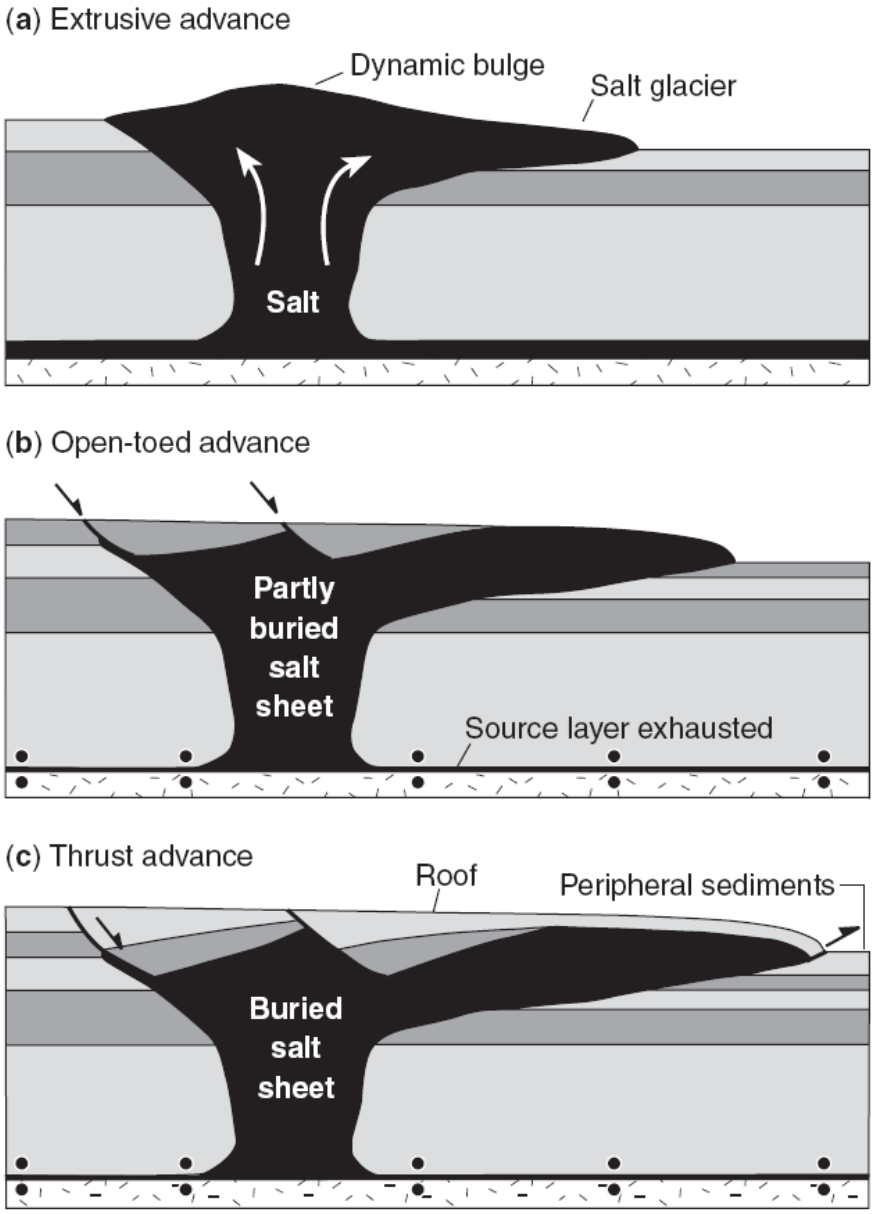

Fig. 6. Schematic cross-sections showing three ways in which salt sheets can advance, depending on their state of burial. After Hudec & Jackson (2009).

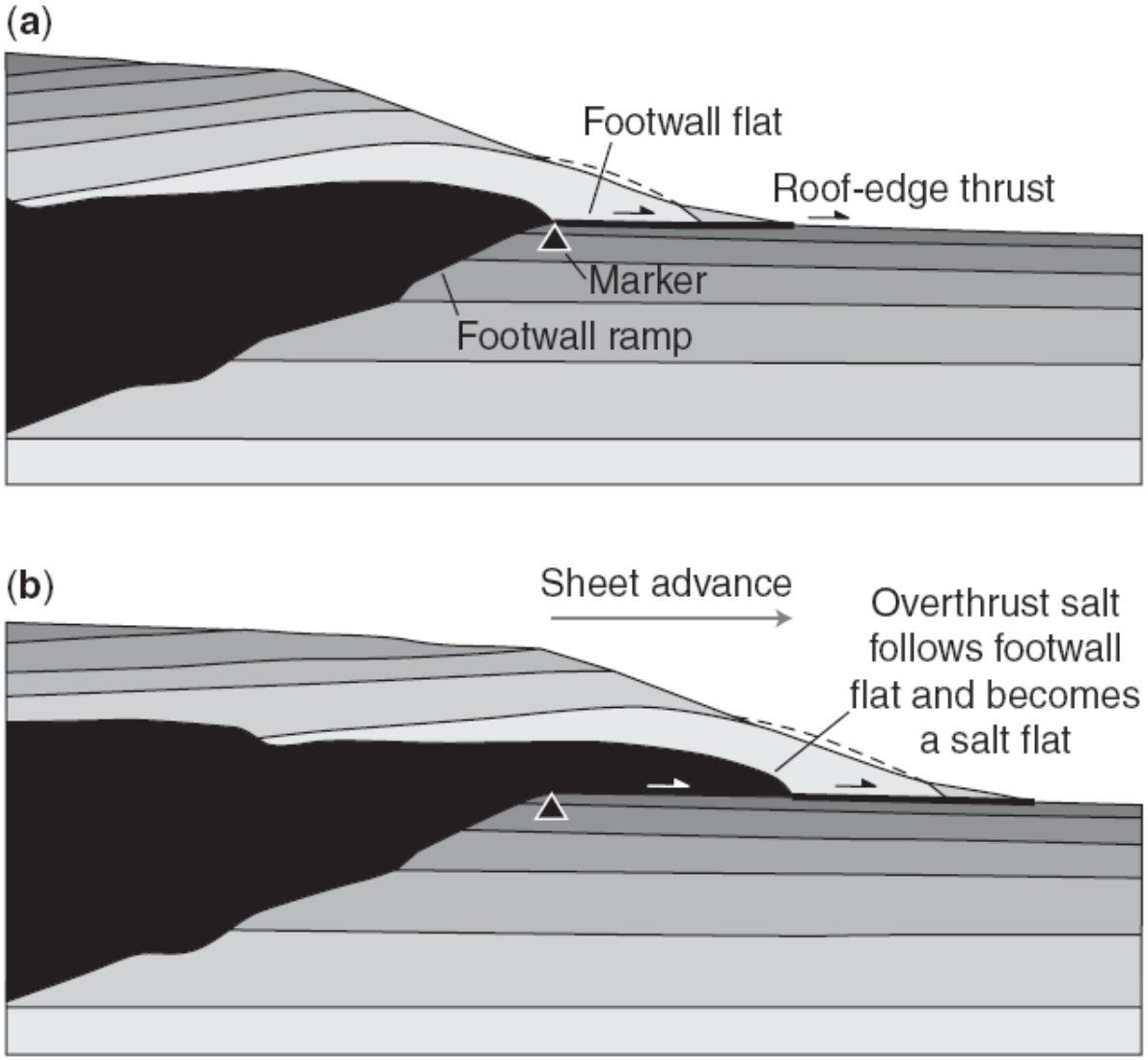

Fig. 9. Schematic cross-sections showing how a thrust flat (**a**) can later become a salt flat (**b**) as a salt canopy advances along the thrust. This change creates ambiguities in interpreting a stepped base of salt.

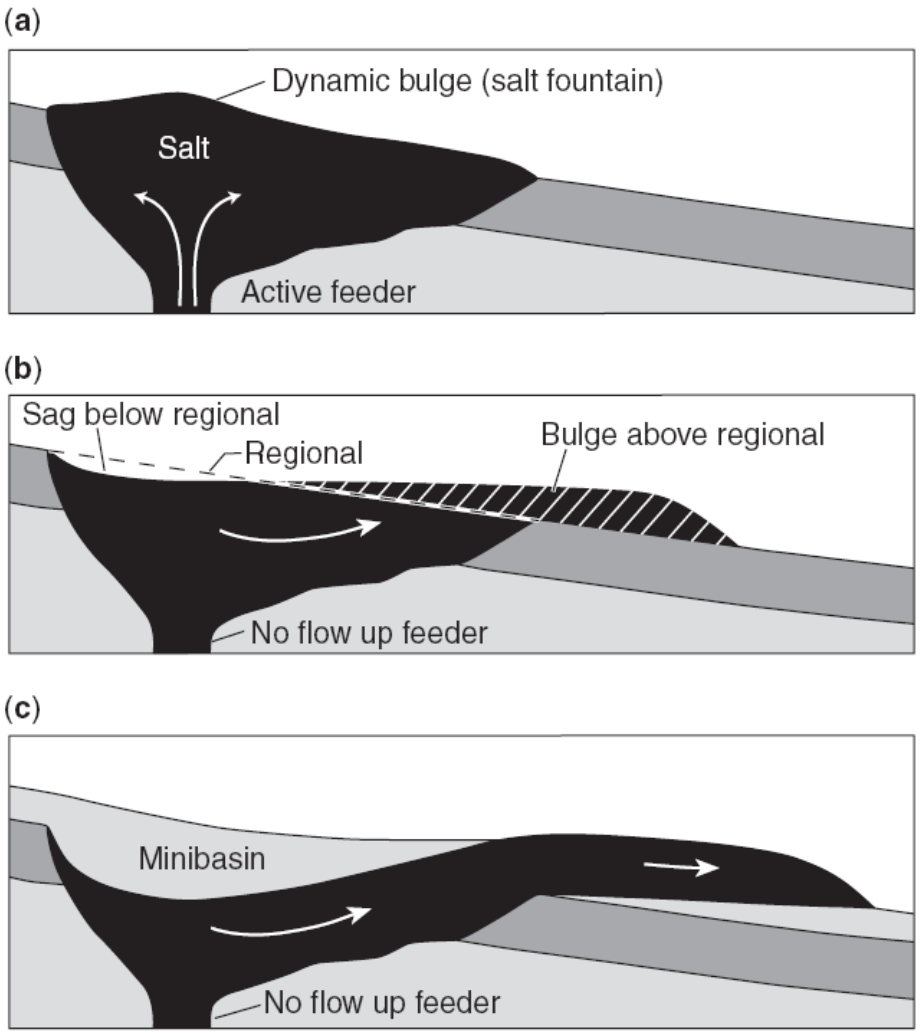

Fig. 15. Schematic cross-sections showing how decay of a dynamic bulge of salt can create a minibasin. (**a**) Above an active feeder, the dynamic pressure of rising salt supports a salt fountain. (**b**) After salt supply wanes, the unsupported salt bulge sags by gravity spreading to form a flat-topped droplet of salt. The updip part of the salt surface sags below regional, creating space for a local depocentre. (**c**) Sediments can gather in the depocentre and further deepen it to form a minibasin. After Hudec *et al.* (2009).

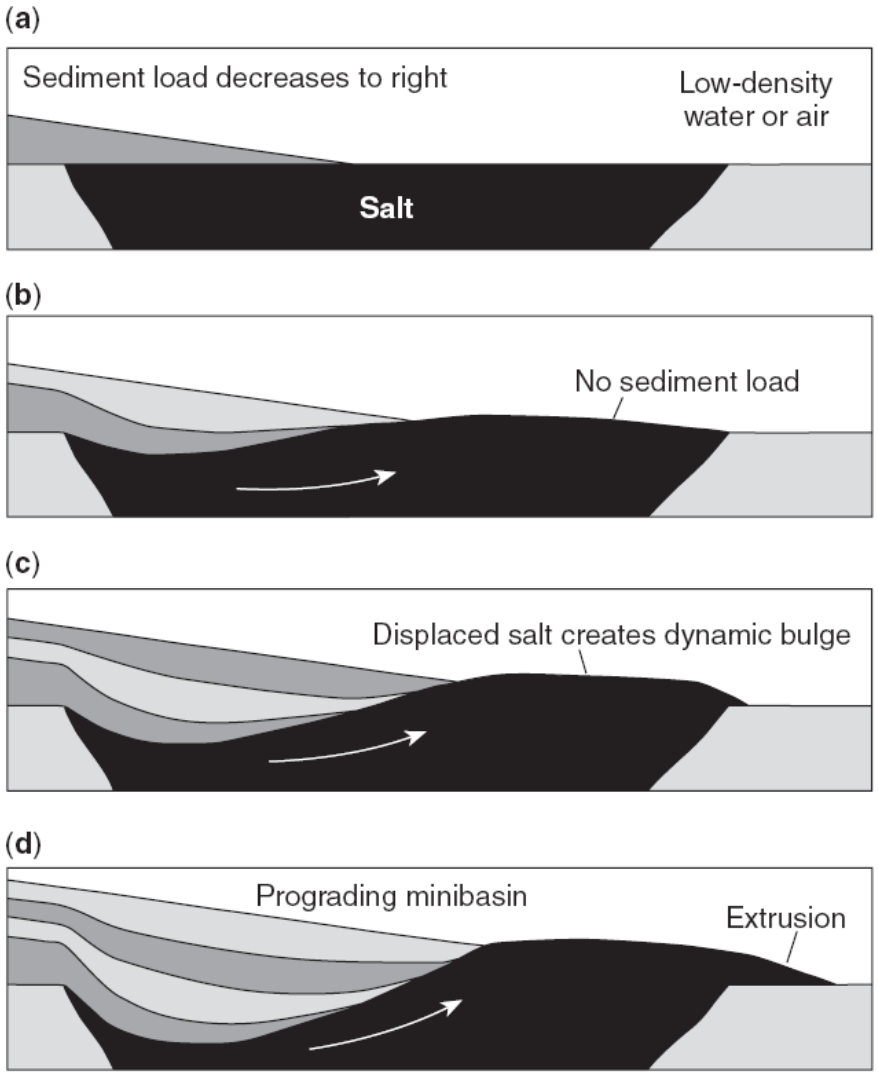

Fig. 16. Schematic cross-sections showing how the differential load of a prograding sedimentary wedge can initiate a minibasin. (**a**) A wedge of uncompacted sediments imposes a differential load because it is much denser than adjoining air or water. (**b**) The differential load causes the thick end of the sedimentary wedge to sink into salt, displacing salt seawards (**c**) and (**d**). After Hudec *et al.* (2009).

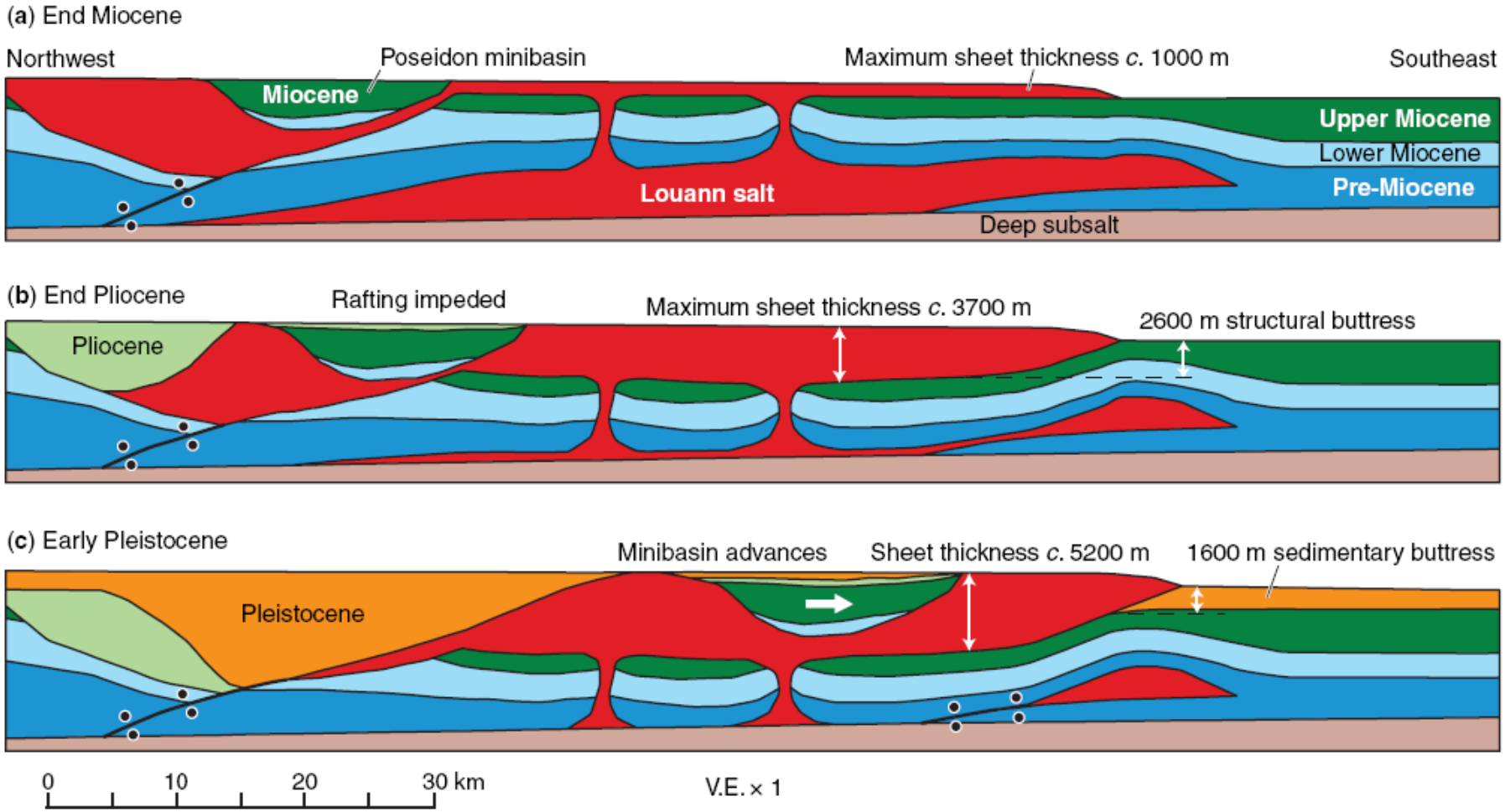

Fig. 20. Schematic restoration showing how a spreading salt canopy can carry an allochthonous minibasin seawards during the Pleistocene. (**a**) The original Miocene location of the minibasin is unknown, but the restoration shows a stratigraphic gap into which the Miocene strata may have fitted. (**b**) The salt canopy thickened by ponding against a late Miocene anticline, but this thickening was still not enough to carry the minibasin. (**c**) Rapid aggradation of lower Pleistocene sediments further thickened the salt canopy enough to transport the minibasin seawards. Vertical scale is only approximate but shows the initial thickness of Louann salt as *c.* 4 km, a thickness used in other restorations (Peel *et al.* 1995). However, the autochthonous salt layer has been variably inflated and deflated, expelled to several canopy levels, and lost to the world ocean, so estimates of the original thickness are highly speculative.

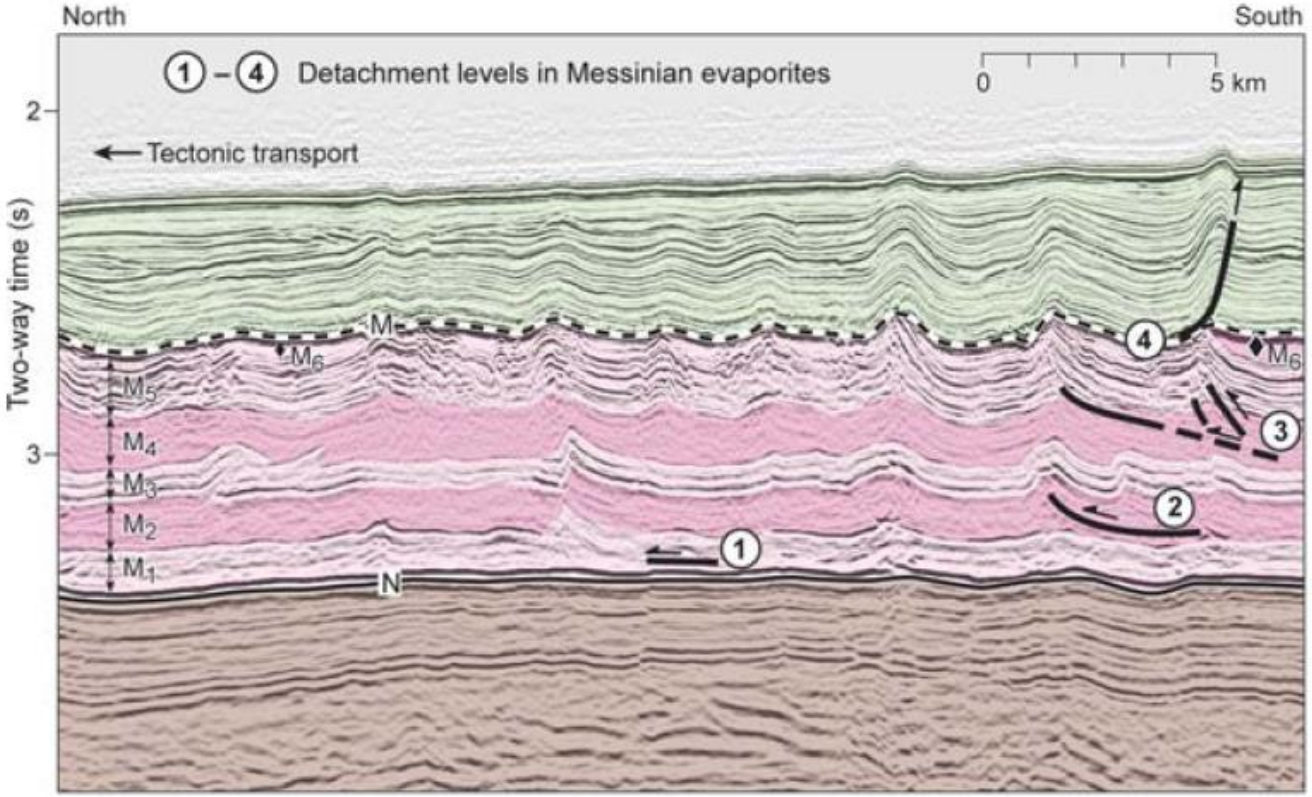

Fig. 3. Seismic profile from the Area A 3D seismic survey showing the deformed and layered Messinian evaporite sequence, consisting of units M1–6, overlain by a less-deformed and partially decoupled post-Messinian succession and underlain by relatively undeformed pre-Messinian strata.

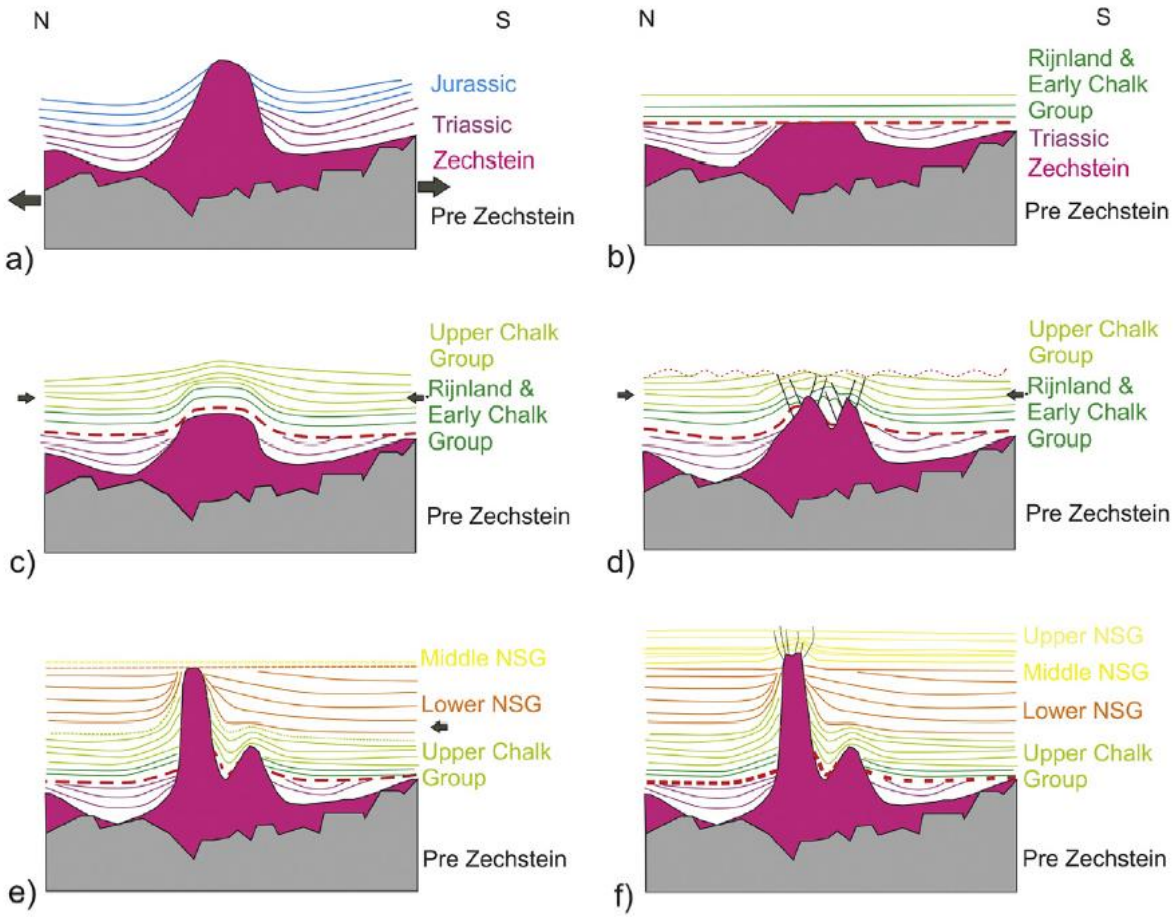

Figure 13. Schematic diagrams of the evolution of salt diapirs. a) Jurassic (201–154 Ma); b) Rijnland–Early Chalk Group (139–100 Ma); c) Upper Chalk Group (75–61.6 Ma); d) Base Lower North Sea Group (61.6 Ma); e) Middle North Sea Group (61.6–12 Ma); f) present day geometry.

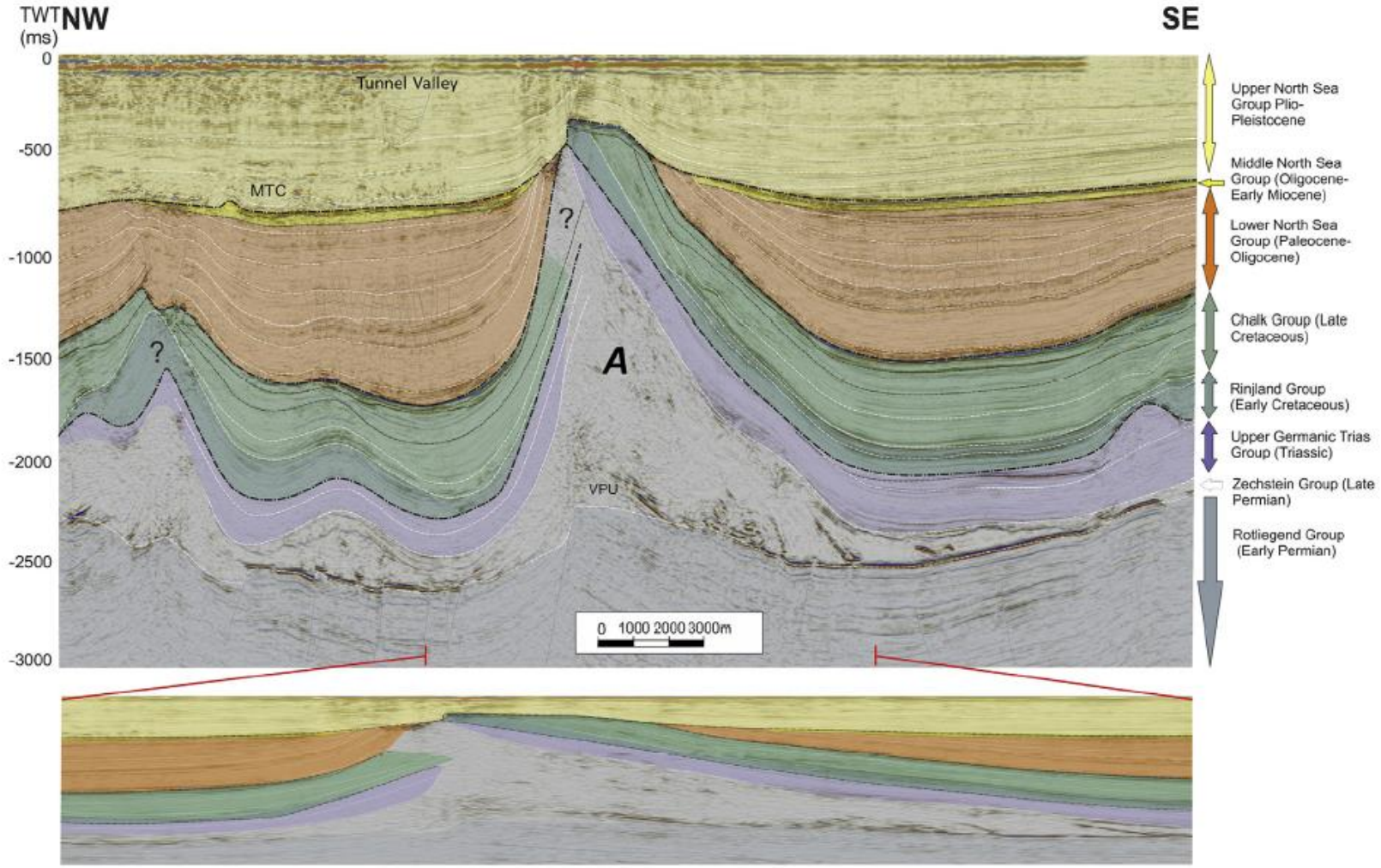

Figure 6. Interpreted seismic cross section NW–SE through *Salt Diapir A*. The complex asymmetrical salt structure and the geometry of the overburden are illustrated here. VPU = Velocity Pull Up; MTC = Neogene Mass Transport Complex. White dotted lines are key reflections, black dotted lines are unconformities. Glacial tunnel valley interpreted in the top 400 ms. Above: vertical exaggeration ×5; below: Vertical exaggeration ×1.5. Location of line in Figure 4a.

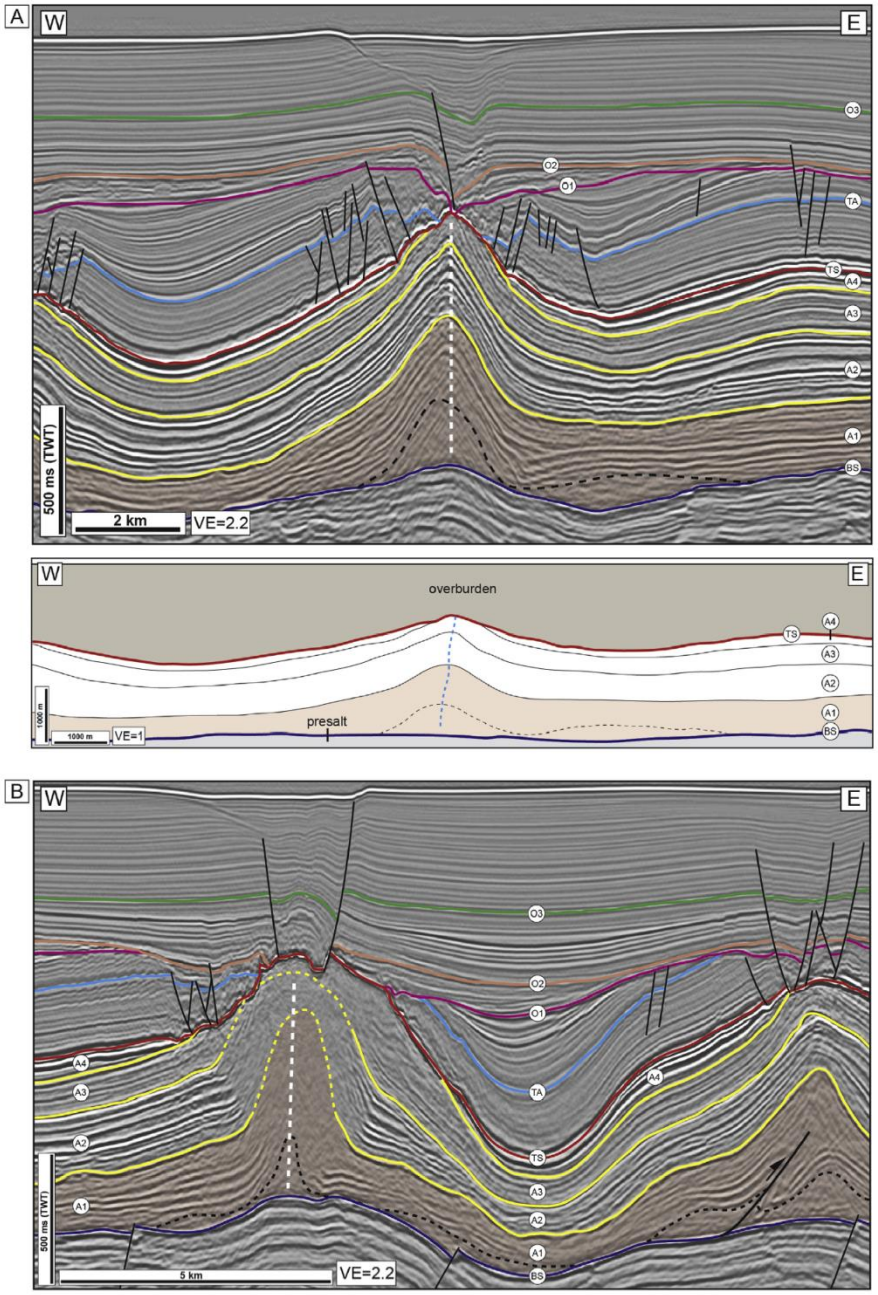
A
W
E
O3
O2
O1
TA
TS
A4
A3
A2
A1
BS
500 ms (TWT)
2 km
VE=2.2
W
E
overburden
TS
A4
A3
A2
A1
BS
presalt
1000 m
1000 m
VE=1
B
W
E
O3
O2
O1
A4
A3
A2
A1
TA
A4
TS
A3
A2
A1
BS
500 ms (TWT)
5 km
VE=2.2

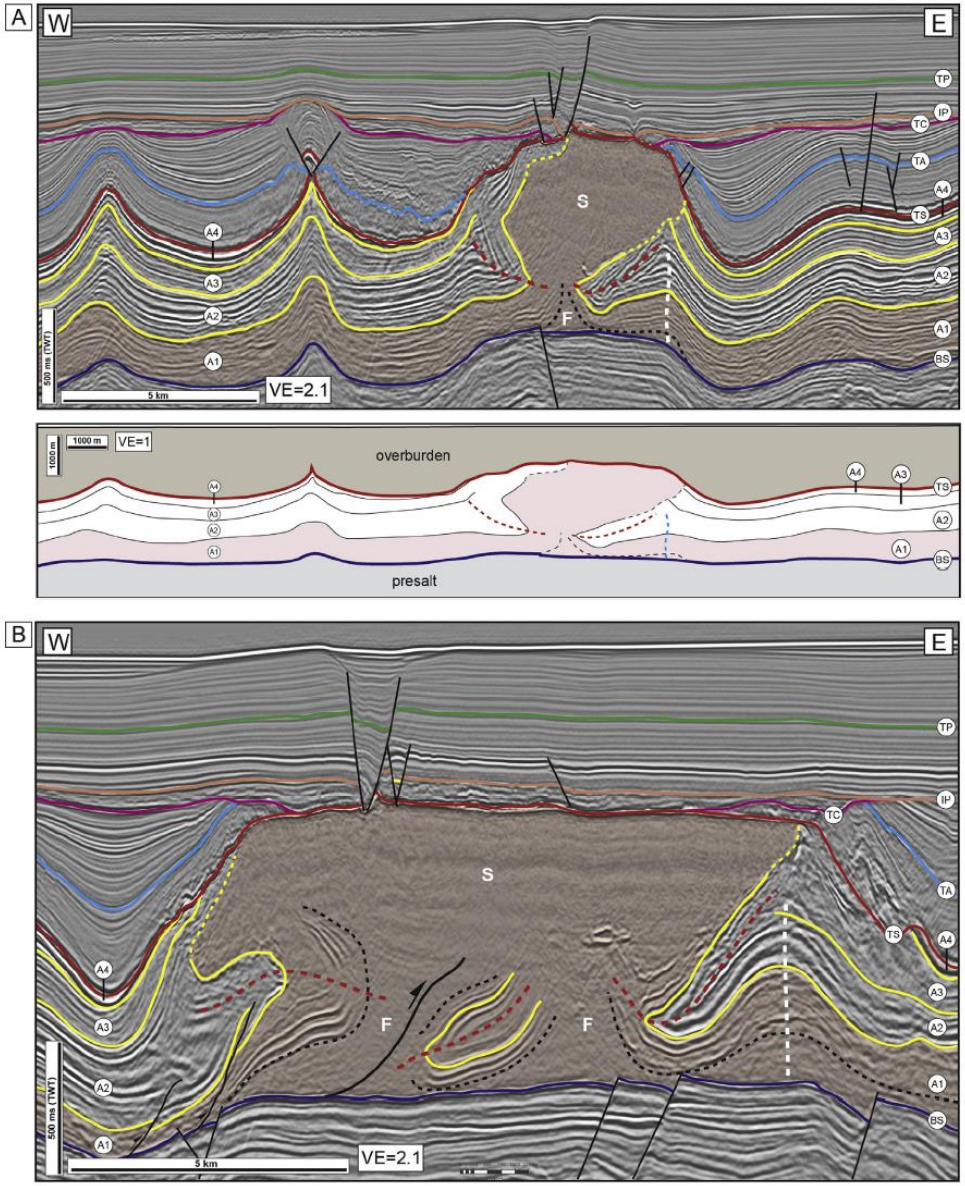

Fig. 11. Time-migrated seismic reflection profiles illustrating intrasalt feeders, sheets and canopies, and synclinal flaps (red dashed line shows axial trace). (A) Martin (Fig. 9A); below is a simple line drawing illstrating the intrasalt structure, based on a depth-converted seismic profile (VE = 1:1). (B) Martin (Fig. 9A); see Data Repository Item 2d for a simple line drawing illustrating the intrasalt structure, based on a depth-converted seismic profile (VE = 1:1). (C) Freddie (Fig. 9D); below is a simple line drawing illstrating the intrasalt structure, based on a depth-converted seismic profile (VE = 1:1). (D) Jimi (Fig. 9C); below is a simple line drawing illstrating the intrasalt structure, based on a depth-converted seismic profile (VE = 1:1). (E) Jimi (Fig. 9C); see Data Repository Item 2e for a simple line drawing illustrating the intrasalt structure, based on a depth-converted seismic profile (VE = 1:1). (F) Liam (Fig. 9B). (G) Liam (Fig. 9B); below is a simple line drawing illstrating the intrasalt structure, based on a depth-converted seismic profile (VE = 1:1). F = feeder; S = sheet. See Fig. 5B for spatial context of diapirs. Vertical exaggeration (VE) is shown on the profiles.

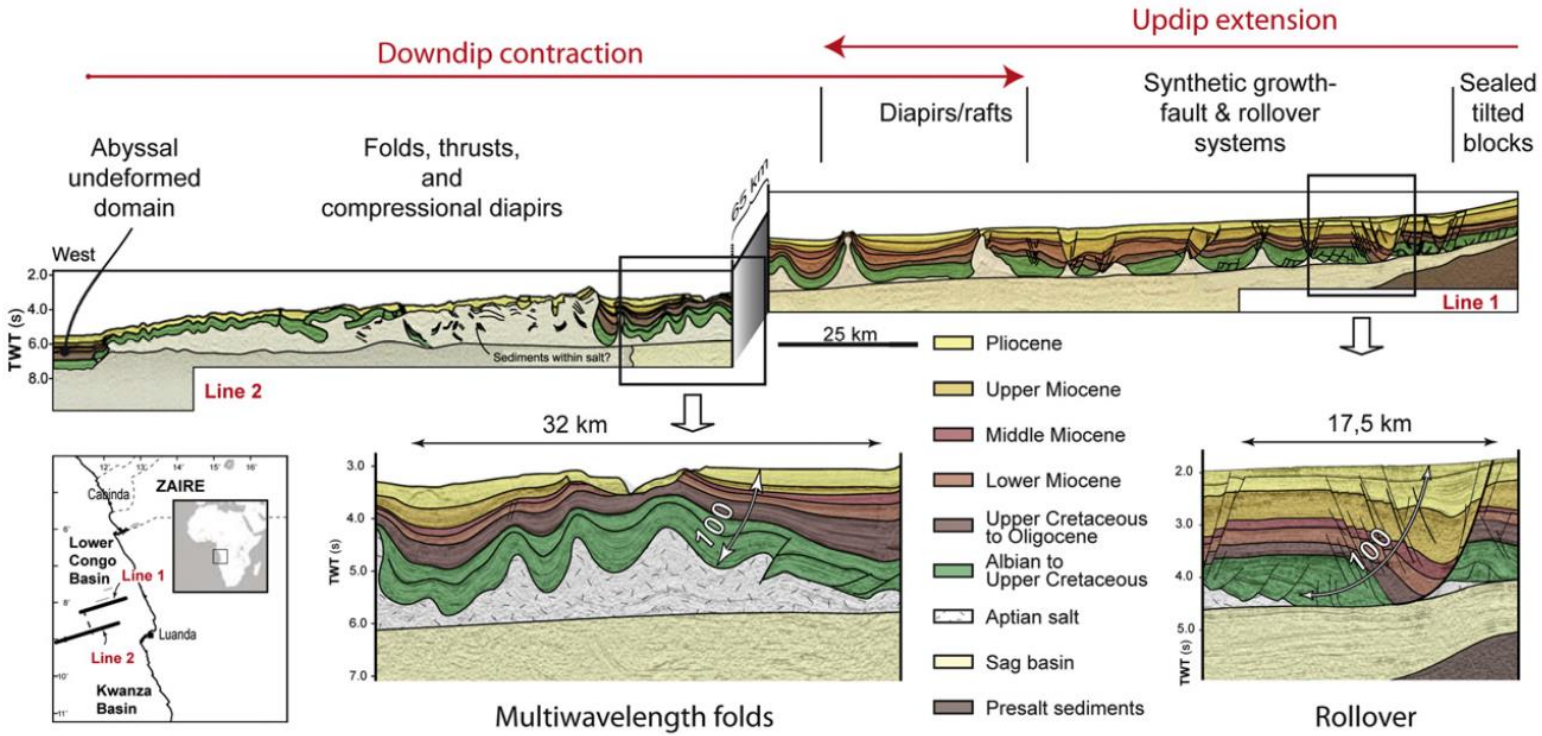

Fig. 1. Composite regional-scale cross-section of the north Angolan margin showing the extensional and contractional deformation domains and the type of individual structures. See location of the two sub-lines 1 and 2 in the lower left insert (modified after Fort et al., 2004a). The two enlargements of the cross-section show the growth character of structures since 100 Ma, in extension to the right and contraction to the left.

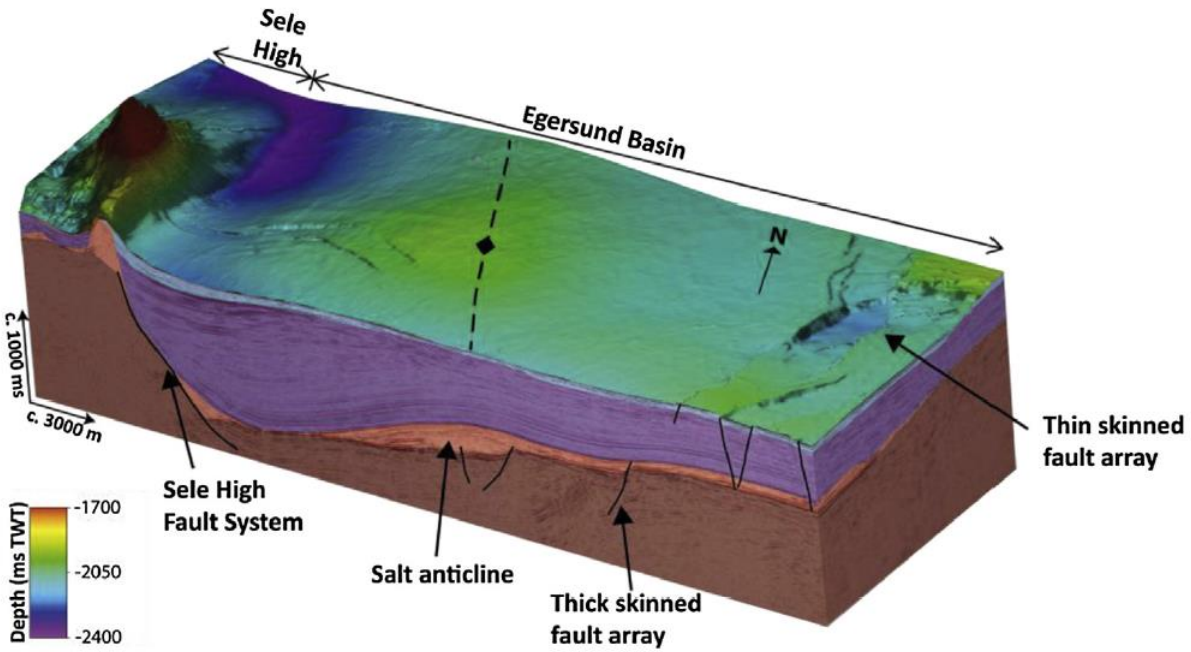

Fig. 2. Block diagram indicating the location of the studied fault array related to the salt anticline to the east. Horizon displayed on the top of the block is the top of the Bryne Formation. The colours on the sides of the block represent the age of the stratigraphy: Brown = Permian, Light red = Zechstein Supergroup, Purple = Triassic and Blue = Jurassic. (For interpretation of the references to colour in this figure legend, the reader is referred to the web version of this article.)

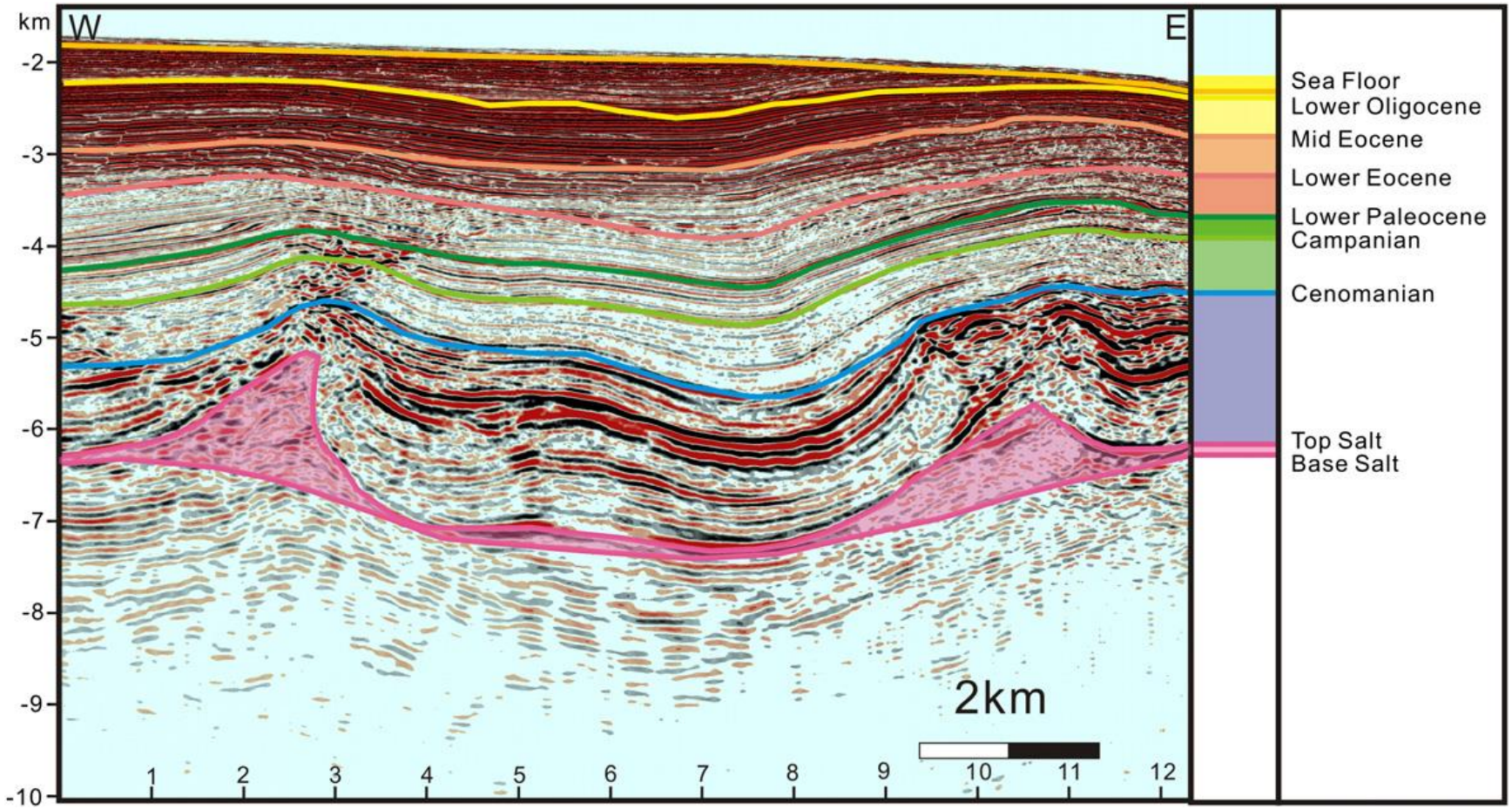

Seismic stratigraphy in the slope of the central Jequitinhonha Basin and seismic marker horizons of basinwide unconformities used for interpretation of the 2D seismic
data in the study area.

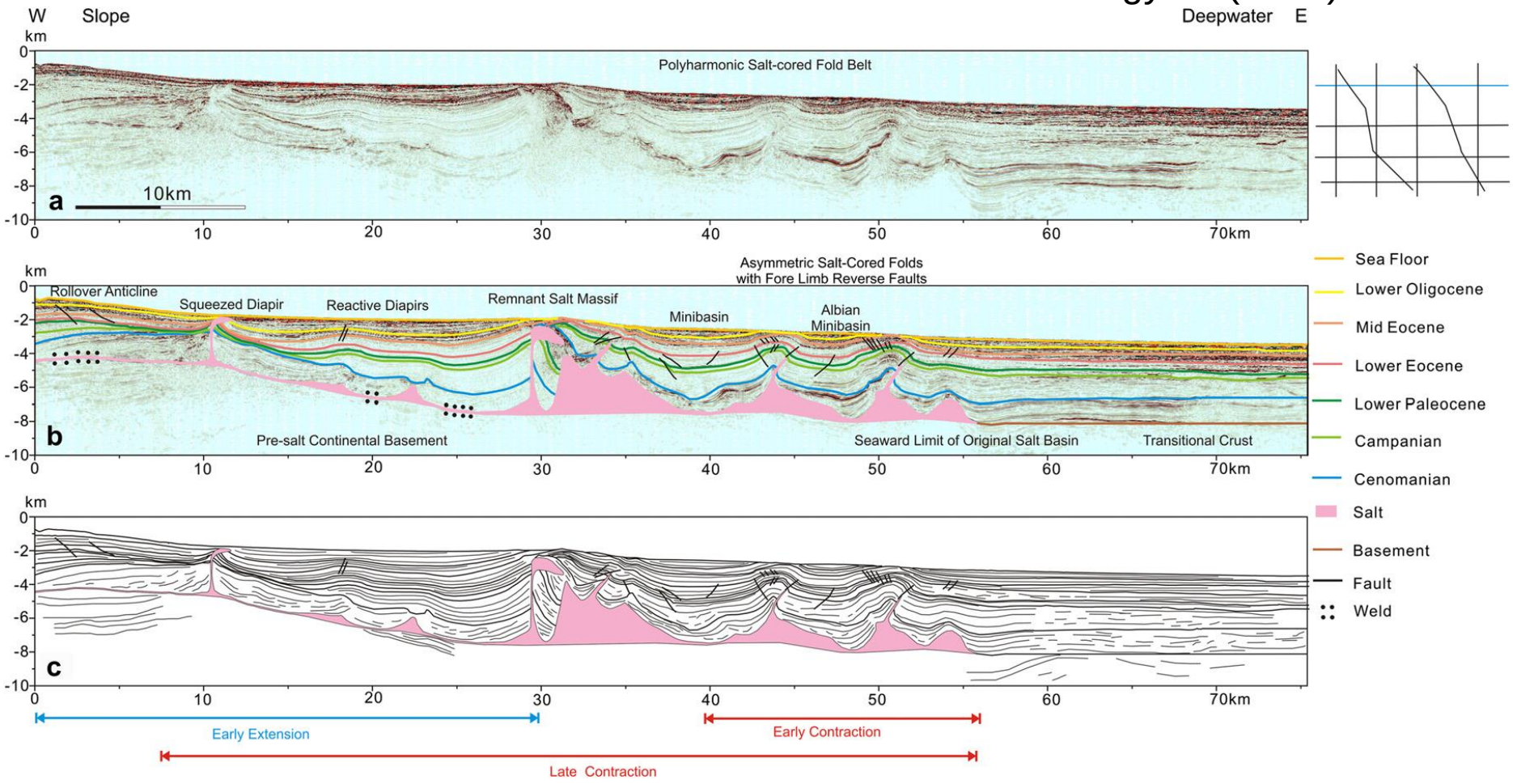

Interpretation of 2D seismic section D1. a) seismic section; b) seismic section with interpretation; c) line interpretation.

J. Adam et al. / Marine and Petroleum Geology 37 (2012) 101e120

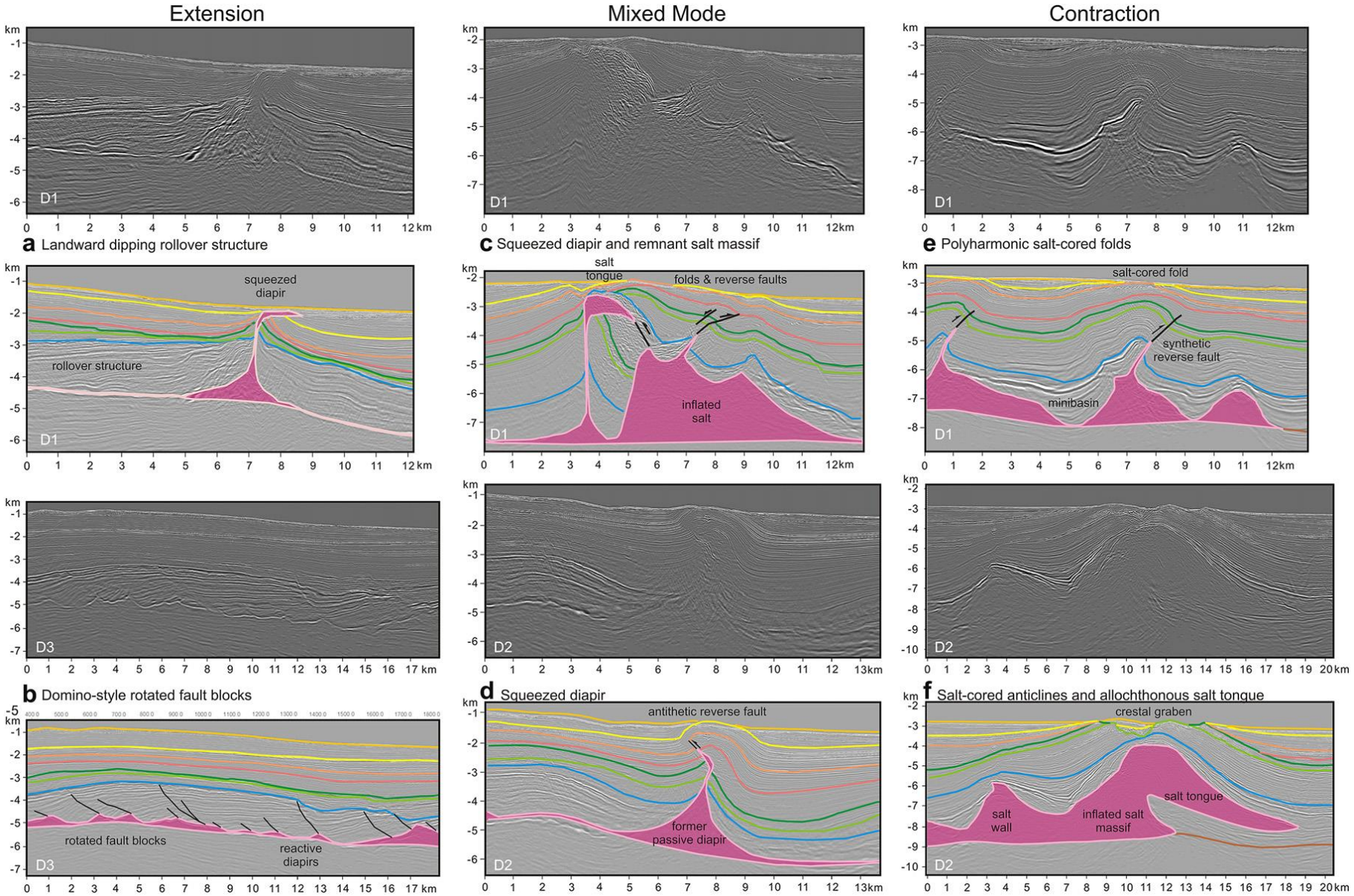

Detailed seismic sections and interpretations of extensional (a, b), mixed mode (c, d) and contractional salt structures (e, f) observed in the seismic dip sections D1eD3.

J. Adam et al. / Marine and Petroleum Geology 37 (2012) 70e100

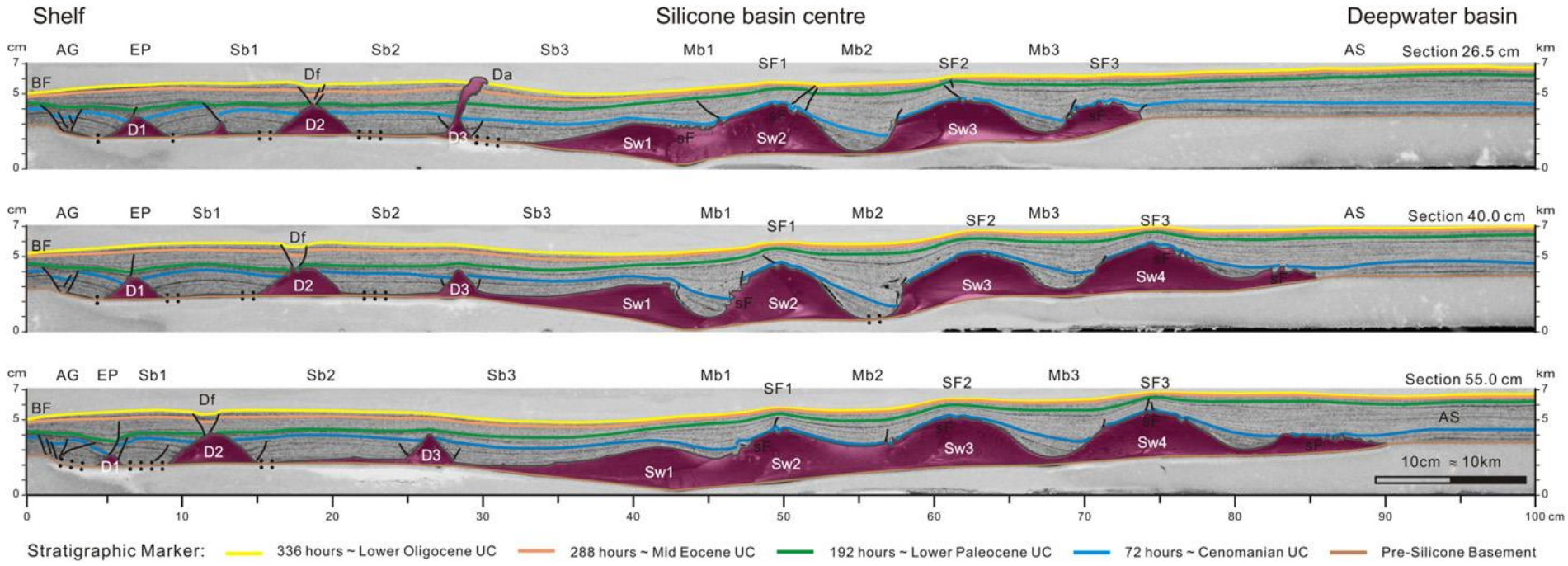

Representative sections of experiment JB4 (location shown in Fig. 12). Experiment scale (in cm) is comparable to the seismic sections (in km) in accordance with
the geometric scaling factor. Silicone features and depocentres numbered sequentially from shelf to deepwater basin; D e diapir, Df e late diapir collapse, Da e active diapir,
Sw e silicone wall, SF e silicone-cored fold, sF e early small-wavelength folds, BF e basinward listric fault, AG e asymmetric graben, EP e expulsion rollover, Sb e silicone
withdrawal basin, Mb e minibasin, AS e aggradational deepwater sequence, : e primary silicone weld.

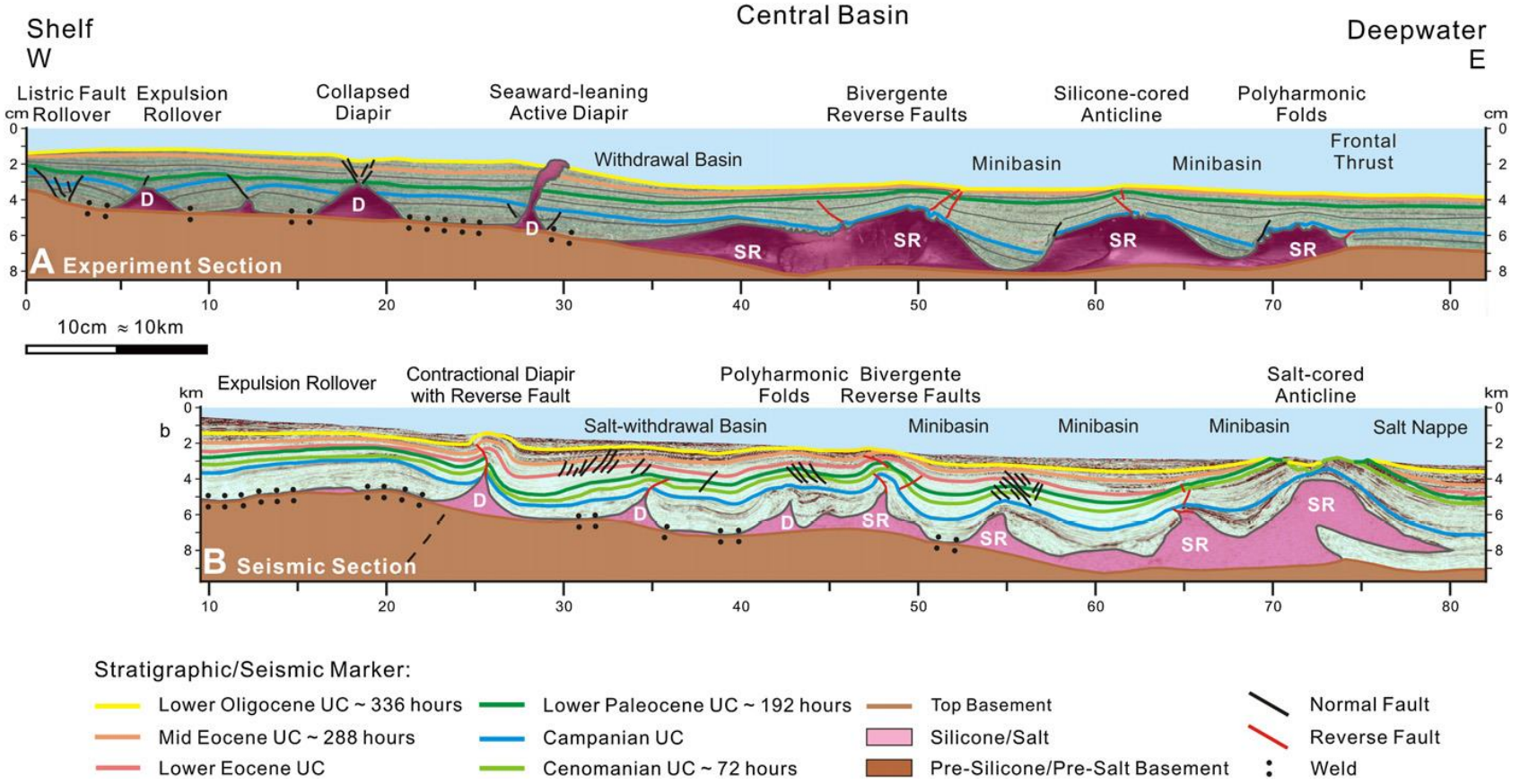

Comparison of structural styles and depocentres in the JB4 experiment section (26.5 cm) and seismic interpretation of line D2. Both sections show a comparable
structural architecture, e.g. polyharmonic folds, bivergent reverse faults, squeezed diapirs, minibasins and salt/silicone-cored anticlines in the deepwater basin. Position of
experiment section shown in Figure 10 and in Figure 12. Due to technical limitations the experiment ended at the Lower Oligocene equivalent experiment time when final kinematic
and depositional pattern were established. Consequently, structures in seismic section underwent an additional 24 Ma years of shortening.

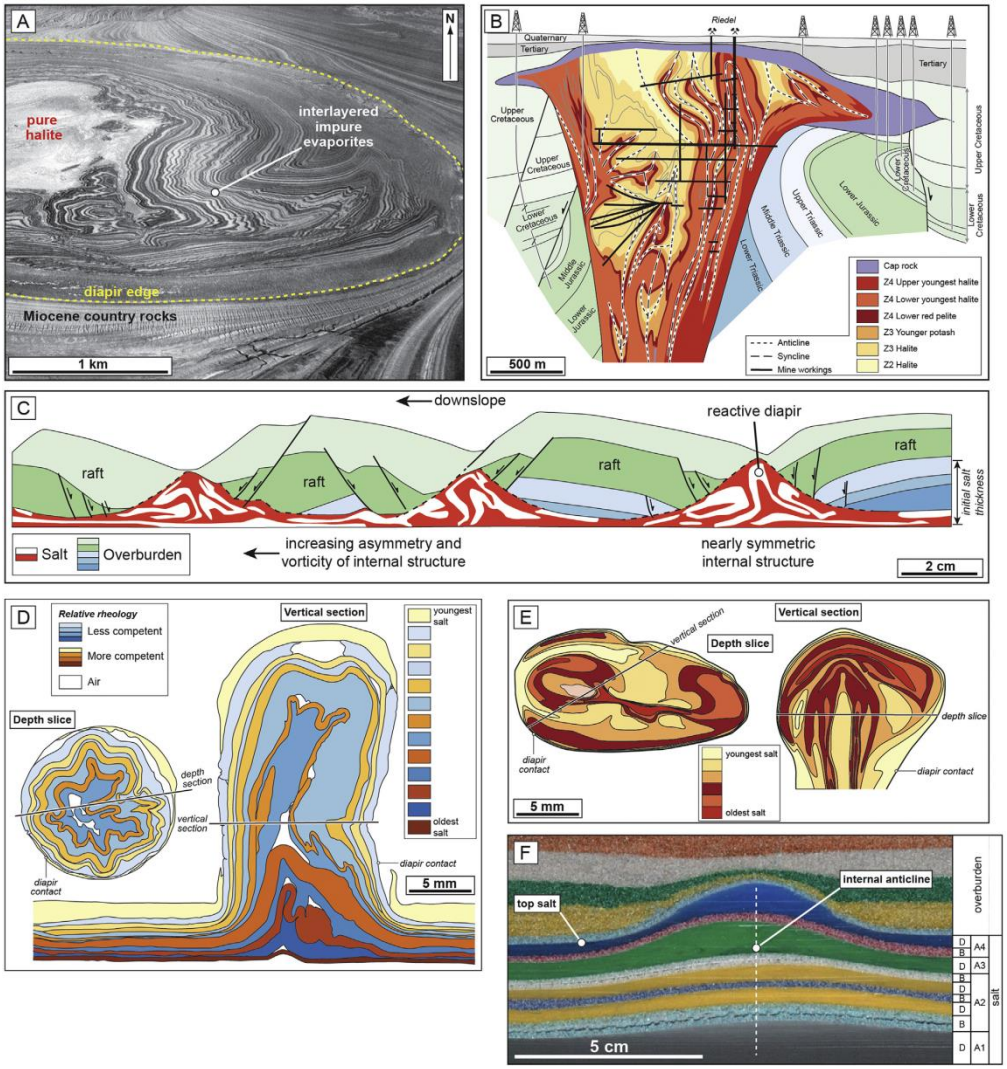

Examples of intrasalt structures. (A) Natural diapir exposed in the Great Kavir, Iran (Jackson et al., 1990). The intrasalt stratigraphy here is similar to that in the Santos Basin, with massive halite-dominated sequences being overlain by impure, interlayered evaporites (see Fig. 4). (B) Intrasalt structure revealed by mining of a natural diapir (H€anigsen-Wathlingen salt dome, Germany) (modified from Schachl, 1987). Much of the intrasalt structure is inferred from limited three-dimensional coverage provided by galleries and boreholes. (C) Physical model of intrasalt structure in salt rollers formed by thin-skinned extension (modified from Brun and Mauduit, 2009). The strain markers were initially vertical rather then horizontal so do not track bedding strain. However, these markers clearly reveal intrasalt vorticity. (D) Physical model of intrasalt structure formed in a simple salt stock (Escher and Kuenen, 1929). Note extreme thickness changes in incompetent units (blue shading) caused by enhanced migration of material from these more mobile layers from the source layer into the diapir. (E) Physical model of intrasalt structure in a density-neutral salt analogue inside a salt stock (modified from Jackson and Talbot, 1989). (F) Physical model of a relatively simple internal (i.e. intrasalt) anticline formed at the end of a salt wall in a density-inverted salt analogue. A1-4 are analogues for the similarly named intrasalt units referred to in the text. D j relatively low density, ductile layers; B j relatively dense, brittle layers. See Dooley et al. (2015b) for full details.

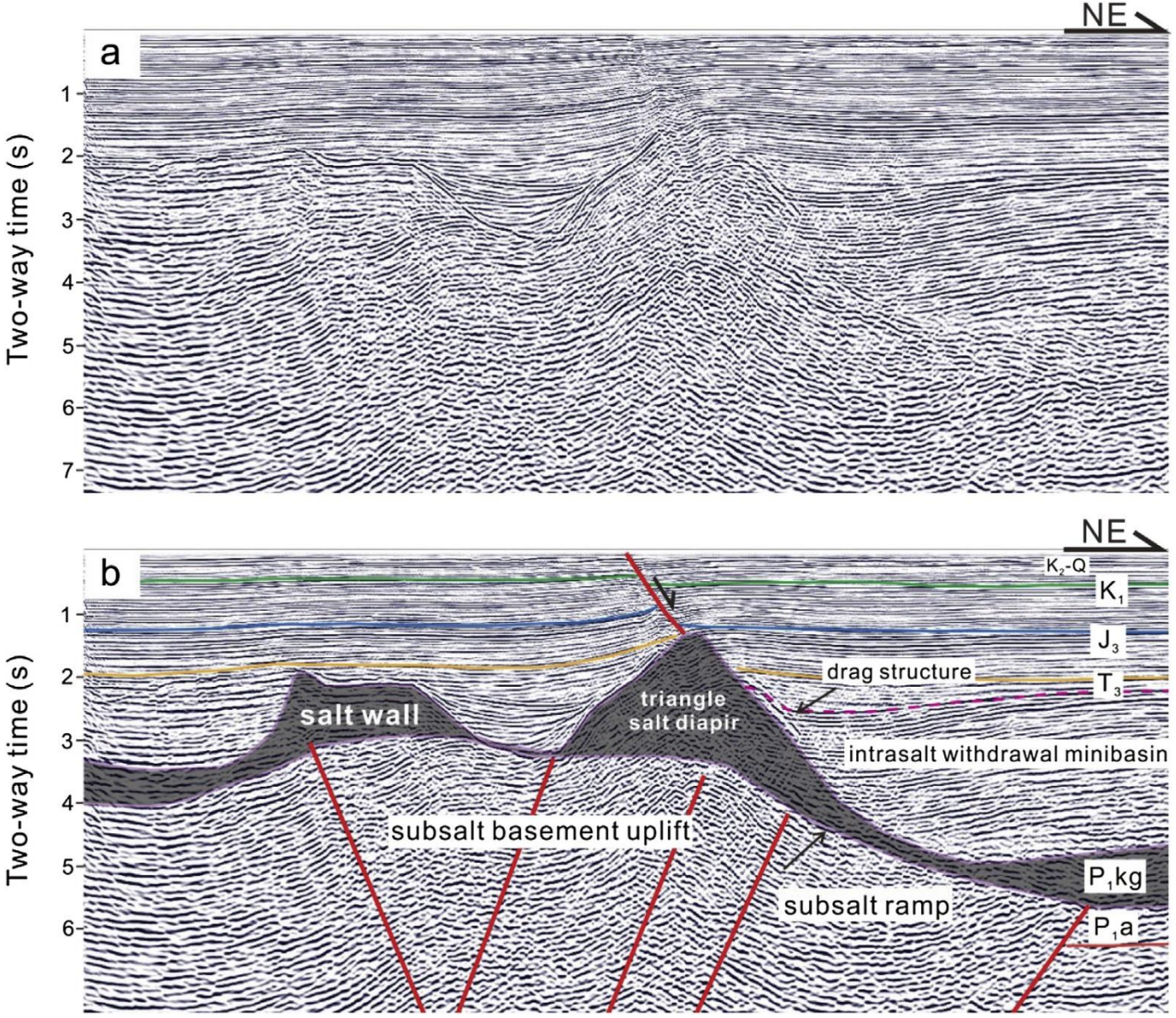

7. (a) Uninterpreted and (b) interpreted seismic section line 2 (see Fig. 5a for location) showing salt structures on the uplift basement in the M block of the Southern Precaspian Basin. The salt diapir was formed at the margin (the hinge between the uplift and the slope) of the subsalt uplift.

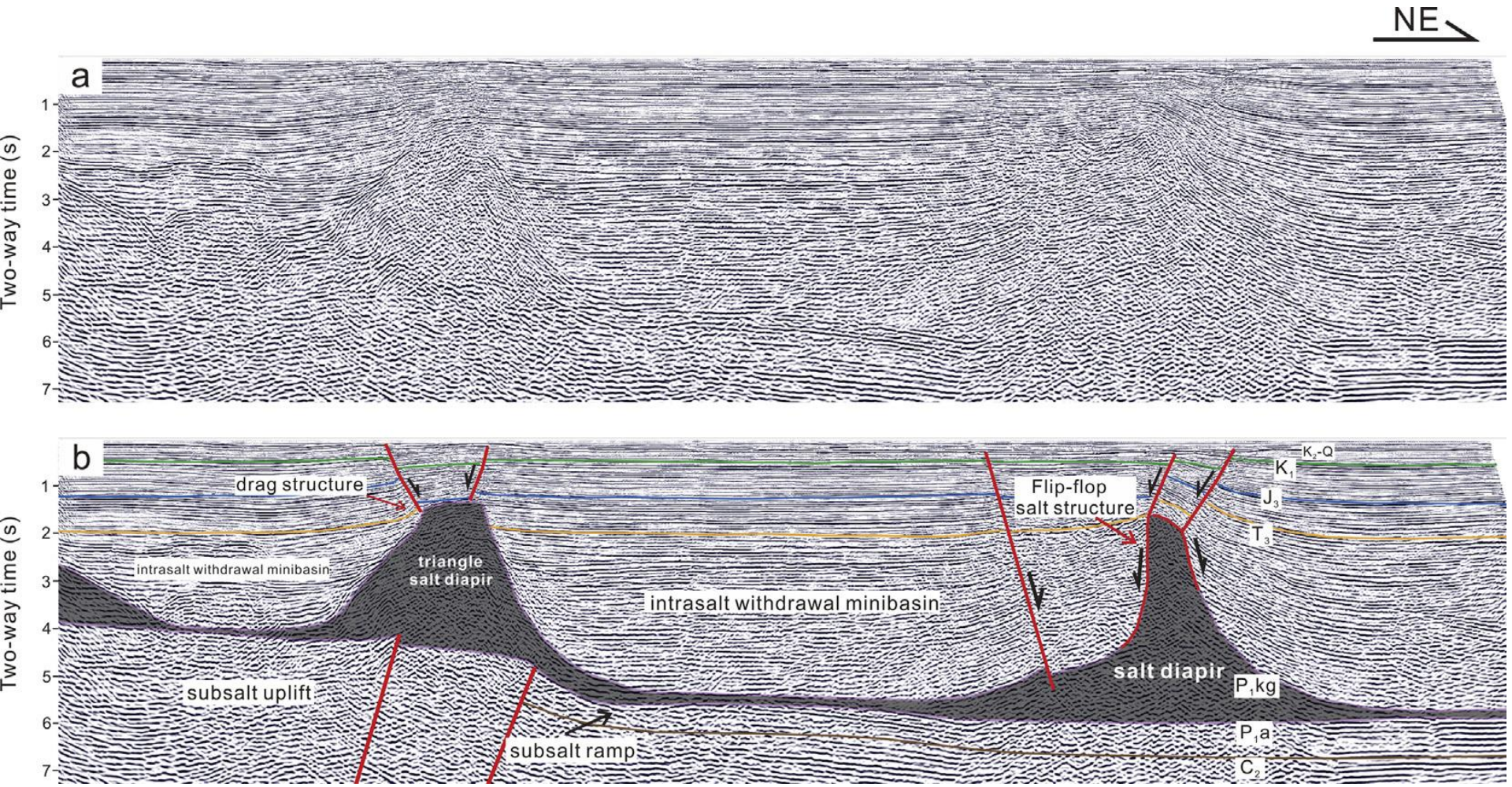

Figure 8. (a) Uninterpreted and (b) interpreted seismic section Line 3 (see Fig. 5a for location) showing salt structures of the M block in the Southern Precaspian Basin. Note the
asymmetric reflection geometry in the overburden on the salt diapir (right) could be characteristic of 'flip-flop' salt structure, which is a type of salt structures that bears similarity
to reactive salt diapir except that it is asymmetric and can itself drive normal faulting as it grows (Quirk and Pilcher, 2012).

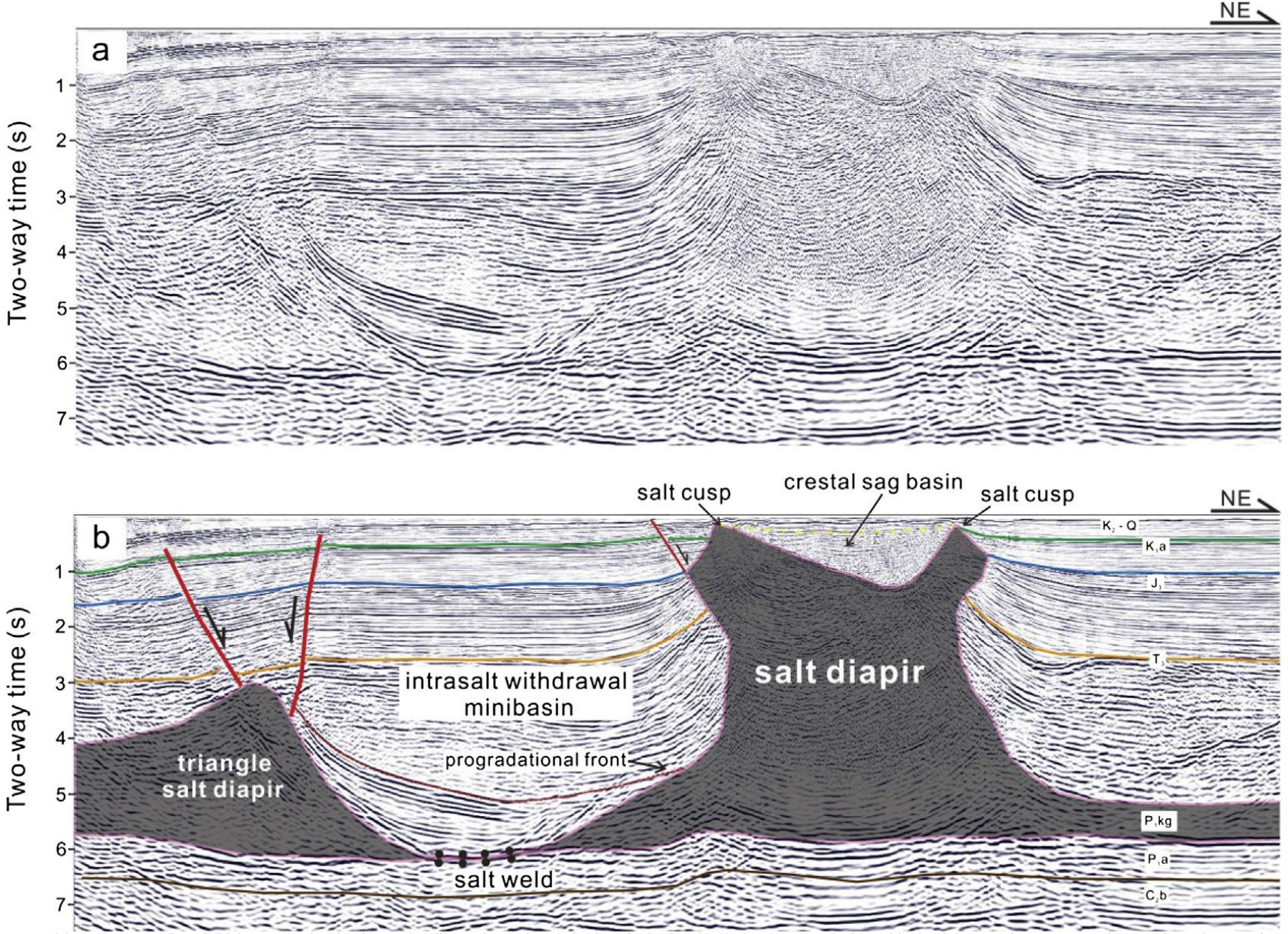

Figure 11. (a) Uninterpreted and (b) interpreted seismic section line 6 (see Fig. 5b for location) showing salt structures in the B block of the Southern Precaspian Basin. A large salt diapir (indented diapir, right) occurred at the progradational front. Moreover, the crestal sag basin between salt cusps suggested that lateral extension occurred in the research area (see Vendeville and Jackson, 1992). The lateral extension made the main salt diapir spreading and downbuilding (with the development of the crestal sag basin between salt cusps), and triggered a minor triangle reactive salt diapir (left).

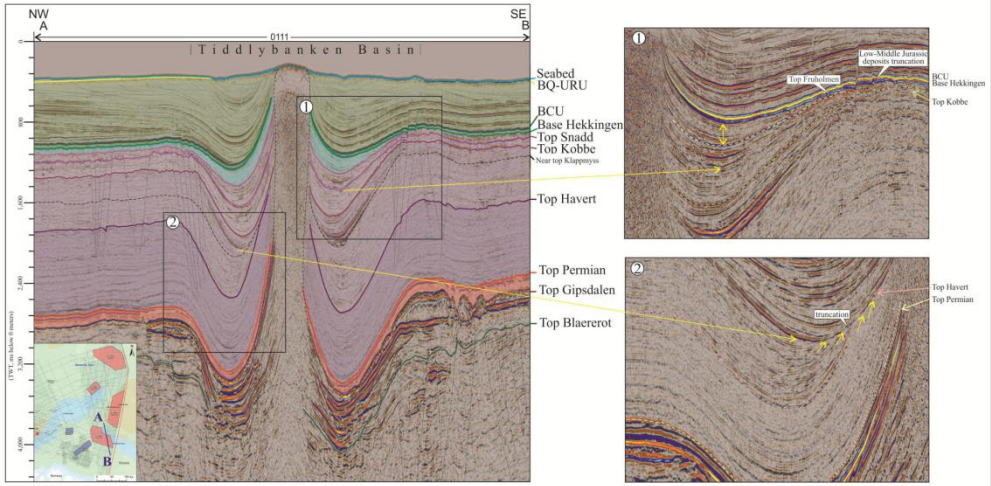

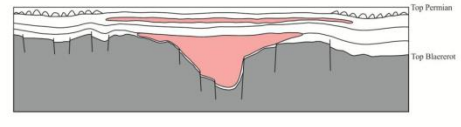

b) T_1 (~250Ma)

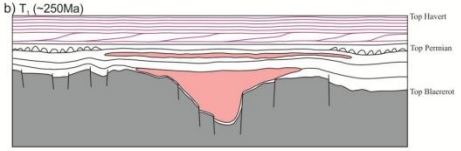

c) T_1 (~247 Ma)

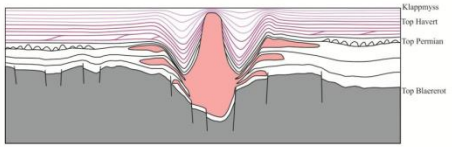

d) T_2 (~242 Ma)

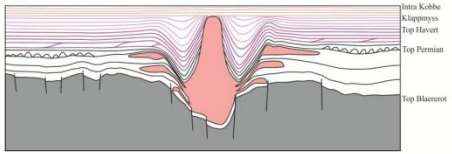

e) J_1 (~145 Ma)

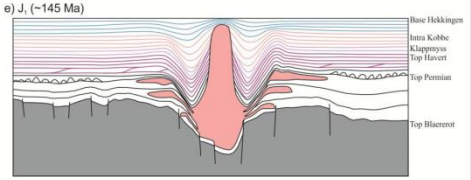

f) K_1 (~100 Ma)

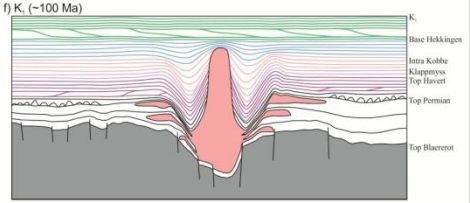

g) K_2 - Pg (~60 Ma)

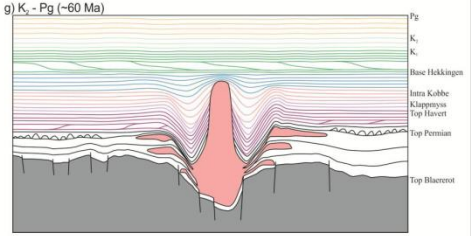

h) Recent

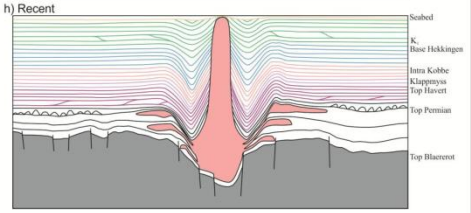

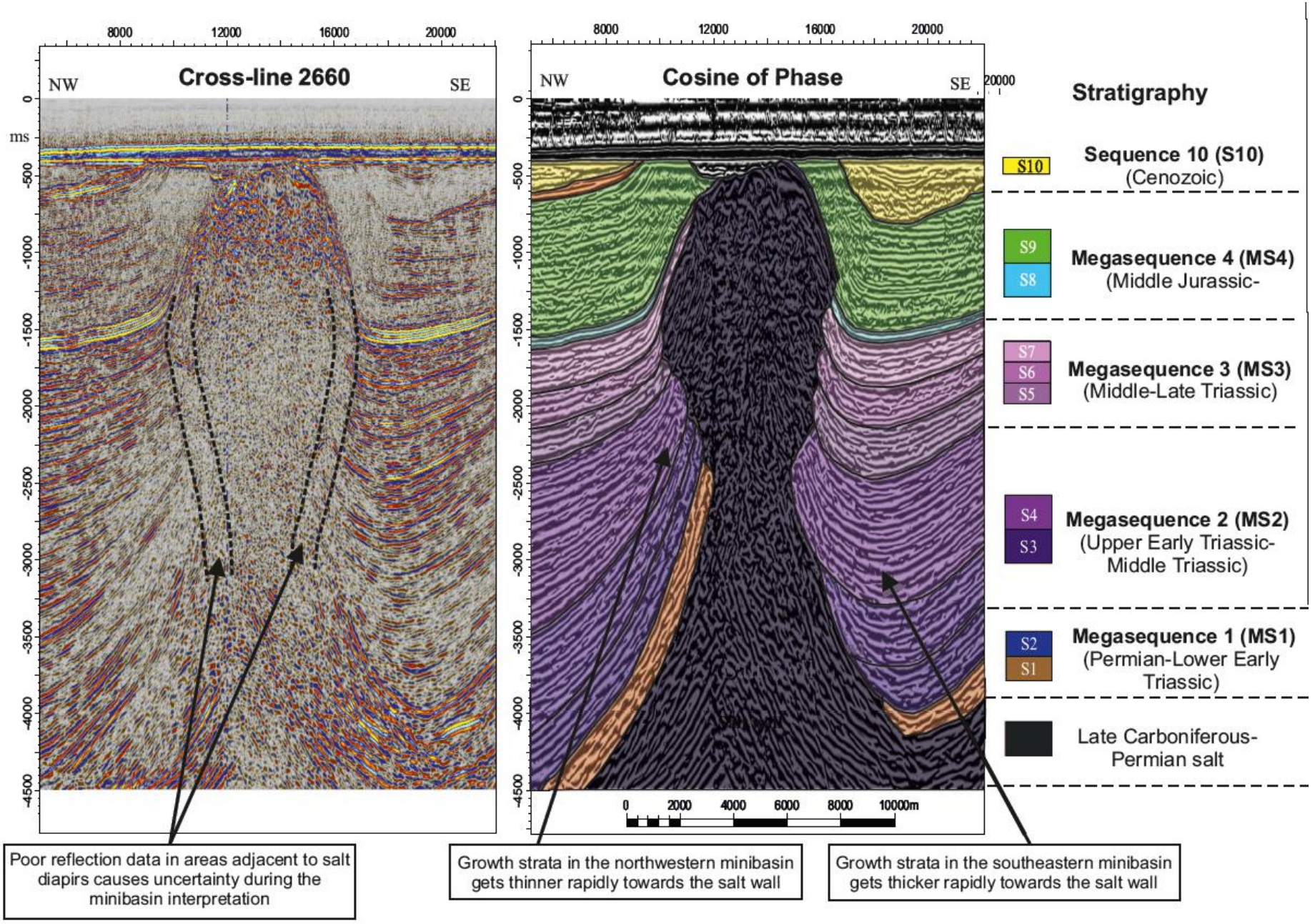
Cross-line 2660
NW
SE
ms
8000
12000
16000
20000
0
-500
-1000
-1500
-2000
-2500
-3000
-3500
-4000
-4500
Cosine of Phase
NW
SE
20000
0
2000
4000
6000
8000
10000m
Stratigraphy
S10
Sequence 10 (S10)
(Cenozoic)
S9
S8
Megasequence 4 (MS4)
(Middle Jurassic-
S7
S6
S5
Megasequence 3 (MS3)
(Middle-Late Triassic)
S4
S3
Megasequence 2 (MS2)
(Upper Early Triassic-
Middle Triassic)
S2
S1
Megasequence 1 (MS1)
(Permian-Lower Early
Triassic)
Late Carboniferous-
Permian salt
Poor reflection data in areas adjacent to salt diapirs causes uncertainty during the minibasin interpretation
Growth strata in the northwestern minibasin gets thinner rapidly towards the salt wall
Growth strata in the southeastern minibasin gets thicker rapidly towards the salt wall

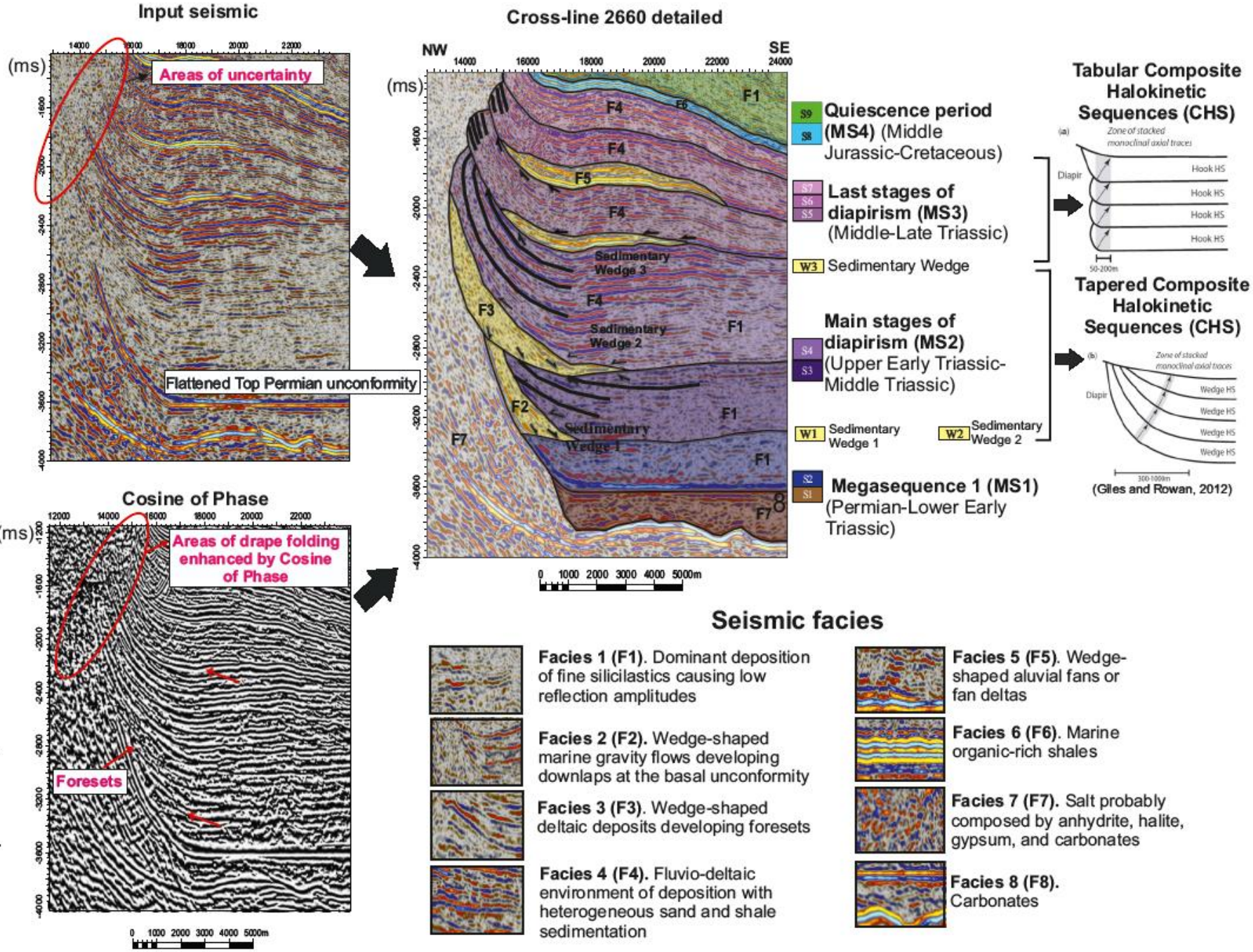
Input seismic
(ms)
Areas of uncertainty
Flattened Top Permian unconformity
Cross-line 2660 detailed
NW
SE
(ms)
F1
F2
F3
F4
F5
F6
F7
F8
Sedimentary Wedge 1
Sedimentary Wedge 2
Sedimentary Wedge 3
0 1000 2000 3000 4000 5000m
S9
S8
Quiescence period (MS4) (Middle Jurassic-Cretaceous)
S7
S6
S5
Last stages of diapirism (MS3) (Middle-Late Triassic)
W3
Sedimentary Wedge
S4
S3
Main stages of diapirism (MS2) (Upper Early Triassic-Middle Triassic)
W1
Sedimentary Wedge 1
W2
Sedimentary Wedge 2
S2
S1
Megasequence 1 (MS1) (Permian-Lower Early Triassic)
Tabular Composite Halokinetic Sequences (CHS)
Zone of stacked monoclinal axial traces
Diapir
Hook HS
50-200m
Tapered Composite Halokinetic Sequences (CHS)
Wedge HS
300-1000m
(Giles and Rowan, 2012)
Cosine of Phase
(ms)
Areas of drape folding enhanced by Cosine of Phase
Foresets
0 1000 2000 3000 4000 5000m
Seismic facies
Facies 1 (F1). Dominant deposition of fine silicilastics causing low reflection amplitudes
Facies 2 (F2). Wedge-shaped marine gravity flows developing downlaps at the basal unconformity
Facies 3 (F3). Wedge-shaped deltaic deposits developing foresets
Facies 4 (F4). Fluvio-deltaic environment of deposition with heterogeneous sand and shale sedimentation
Facies 5 (F5). Wedge-shaped aluvial fans or fan deltas
Facies 6 (F6). Marine organic-rich shales
Facies 7 (F7). Salt probably composed by anhydrite, halite, gypsum, and carbonates
Facies 8 (F8). Carbonates

Salt-related Gilbert deltas

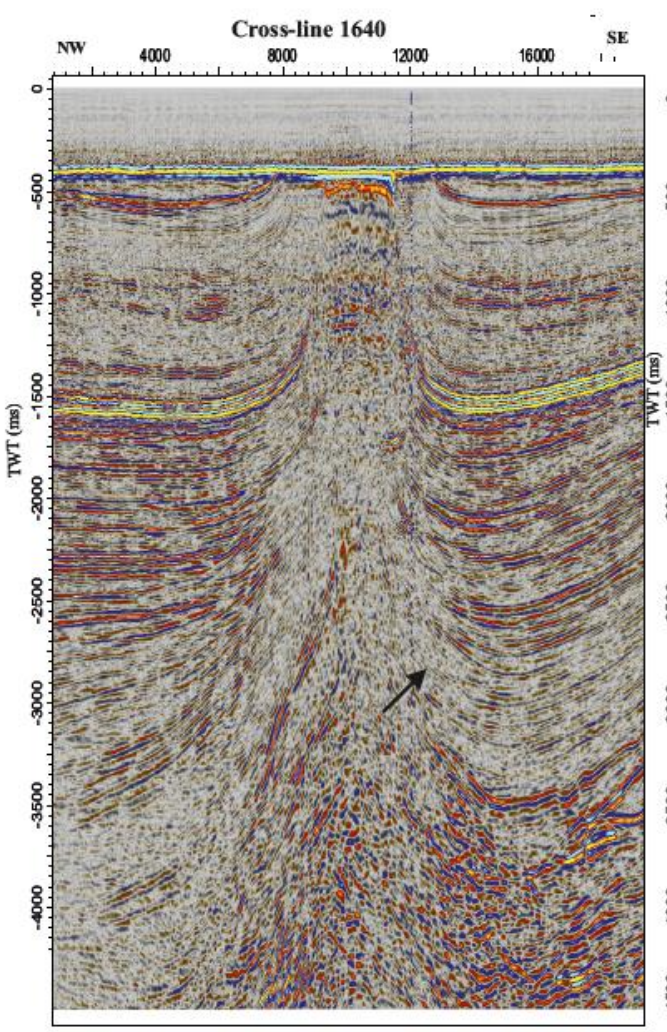

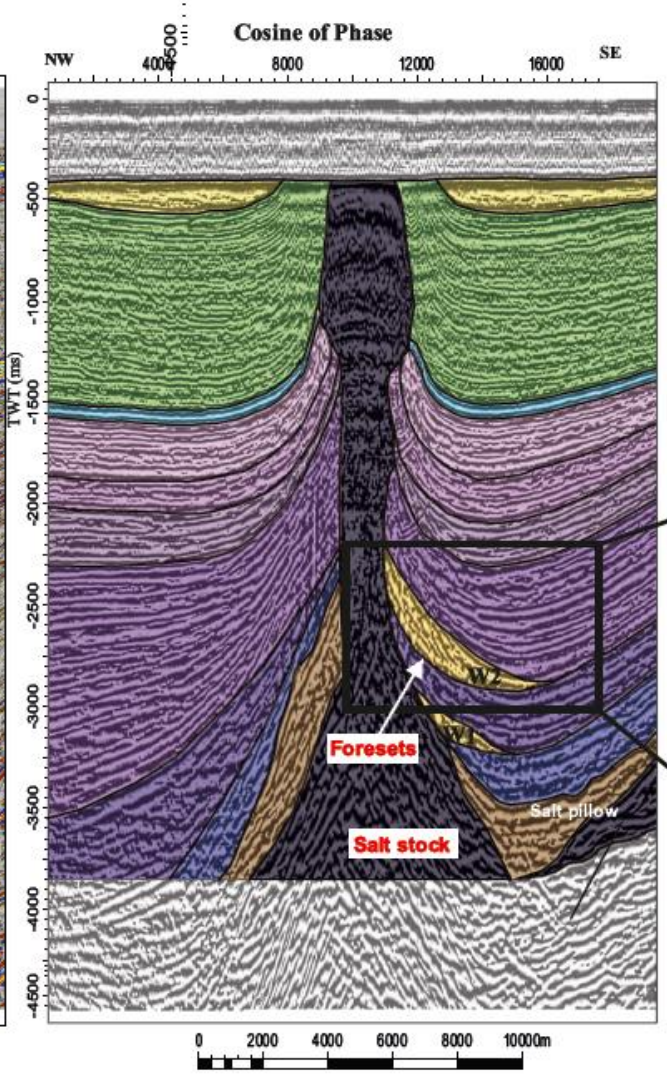

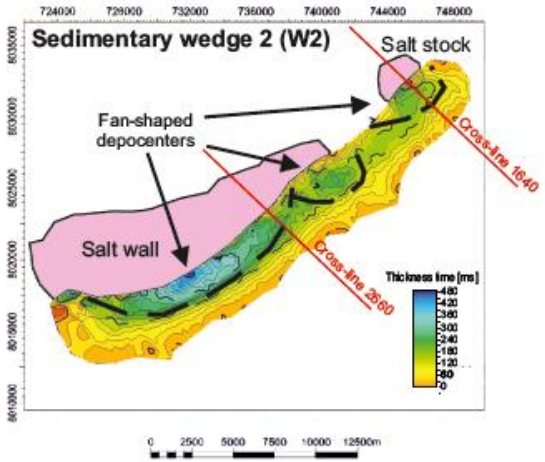

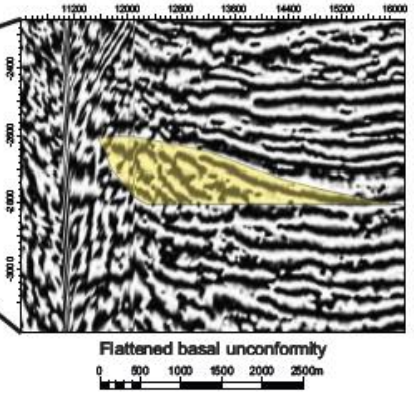

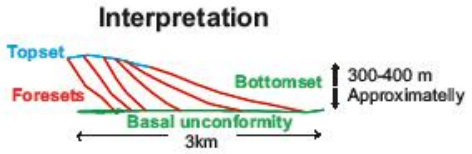

Conceptual model of the Nordkapp Basin

UPLIFT AND EROSION (Cenozoic)

- Cenozoic, Cretaceous, and Jurassic strata strongly truncated
- Salt structures are covered by glacial Quaternary sediments

REACTIVATION (Cenozoic)

- Reactivation caused by regional contraction (Nilsen et al., 1995)
- Syn-kinematic deposition of S10
- Marine fine grain silicilastics to fluvial environments of deposition
- Presence of salt-related sedimentary wedges

QUIESCENCE (Middle Jurassic - Late Cretaceous)

- Deposition of S8 and S9
- Organic-rich shales to fine grain silicilastics

LATE STAGES OF DIAPIRISM (Middle Triassic - Late Triassic)

- Low sedimentation rates vs salt supply
- Exposure of salt structures
- Salt widening and divergent migration of depocenters
- Deposition of Tabular Composite Halokinetic Sequences (S5, S6, and S7)
- Third generation of rim-synclines
- Total depletion of salt source layer at the end of this period

Conceptual model: deposition of S5,S6, and S7

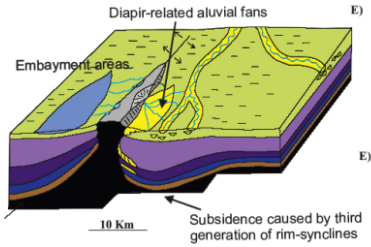

MAIN STAGE OF DIAPIRISM (Upper Early Triassic - Middle Triassic)

- High sedimentation rates vs salt supply
- Salt structures working as salt rollers
- Deposition of Tapered Composite Halokinetic Sequences (S3 and S4)
- Generation of primary and secondary rim synclines
- Major salt source layer depletion
- Inner shelf to fluvio-deltaic environments of deposition with development of Gilbert-deltas on salt rollers hanginwalls

Conceptual model: deposition of S3,S4, and S5

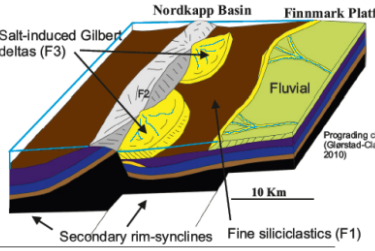

PRE-KINEMATIC (Late Permian - Lower Early Triassic)

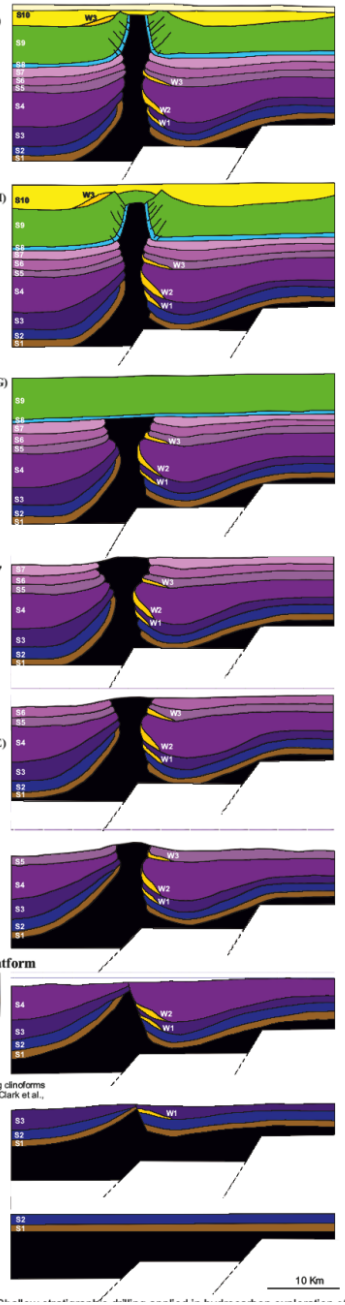

REFERENCES

Deep-Water Gulf of Mexico

With 12 recently announced deep-water discoveries and an aggressive leasing schedule for the Western and Central Gulf of Mexico, exploration and production technology is being pushed to its limits. To meet industry needs to image deeper and more obscure targets, TGS-NOPEC Geophysical Company has over 2.5 million km of 2-D and 88,000 km² of 3-D seismic data available in the Gulf, of which this line is an example.

Photo: MMS

The Ocean Confidence semi-submersible rig is used to drill deep prospects in the deep-water Gulf of Mexico.

Photo: Liam Gumley, MODIS/NASA

Sediments, similar to these off the current Mississippi delta, derived from the north, have been filling in the Gulf of Mexico since Jurassic time.

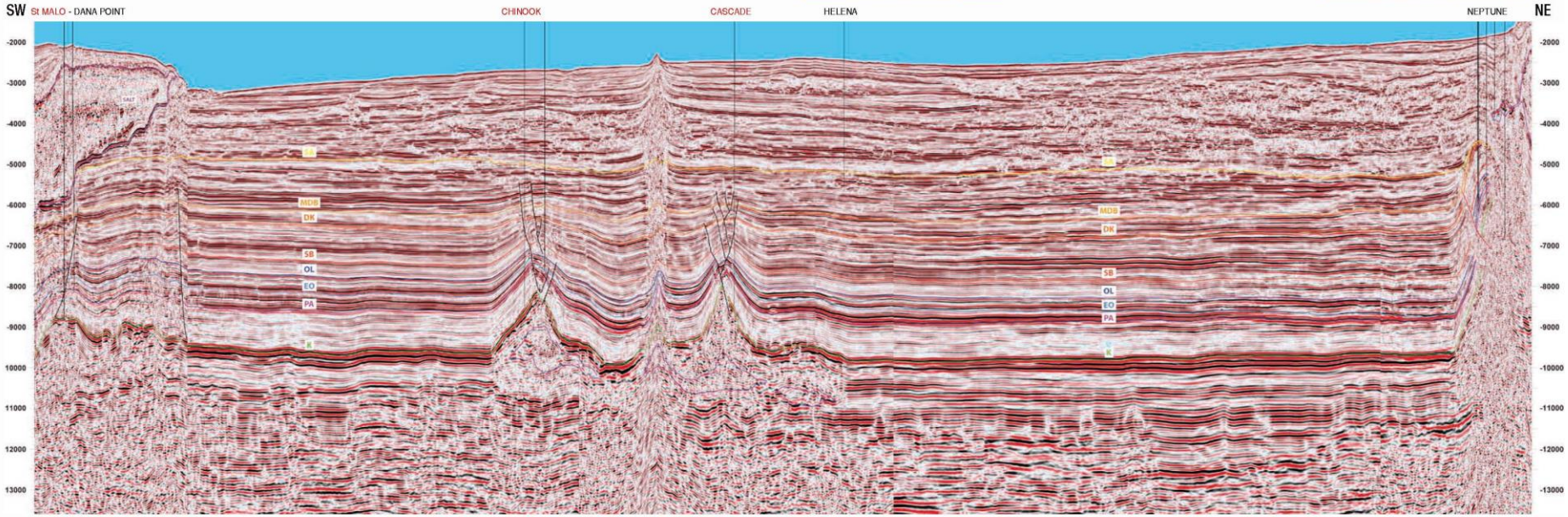

THE ONLY COMPLETE REGIONAL PERSPECTIVE

RTM re-processing gives a new look at the Gulf of Mexico Continental Margin

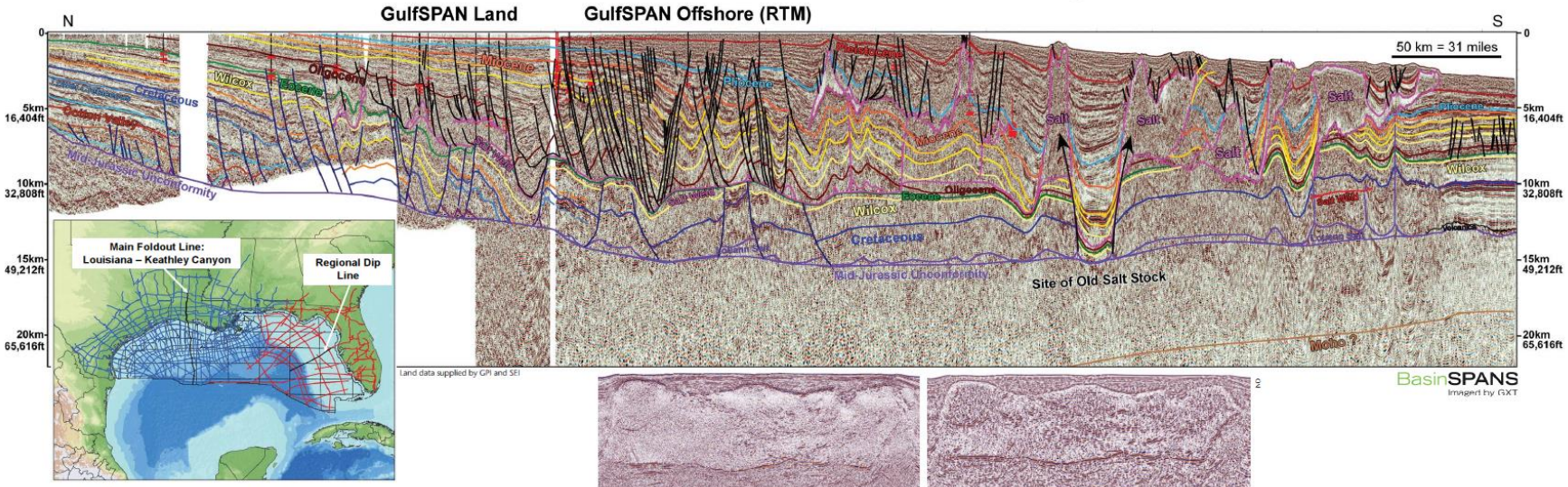

Regional GulfSPAN dip profile north to south from Central Louisiana to Keathley Canyon. This profile highlights the Cretaceous to Pleistocene prograding shelf margins and the interpretation of the deep water equivalent systems. The regional Eocene salt weld (pre-existing canopy) forms a major detachment surface accommodating Oligocene and Miocene expansion updip and the linked contraction to the south.

Inset base map shows the location of seismic profile and the complete GulfSPAN program. Red lines in the eastern Gulf of Mexico and onshore Florida are the recent continuation of this program to better understand the northern and eastern margins of the basin. Some of these lines have already been acquired and processed and some are in the planning stage.

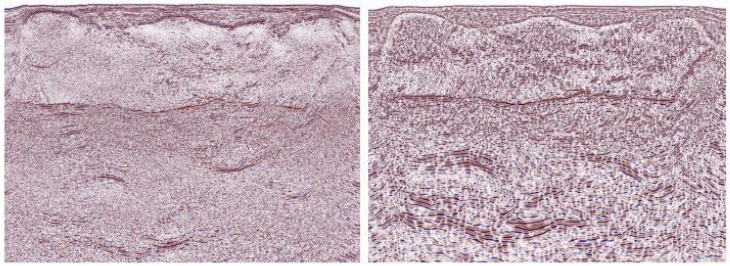

Comparison of original Kirchhoff migration (left) and the reimaged RTM (right). Note the improved image of base salt and the coherent signal for the subsalt deeper strata. Improved deep imaging should provide new exploration targets.

North Sea Renaissance

This example from the 2D North Sea Renaissance (NSR) seismic program is from the Norwegian Danish Basin. The middle part of the section is dominated by 2-4 km of heavily structured Triassic sediments and Permian salt. The parallel layers below the salt are assumed to represent the Rotliegendes Formation underlain by pre Permian sedimentary basins and highs.

Desert Sandstones
The top of the deeply buried Rotliegendes Formation, extensive desert deposits of Early Permian age, is easily identified on the NSR regional lines in spite of lying beneath Upper Permian salt. Few wells have drilled through these sandstones, and we know little of the Carboniferous, Devonian and deeper strata.

Photo: Jolanta Kosonina

Deep Water Shales
The Cretaceous rests unconformably on Jurassic strata in the North Sea. It is a pronounced reflector that is difficult to miss. The Jurassic below the reflector consists of Upper Jurassic shales (source rock) or Middle Jurassic sandstones (reservoir rock). Along the coast of Dorset we find the type section for the Upper Jurassic Kimmeridge shales.

Photo: Matthew Cimitrova

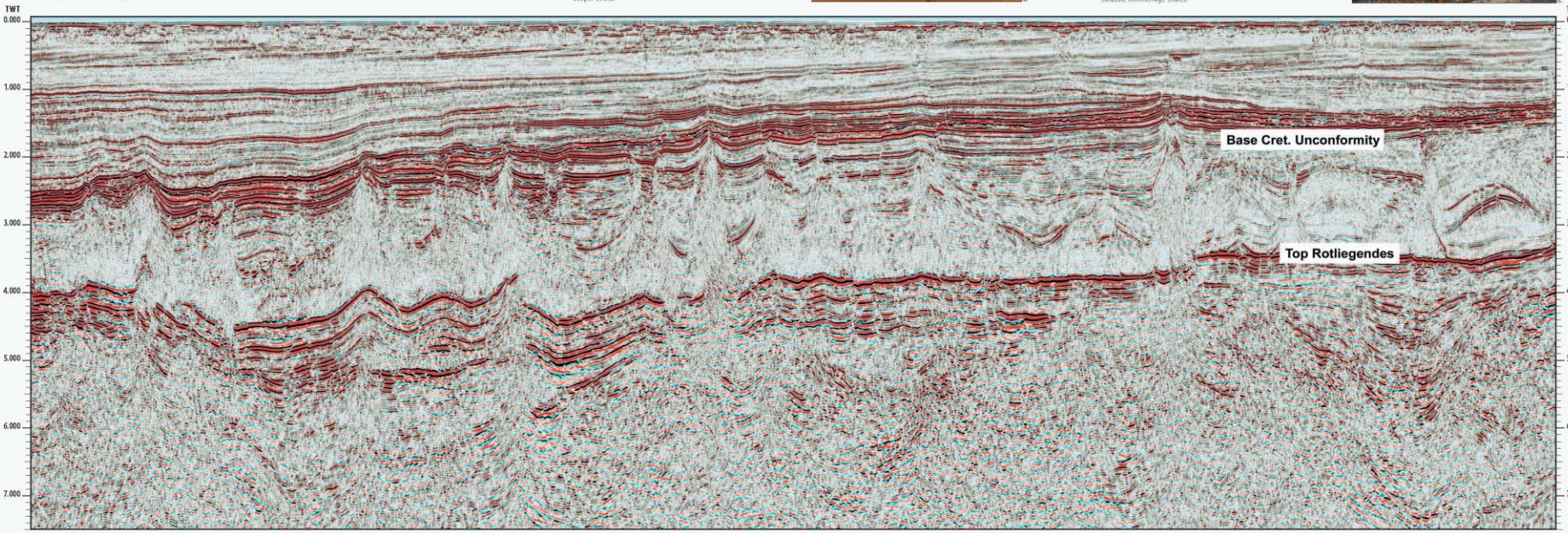

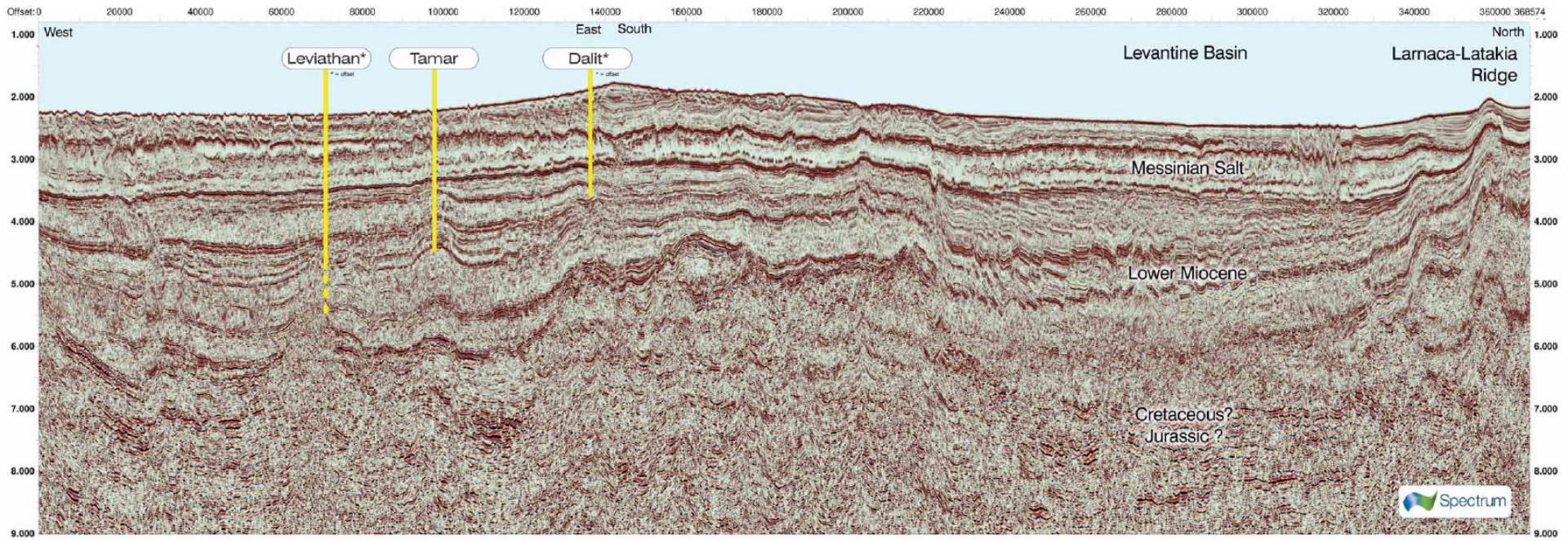
Offset: 0
20000
40000
60000
80000
100000
120000
140000
160000
180000
200000
220000
240000
260000
280000
300000
320000
340000
360000 368574
West
East
South
North
Leviathan*
* = offset
Tamar
Dalit*
* = offset
Levantine Basin
Larnaca-Latakia Ridge
Messinian Salt
Lower Miocene
Cretaceous?
Jurassic ?
Spectrum
1.000
2.000
3.000
4.000
5.000
6.000
7.000
8.000
9.000

Petroleum Potential of the Offshore Namibe Basin

The frontier Namibe Basin holds tremendous potential for hydrocarbons. The offshore West African basins have proven similarities with the equivalent sediments of the Brazilian margin, both part of the Aptian Salt Basin geological province, which formed as the Atlantic Ocean opened.

A GeoStreamer® dual-sensor regional 2D seismic survey, acquired in 2011 in association with Sonangol, covers the Angolan sector of the Namibe Basin and has been used to improve regional understanding of the tectonic evolution, geology and prospectivity of the Namibe Basin.

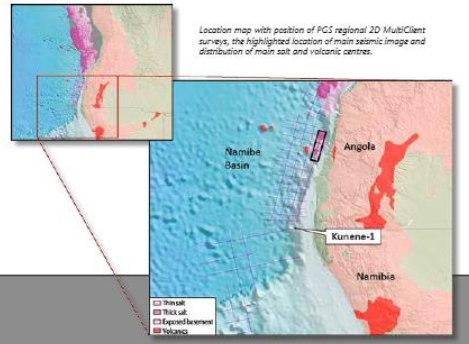

Location map with position of PGS regional 2D MultiClient surveys, the highlighted location of main seismic image and distribution of main salt and volcanic centres.

Section of a regional MultiClient GeoStreamer strike line, showing a salt-filled, perched basin in the Angolan sector of the Namibe Basin

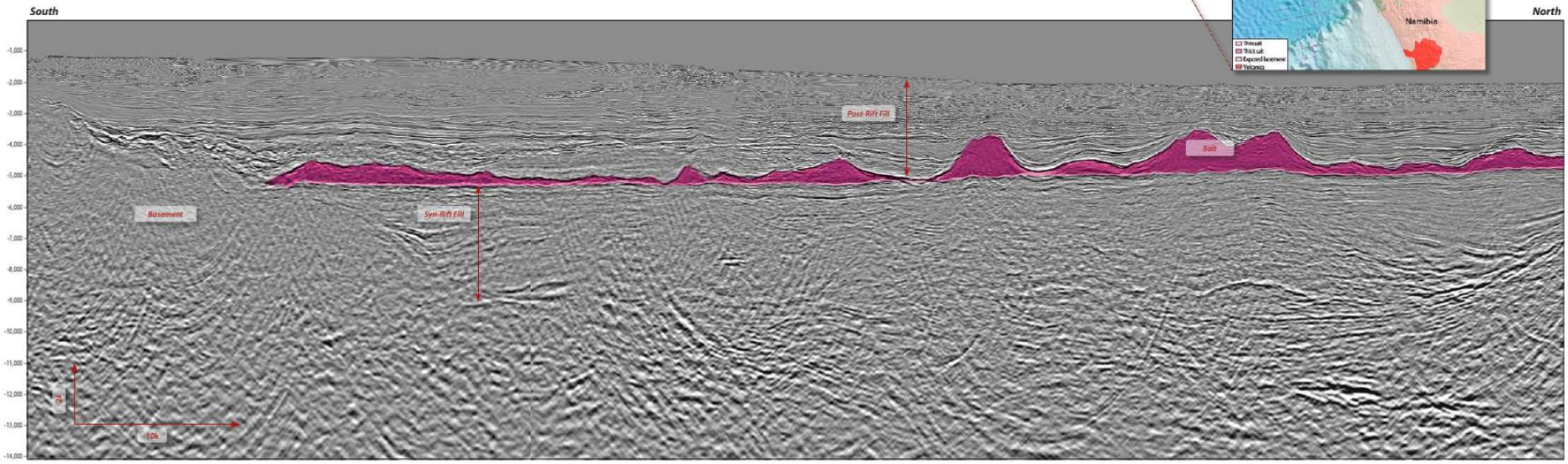

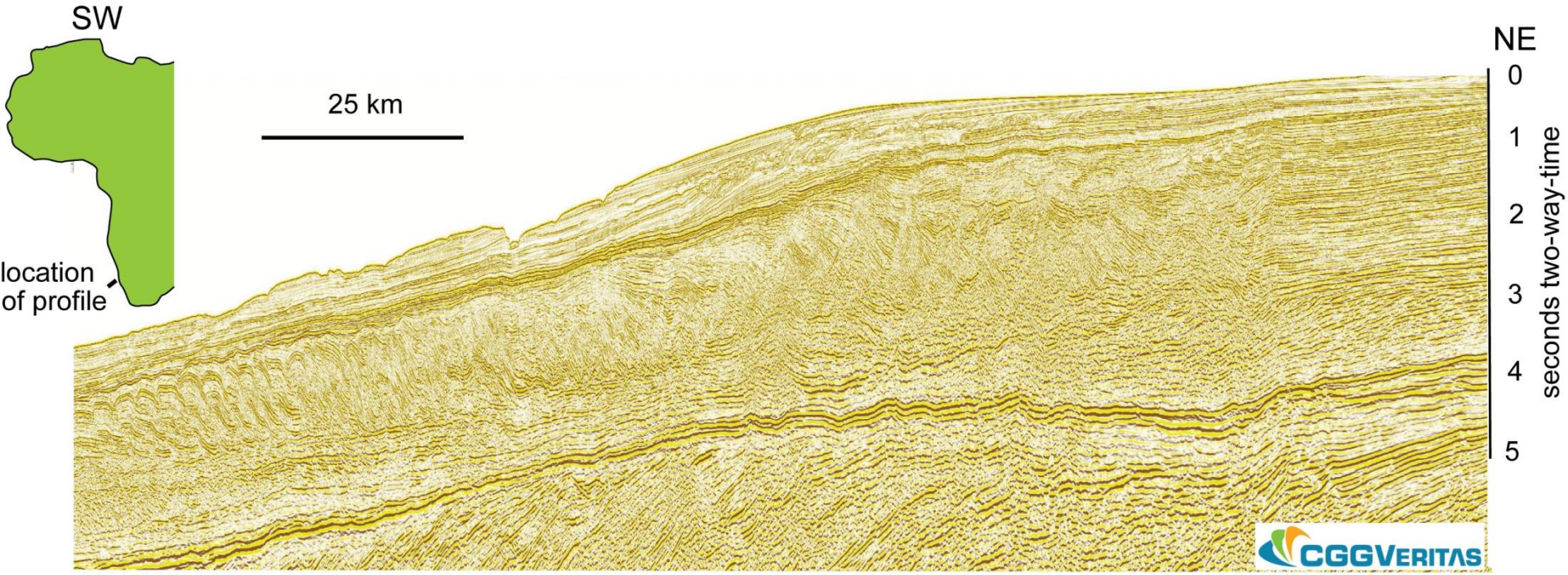
SW
NE
25 km
location
of profile
0
1
2
3
4
5
seconds two-way-time
CGGVERITAS

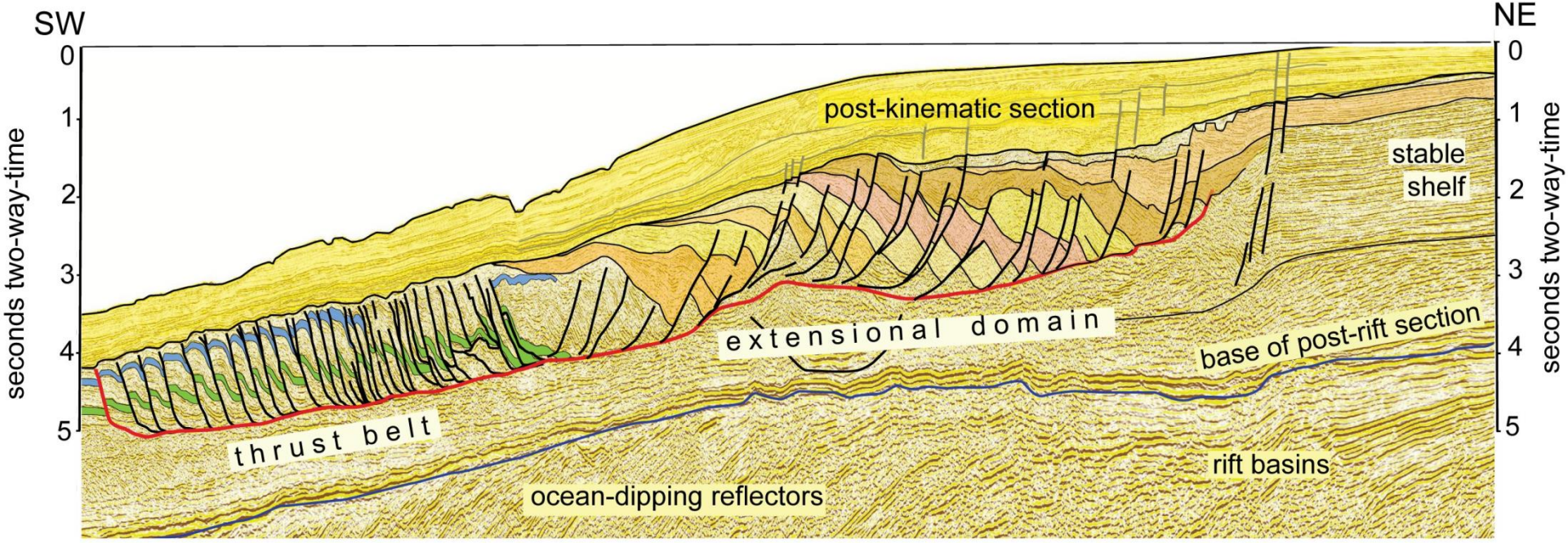
SW
NE
seconds two-way-time
0
1
2
3
4
5
post-kinematic section
stable shelf
extensional domain
base of post-rift section
thrust belt
rift basins
ocean-dipping reflectors

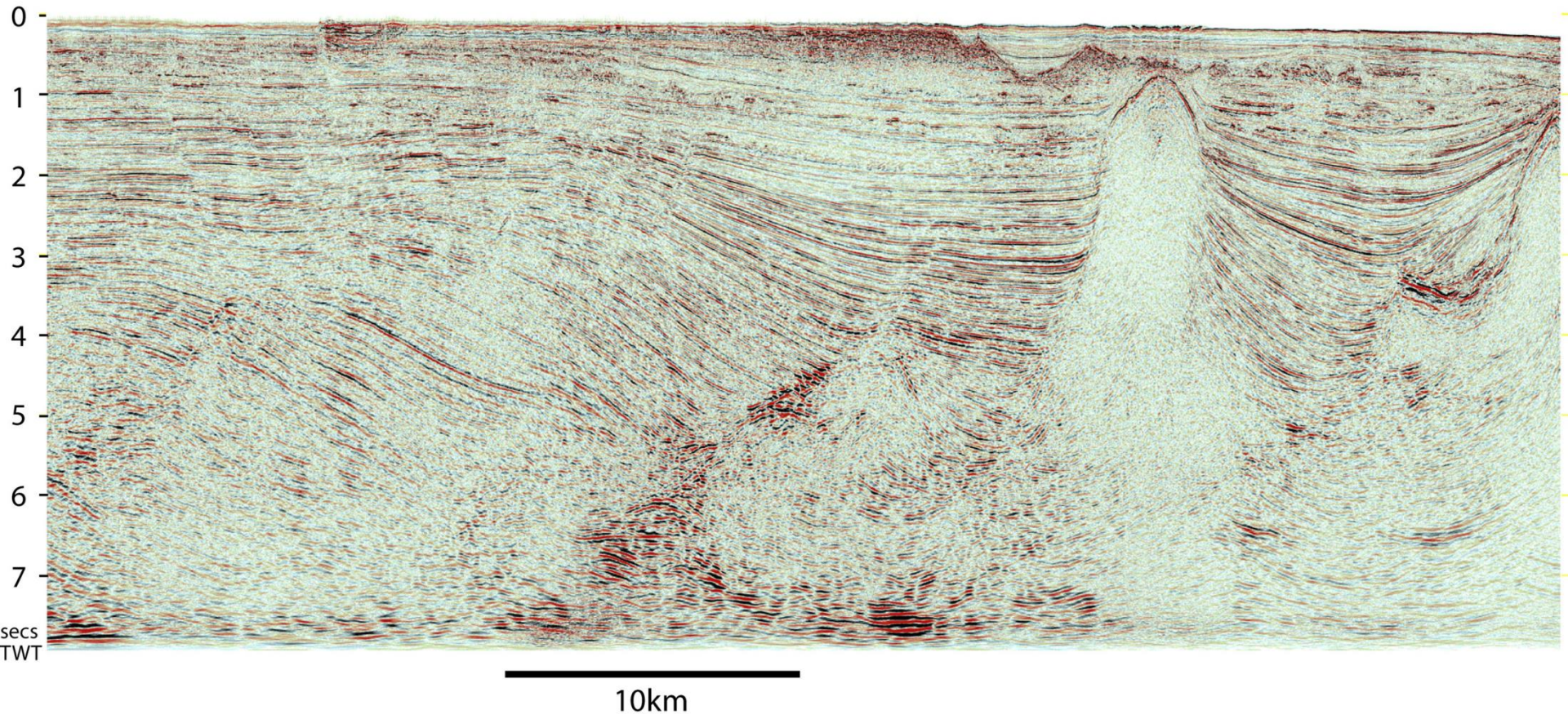
0
1
2
3
4
5
6
7
secs
TWT
10km

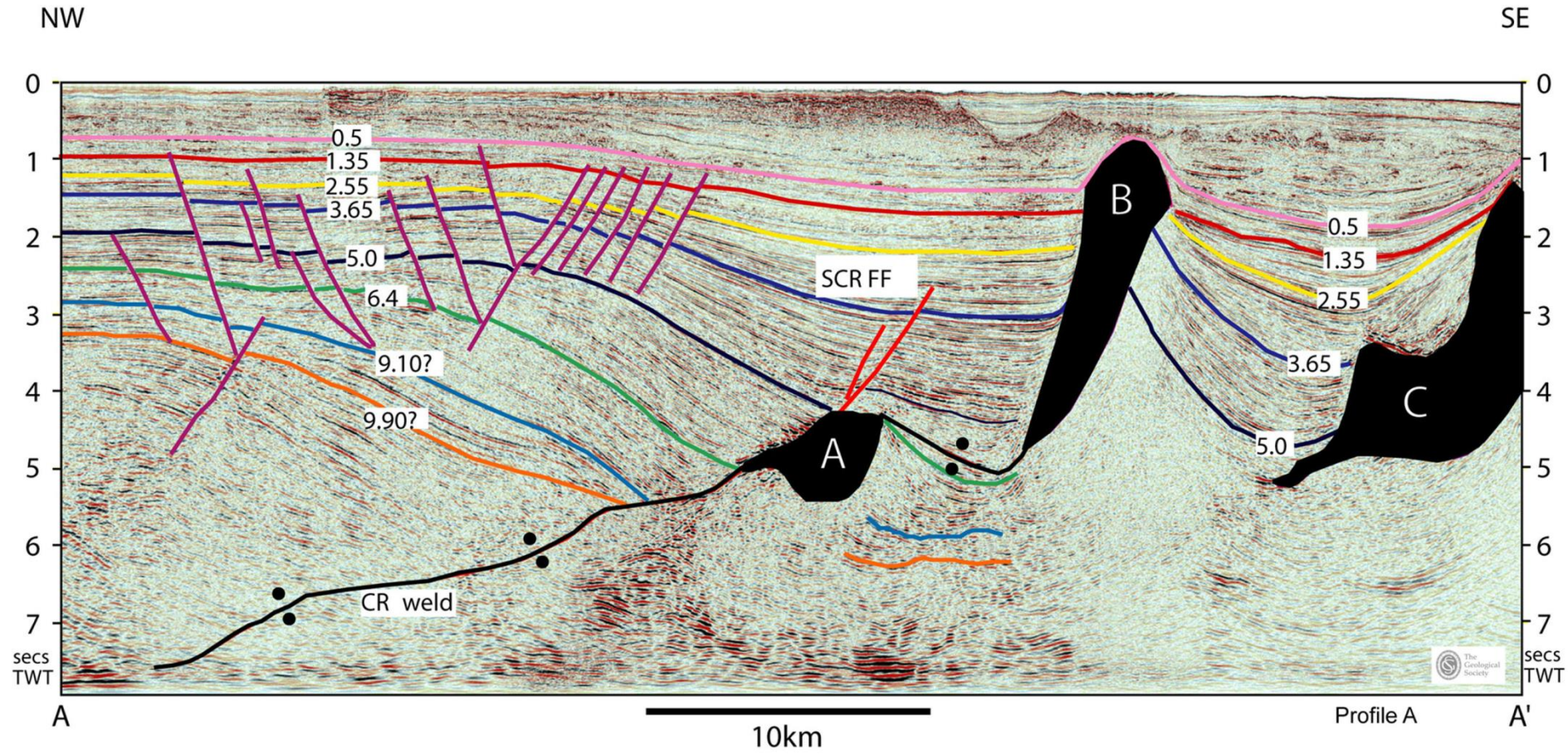
NW
SE
0
1
2
3
4
5
6
7
secs TWT
0.5
1.35
2.55
3.65
5.0
6.4
9.10?
9.90?
CR weld
SCR FF
A
B
C
A
A'
10km
Profile A

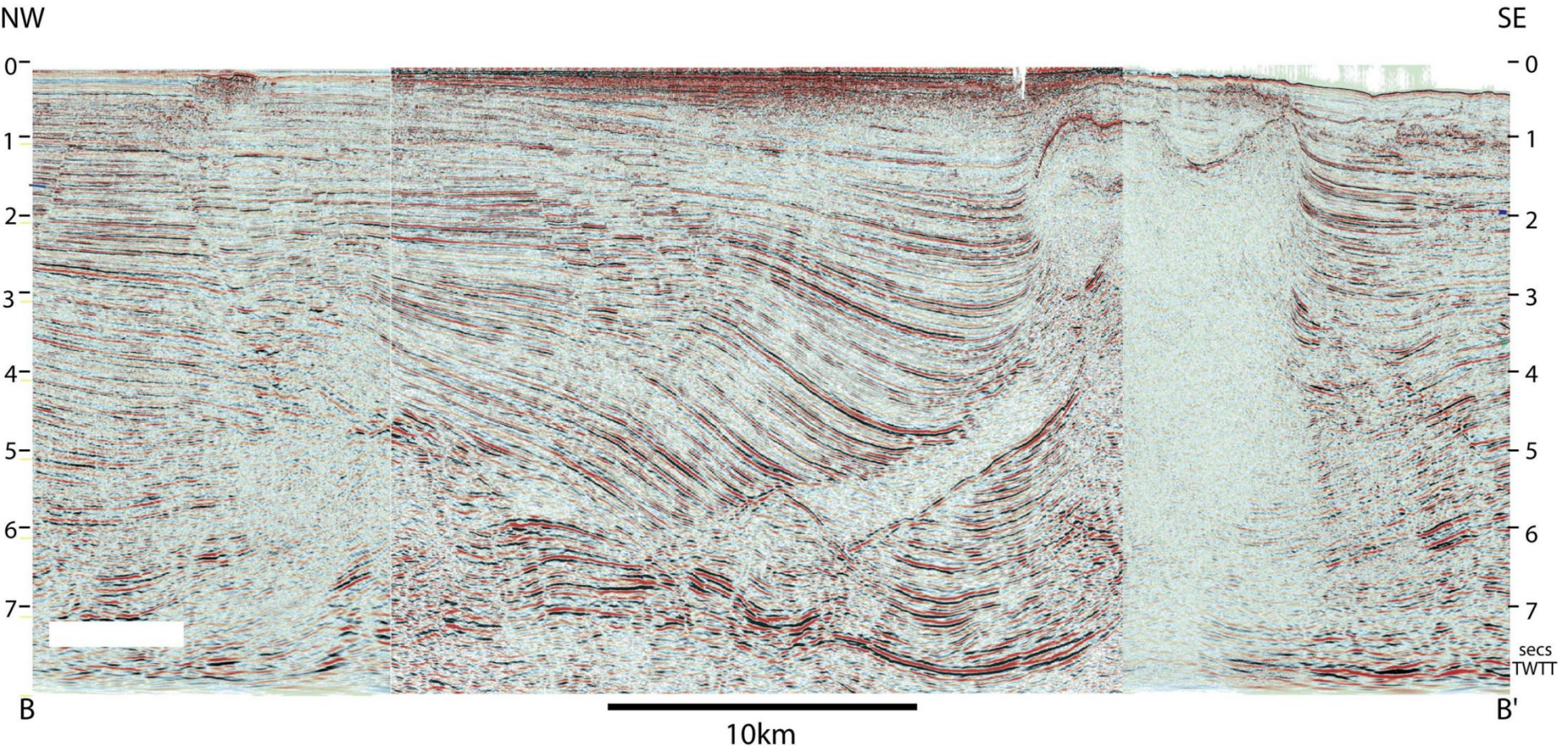
NW
SE
0
1
2
3
4
5
6
7
secs
TWTT
B
B'
10km

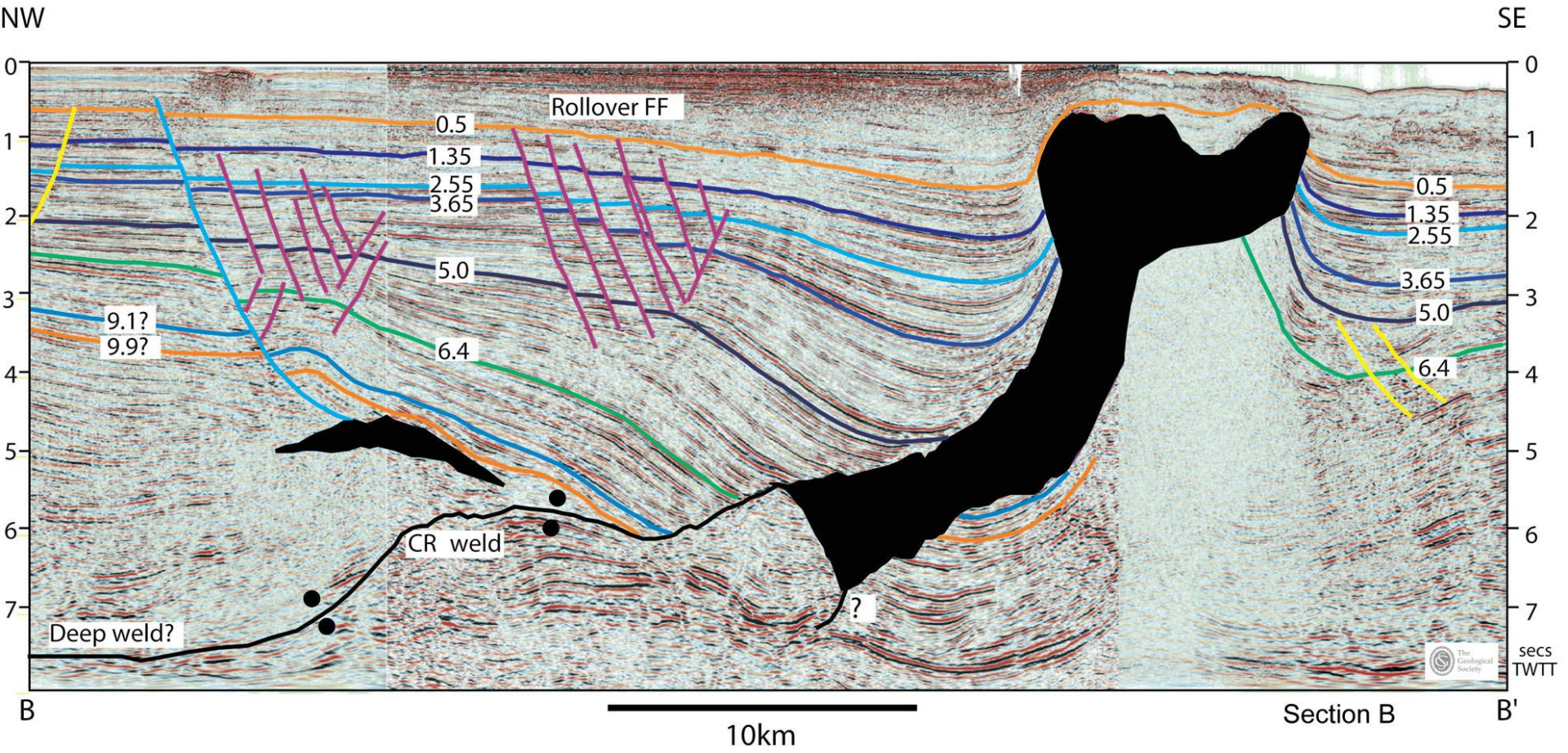
NW
SE
0
1
2
3
4
5
6
7
Rollover FF
0.5
1.35
2.55
3.65
5.0
6.4
9.1?
9.9?
CR weld
Deep weld?
?
secs TWTT
B
B'
Section B
10km